TESE DE DOUTORAMENTO

SEARCH FOR NEW STRATEGIES FOR CONTROLLING VIRAL DISEASES IN AQUACULTURE

Raquel Lama López

ESCOLA DE DOUTORAMENTO INTERNACIONAL

PROGRAMA DE DOUTORAMENTO EN AVANCES EN BIOLOXÍA MICROBIANA E PARASITARIA

SANTIAGO DE COMPOSTELA

ANO 2021

USC
UNIVERSIDADE
DE SANTIAGO
DE COMPOSTELA

BEATRIZ NOVOA GARCÍA, PROFESORA DE INVESTIGACIÓN DEL CSIC, Y MARÍA YSABEL SANTOS RODRÍGUEZ, CATEDRÁTICA DE LA USC,

CERTIFICAN:

Que la presente memoria titulada “Search for new strategies for controlling viral diseases in aquaculture”, que para optar al Grado de Doctor en Biología presenta Dña. RAQUEL LAMA LÓPEZ, ha sido realzada bajo nuestra dirección y/o tutela. Y considerando que constituye su trabajo de tesis, autorizamos su presentación a la Comisión Académica correspondiente.

Y para que así conste, expedimos el presente certificado en Vigo, 27 de Enero de 2021.

La Doctoranda **La Tutora**

Fdo: Raquel Lama López Fdo: Ysabel Santos Rodríguez

La Directora de Tesis

Fdo: Beatriz Novoa García

USC
UNIVERSIDADE
DE SANTIAGO
DE COMPOSTELA

AUTORIZACIÓN DO DIRECTOR / TITOR DA TESE

[incluír título da tese]

D./Dna. .....BEATRIZ NOVOA GARCÍA

INFORMA:

Que a presente tese, correspóndese co traballo realizado por Dna. RAQUEL LAMA LÓPEZ, baixo a miña dirección, e autorizo a súa presentación, considerando que reúne os requisitos esixidos no Regulamento de Estudos de Doutoramento da USC, e que como director desta non incorre nas causas de abstención establecidas na Lei 40/2015.

De acordo co indicado no Regulamento de Estudos de Doutoramento, declara tamén que a presente tese de doutoramento é idónea para ser defendida en base á modalidade de Monográfica con reproducción de publicacións, nos que a participación da doutoranda foi decisiva para a súa elaboración e as publicacións se axustan ao Plan de Investigación.

En Vigo, 4 de marzo de 2021

NOVOA GARCIA BEATRIZ - DNI 36069487J

Firmado digitalmente por NOVOA GARCIA BEATRIZ - DNI 36069487J
Nombre de reconocimiento (DN): c=ES, o=CONSEJO SUPERIOR DE INVESTIGACIONES CIENTIFICAS, ou=CERTIFICADO ELECTRONICO DE EMPLEADO PUBLICO, ou=INSTITUTO DE INVESTIGACIONES MARINAS, ou=36069487, serialNumber=IDCES-36069487J, sn=NOVOA GARCIA, givenName=BEATRIZ, cn=NOVOA GARCIA BEATRIZ - DNI 36069487J
Fecha: 2021.03.04 09:18:43 +01'00'

The work presented in this Doctoral Thesis has been supported by the projects:

- European Union through the funding Programme Horizon 2020 (Performfish-727610).
- Ministerio de Economía, Industria y Competitividad of Spain (BIO2017-82851-C3-2-R).
- EU Feder Programa Interreg España-Portugal 0474_BLUEBIOLAB.
- Consellería de Economía, Emprego e Industria (GAIN, Xunta de Galicia) IN607B 2019/01.
- Axencia Galega de Innovación (GAIN, Xunta de Galicia), for the predoctoral contract IN606A-2017/011.

USC
UNIVERSIDADE
DE SANTIAGO
DE COMPOSTELA

LIST OF PUBLICACIONS

Scientific publications included in this doctoral thesis:

- **Chapter 2: Lama R**, Pereiro P, Valenzuela-Muñoz V, Gallardo-Escárate C, Tort L, Figueras A, Novoa B (**2020**) RNA-Seq analysis of European sea bass (*Dicentrarchus labrax* L.) infected with nodavirus reveals powerful modulation of the stress response. *Veterinary Research* 51:64.

Author contribution in publication Chapter 2: Raquel Lama conducted the laboratory experiments, performed the bioinformatic analyses and data curation, and wrote the manuscript.

- **Chapter 3:** Pereiro P, **Lama R**, Moreira R, Valenzuela-Muñoz V, Gallardo-Escárate C, Novoa B, Figueras A (**2020**) Potential involvement of lncRNAs in the modulation of the transcriptome response to nodavirus challenge in European sea bass (*Dicentrarchus labrax* L.). *Biology* 9:165.

Author contribution in publication Chapter 3: Raquel Lama conducted the laboratory experiments, validated the lncRNAs, and participated in the writing and review of the manuscript.

- **Chapter 4: Lama R**, Pereiro P, Novoa B, Coll J (**2019**) Sea bass immunization to downsize the betanodavirus protein displayed in the surface of inactivated repair-less bacteria. *Vaccines* 7:94.

Author contribution in publication Chapter 4: Raquel Lama participated in the methodology, investigation, and the formal analysis of data.

Quality criteria of the journals:

ISO titles	Impact factor	5-YEAR Impact Factor	Q1	Rank	eISSN
Vaccines	4.760 (2018)	n/a	Immunology - SCIE	39/158	2076-393X
BMC Vet. Res	1.835 (2019)	2.179	Veterinary sciences - SCIE	32/141	1746-6148
Biology-Basel	3.796 (2019)	n/a	Biology - SCIE	19/93	2079-7737

Other scientific publications:

Vazquez-Rodríguez S, **Lama López R**, João Matos M, Armesto G, Serra S, Uriarte E, Santana L, Borges F, Muñoz Crego A, Santos Y (**2015**) Design, synthesis and antibacterial study of new potent and selective coumarin-chalcone derivatives for the treatment of tenacibaculosis. *Bioorganic & Medicinal Chemistry* 23:7045-7052.

Lama R, Pereiro P, Costa MM, Encinar JA, Medina-Gali RM, Pérez L, Lamas J, Leiro J, Figueras A, Novoa B (**2018**) Turbot (*Scophthalmus maximus*) Nk-lysin induces protection against the pathogenic parasite *Philasterides dicentrarchi* via membrane disruption. *Fish and Shellfish Immunology* 82:190-199.

AGRADECIMIENTOS

En primer lugar, dar las gracias a mis directores de tesis, Bea y Antonio. Antonio, aunque no seas mi director de manera oficial, tengo que agradecerte toda la ayuda que me has dado durante estos años y tus consejos para mejorar en mi trabajo. Gracias a los dos por haber confiado en mí y haberme dado la oportunidad de entrar en vuestro laboratorio, por guiarme y darme esta magnífica oportunidad de trabajar durante tantos años con vosotros.

No puedo olvidarme de mis inicios con Ysa Santos, de no ser por ti no habría llegado aquí. Recuerdo la ilusión que me hizo comenzar en el laboratorio en cuarto de carrera y los 5 años que estuve contigo en los que tanto me animaste. Gracias por ayudarme a conseguir este trabajo, aunque eso significara irme de Santiago.

En este laboratorio encontré a las mejores compañeras que podría haber soñado jamás!! Hablo en femenino porque ganamos por goleada! A las que todavía están y las que ya se han ido, gracias por vuestros conocimientos, vuestro apoyo y por haberos convertido en una parte muy importante de mi vida.

Gracias a mis compañeros de Chile por acogerme y enseñarme tantas cosas! Por hacerme sentir parte del grupo, siempre os estaré agradecida.

También me gustaría dar las gracias a mi madre que siempre me ha apoyado a la hora de estudiar y formarme y me ha dado libertad para viajar y abrir mis horizontes desde muy joven. Gracias también a mi familia, que sin saberlo, me han hecho mejorar en mi trabajo ayudándome a formarme mejor. A mis amigas, por apoyarme siempre y darme tantos ánimos, por creer que soy lo más cuando solo hago mi trabajo, me levantáis el ánimo! Y gracias Jose por hacer esta etapa más fácil y creer siempre en mí.

Soy escueta en palabras, lo sé, los que me conocéis sabéis cuánto me cuesta escribir, pero cada uno de vosotros sabéis lo agradecida que estoy y se me da mejor demostrar que escribir.

A TODOS, MIL GRACIAS!

SANTIAGO DE COMPOSTELA

ANO 2021

Index contents

List of abbreviations

3BHSD: 3 beta-hydroxysteroid dehydrogenase
5HT3E: 5-hydroxytryptamine receptor 3E
ACTH: adrenocorticotropic hormone
ALDOA: fructose-bisphosphate aldolase a
AMP: antimicrobial peptides
ATP2A1: sarcoplasmic endoplasmic reticulum calcium atpase 1-like (SERCA1)
B4GALT1: beta-1,4-galactosyltransferase 1
BAPTA-AM: 1,2-Bis(2-aminophenoxy)ethane-N,N,N',N'-tetraacetic acid tetrakis(acetoxymethyl ester)
BDKRB2: b2 bradykinin receptor
BFNNV: barfin flounder nervous necrosis virus
BSA: bovine serum albumin
C1QT1: complement c1q tumour necrosis factor-related protein 1
C3: complement component C3
Ca, Ca^{2+}: calcium
CAI: Carboxyamidotriazole
CALR: calreticulin
CART4: cocaine- and amphetamine-regulated transcript 4
CBLN1: cerbellin 1
CCRV: channel catfish hemorrhage reovirus
CD40: CD40 molecule, TNF receptor superfamily
cDNA: complementary DNA
CNS: central nervous system
CPFX: ciprofloxacin
CRH: corticotropin-releasing hormone
CTL: cytotoxic-T lymphocytes
CYP: cytochrome p450
DAB: 3,3′-Diaminobenzidine
DAPI: 4′,6-diamidino-2-phenylindole
DC: duct of Cuvier
DDIT4L: DNA damage-inducible transcript 4-like protein
DEG: differentially expressed gene
DLB-1: European sea bass brain cell line
DMSO: dimethyl sulfoxide
dpf: days post-fertilization
dpi: days post-infection
dsRNA: double strand RNA
EDTA: ethylenediaminetetra-acetic acid

EGTA: ethylene glycol tetra-acetic acid
ELISA: enzyme linked immunosorbent assays
ENOX1: ecto-NOX disulphide-thiol exchanger 1
ER: endoplasmic reticulum
ERO1A: ero1-like protein alpha
ESV: European sheatfish virus
FBS: foetal bovine serum
FC: fold change
FDR: false discovery rate
GABA: γ-aminobutyric acid
GH: growth hormone
GK cell line: grouper kidney cell line
GLHA: gonadotropin
GMEB1: glucocorticoid modulatory element-binding protein 1
GMO: genetically modified organism
GO: Gene Ontology
GRP84: G protein-coupled receptor 84
H_2O_2: hydrogen peroxide
H_2SO_4: sulphuric acid
HBSS: Hanks' balanced salt solution
HPA: hypothalamic-pituitary-adrenal
hpi: hours post-infection
HPI: hypothalamic-pituitary-interrenal
hpt: hours post-treatment
HRP: horseradish peroxidase
HYOU1: hypoxia-upregulated protein 1
i.m.: intramuscularly
i.p.: intraperitonealy
IFN: interferon
Igs: immunoglobulins
IGSF11: immunoglobulin superfamily member 11
IHNV: infectious hematopoietic necrosis virus
IL: interleukin
Ileu: isoleucine
IM: intramuscularly
IPNV: infectious pancreatic necrosis virus
IPTG: isopropil ß-D-1-tiogalactopiranósido
IRAK: interleukin-1 receptor-associated kinase
ISAV: infectious salmon anaemia virus
ISKNV: infectious spleen and kidney necrosis virus
KEGG: Kyoto Encyclopedia of Genes and Genomes
KOH: potassium hydroxide
L15: Leibovitz's medium
LECT2: leukocyte cell-derived chemotaxin-2
lncRNA: long noncoding RNA

LTB4R: leukotriene B4 receptor
***lyz*:** lysozyme gene
MMP: mitochondrial membrane potential
***mpeg*:** macrophage-expressed gen
MPX: myeloperoxidase gene
mRNA: messenger RNA
MS-222: ethyl 3-aminobenzoate methanesulfonate
***mx*:** myxovirus resistance gene
NaCl: sodium chloride
NCC: nonspecific cytotoxic cells
ncRNA: non-coding RNA
NGS: next-generation sequencing
NK: natural killer
NLRC3: NLR family, CARD domain containing 3
NMBB: neuromedin Bb
NMDE2: glutamate receptor ionotropic nmde2
NMU: neuromedin U
NNV: nervous necrosis virus, nodavirus
NO: nitric oxide
NOS1: nitric oxide synthase 1
NPB: neuropeptide B
NPVF: neuropeptide VF precursor
NPY: neuropeptide Y
O/N: overnight
PAGE: polyacrylamide gel electrophoresis
PBS: phosphate-buffered saline
PBST: phosphate-buffered saline containing 0.1% Tween-20
PCA: principal component analysis
PDIA4: protein disulphide-isomerase a4
PENKA: proenkephalin a
PFA: paraformaldehyde
PMA: phorbol myristate acetate
POMC: pro-opiomelanocortin
PRL: prolactin
PTH2: parathyroid hormone 2
PTX4: pentraxin 4
QORX: quinone oxidoreductase pig3
RdRp: RNA-dependent RNA-polymerase
RecA: recombinase A
RGNNV: red-spotted grouper nervous necrosis virus
***rgs6*:** regulator of g-protein signalling 6-like gen
RIN: RNA Integrity Number
RLU: relative luminescence units
RNA-Seq: high-throughput RNA sequencing

ROS: reactive oxygen species
RT: room temperature
RSAD: viperin or radical S-adenosyl methionine domain-containing protein 2
SACS: sacsin
SB cell line: Asian sea bass epithelial cells
SB medium: soy-bean hydrolysate broth
SDS: Sodium Dodecyl Sulfate
SEM: standard error of the mean
SERCA1: sarcoplasmic endoplasmic reticulum calcium atpase 1-like
SHRV: snakehead rhabdovirus
SJNNV: striped jack nervous necrosis virus
SL: somatolantin
SOMA: somatolactin
SRA: Sequence Read Archive
SSN-1 cell line: striped snakehead fish cell line
SST: somatostatin
SSTR2: somatostatin receptor type 2
STAR: steroidogenic acute regulatory protein, mitochondrial
STING: stimulator of interferon genes protein
SVCV: spring viremia of carp virus
TB medium: casein hydrolysate broth
$TCID_{50}$/ml: tissue culture infectious dose infecting 50% of inoculated cultures
TCR: T cell receptor
TetR: resistant to tetracycline
TLR: toll-like receptor
TMEM: transmembrane protein TNF: tumor necrosis factor
TPM: transcripts per million
TPNNV: tiger puffer nervous necrosis virus
TRIM: tripartite motif
Tris-HCl: Tris-hydrochloride
TSH: thyrotopin
UNC93B1: unc-93 homolog B1 (*C. elegans*)
VER: viral encephalopathy and retinopathy
VHSV: viral hemorrhagic septicemia virus
VLP: virus like particles
VNN: viral nervous necrosis
WT: wild type

List of figures

List of tables

Chapter 1

Introduction and Objectives

USC
UNIVERSIDADE
DE SANTIAGO
DE COMPOSTELA

1. Introduction and objectives

1.1. AQUACULTURE

The term "aquaculture" encompasses a whole set of activities, techniques and knowledge of the cultivation of aquatic plant and animal species. Currently, it is an important economic activity for the production of food, raw materials for industrial and pharmaceutical use, and of living organisms for repopulation and ornamentation. Large-scale cultivation of aquatic organisms is a relatively recent success. In the 19th century several countries focused on the repopulation of their rivers and lakes. Currently, more than half of the set of aquatic products consumed all over the world population comes from aquaculture farms. One of the biggest success stories in European aquaculture has been the culture of the European sea bass (*Dicentrarchus labrax* L.), which in less than 15 years grew from a few thousand tonnes to almost 163,131 tons in 2015 (Food and Agriculture Organization, FAO) (Bagni, 2015), whilst 6,435 tons were obtained by fishing according to MAPAMA (Ministerio de Agricultura y Pesca, Alimentación y Medio Ambiente, 2017) data in the same year.

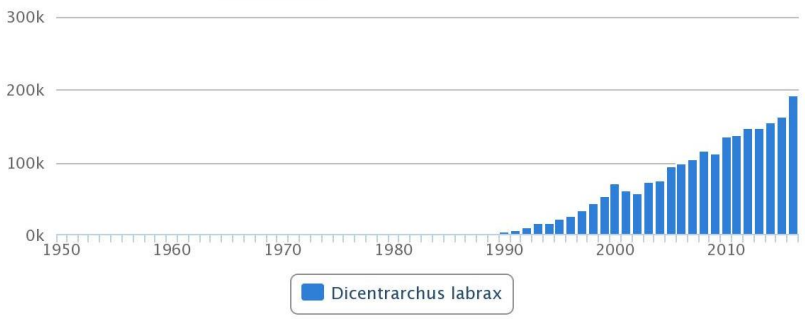

Figure 1.1. Global aquaculture production for *Dicentrarchus labrax* in tons since 1990 to 2016 (FAO, 2019).

Spain occupies the fourth place in the world ranking of sea bass fishing, and the third in sea bass aquaculture production. Figure 1.2 represents the production of sea bass from aquaculture compared with the low production of sea bass by fishing (Asociación Empresarial de Acuicultura en España, APROMAR, 2020).

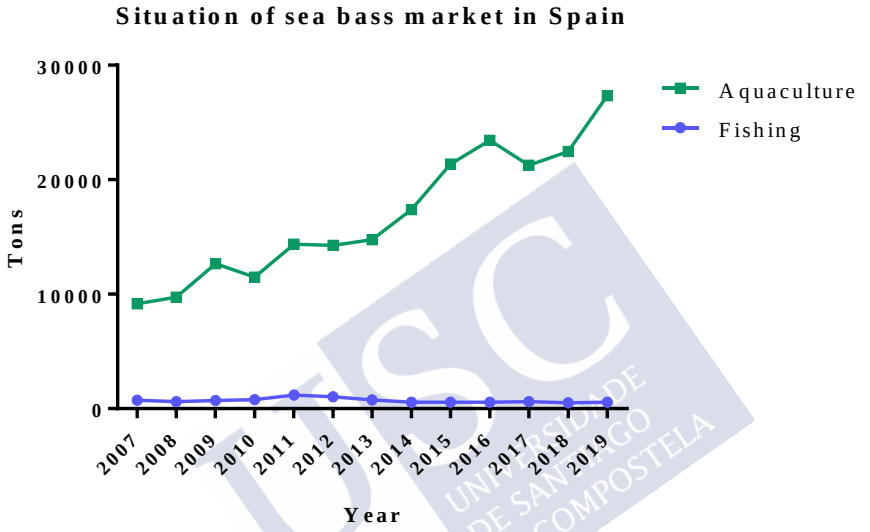

Figure 1.2. The evolution of the sea bass market in Spain in recent years (APROMAR, 2020).

The first intensive rearing trials started in the early 1970's, and afterwards, controlled reproduction in spawning tanks and larval rearing were developed (Figure 1.3). Sea bass needs up to 18 or 24 months to reach commercial size, therefore selective breeding programs leading to an improvement in growth rate or resistance to diseases are major aquaculture approaches that need special attention and deep investigation.

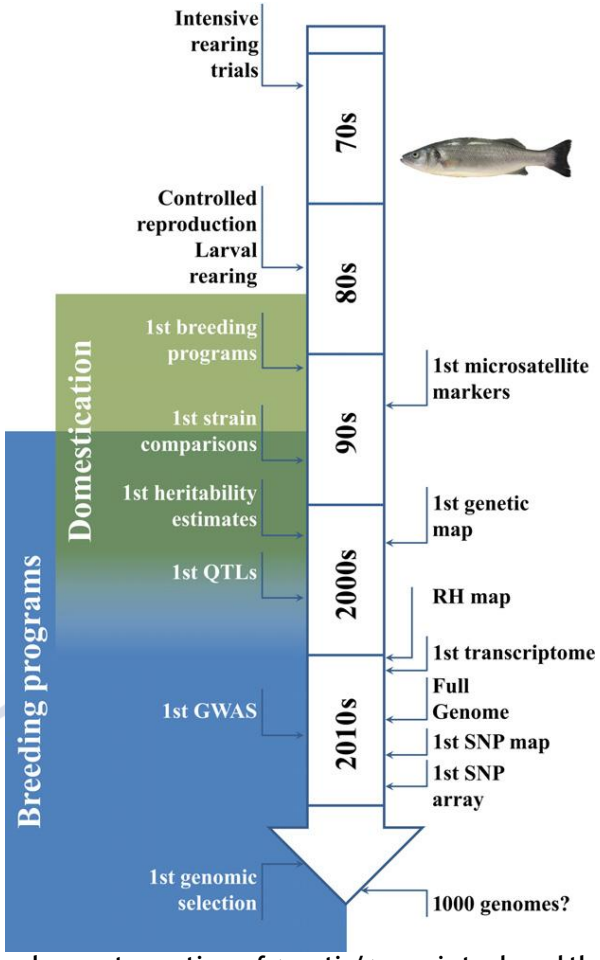

Figure 1.3. Development over time of genetic/genomic tools and their application in European sea bass (Vandeputte et al., 2019).

1.2. DISEASES AFFECTING THE SEA BASS PRODUCTION

Sea bass are susceptible to a wide range of diseases under rearing conditions. These outbreaks have important effects on commercial production and could limit the expansion of the industry in some countries, particularly in the Mediterranean aquaculture.

Stress is considered an important factor co-responsible for disease outbreaks, thus improved husbandry is generally suggested to reduce

stress (Johansen et al., 2006). Another problem is the lack of authorized effective therapeutants in most European countries (FAO).

Knowledge on molecular and genetic mechanisms of resistance to pathogens and specific features of immune response against various infectious agents should greatly benefit the development of effective therapeutants and vaccines that allow avoiding the use of antimicrobials that can reach the environment and cause a detrimental effect on human health.

Sea bass is affected by various diseases caused by bacteria, parasites and viruses. The most representative bacterial diseases are vibriosis and photobacteriosis, mostly caused by *Vibrio anguillarum* and *Photobacterium damselae* subsp. *piscicida*, respectively (Dec et al., 1990; Bakopoulos et al., 1997). The main parasitic agents affecting sea bass culture include *Philasterides dicentrarchi* (Dragesco et al., 1995) or *Anisakis* spp. (Cammilleri et al., 2018). But sea bass is mostly affected by the viral encephalopathy and retinopathy (VER) or the viral nervous necrosis (VNN) disease, caused by the fish nodavirus (NNV) (Office International des Epizooties, OIE, 1995), generating higher mortality in this fish species. This disease was first recorded in the late 80's in several species of fish and described as a picornavirus (Glazebrook et al., 1990; Yoshikoki and Inoue, 1990), and in 1985 the "seed" production of sea bass was completely eliminated by the presence of this virus in the nerve cells of larvae and juvenile sea bass (Bellance and Gallet de Saint-Aurin, 1988). Since then, a lot of studies have been carried out to learn more about this virus and try to eradicate it.

1.2.1. General characteristics of nodavirus

NNV produces a severe pathology in marine and freshwater species around the world, reaching mortalities of 100% in juveniles, and it has also been detected in adult animals (Munday et al., 2002; Doan et al., 2017). Due to its neurotropic nature, NNV affects mainly the central nervous system (CNS), causing vacuolization in the brain, spinal cord and retina of infected fish. This entails a series of symptoms that are characteristic of this disease, such as abnormal swimming behaviour (spiral swimming that provokes curved spinal cord, horizontal looping,

swim bladder hyperinflation), loss of eyes due to a necrotic process, loss of appetite and darkening of the skin.

The piscine nodavirus is included in the genus *Betanodavirus* that, nowadays, consists of 4 recognized genotypes: the striped jack nervous necrosis virus (SJNNV), the barfin flounder nervous necrosis virus (BFNNV), the tiger puffer nervous necrosis virus (TPNNV) and the red-spotted grouper nervous necrosis virus (RGNNV) (Schneemann et al., 2005). The RGNNV is the genotype that affects more areas worldwide and those animals that live at warmer temperatures (25-30 ˚C), and affects the European sea bass (Munday et al., 2002; Doan et al., 2017).

The NNV is a small non-enveloped virus, with a diameter of 25-30 nm and icosahedral symmetry. The viral genome is a bisegmented positive-sense single stranded RNA, composed of RNA1 and RNA2. The RNA1 (3.1 Kb) encodes an RNA-dependent RNA-polymerase (RdRp), also named protein A. The RNA2 (1.4 Kb) encodes a capsid protein, that in addition to having a structural function, it has a terminal nucleolus localization signal, which is associated with cell cycle arrest (Guo et al., 2003a) and, at later stage of infection, the accumulation of the capsid protein induces a caspase-dependent cascade ending up in the cell apoptosis (Guo et al., 2003b; Wu et al., 2008). There is a subgenomic RNA, the RNA3, synthetized from the 3' terminus of RNA1 that encodes two non-structural proteins, the B1 and B2. The protein B1 plays a role as an antinecrotic death factor, which reduces mitochondrial membrane potential (MMP) loss and causes cell cycle arrest at early stages of viral infection (Chen et al., 2009; Su et al., 2018). The viral protein B2 suppresses the cellular RNA interference in infected cells (Iwamoto et al., 2005; Fenner et al., 2006) and also acts as a necrotic death factor, upregulating the expression of the proapoptotic cell gene *Bax* and inducing MMP loss but not mitochondrial cytochrome c release (Chen et al., 2007; Su et al., 2009) (Figure 1.4).

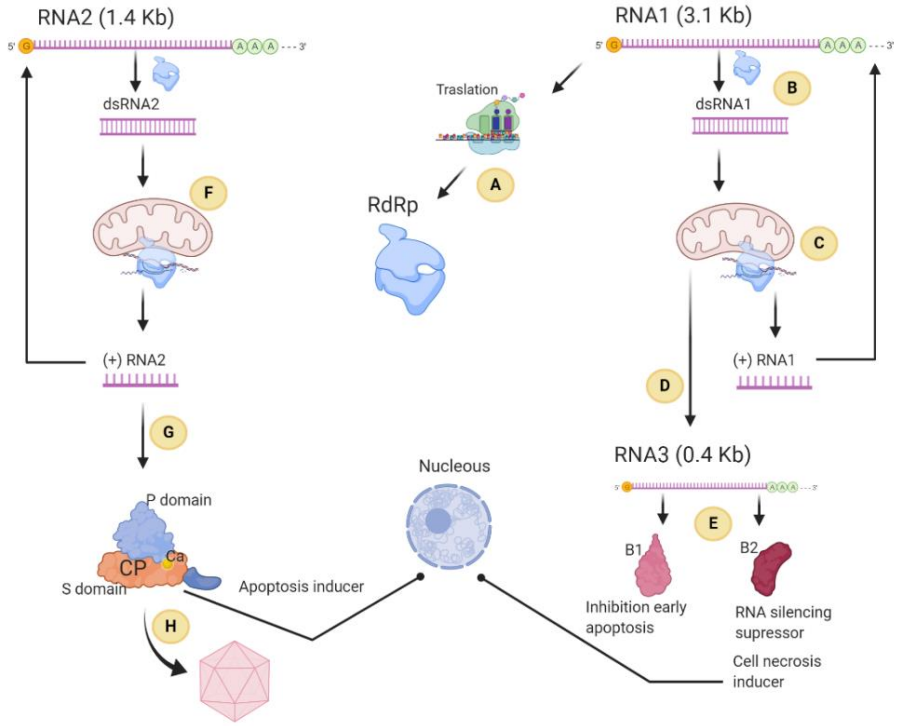

Figure 1.4. Schematic overview of the betanodavirus replication cycle: After entry, the viral bisegmented single stranded positive RNA genome is released into the cytoplasm. Subsequently, host ribosomes translate the viral RNA1 into the viral RNA-depentent RNA polymerase (RdRp) **A** The RdRp is then used to copy the genomic (+) RNA1, synthetizing a (-) RNA strand and generating a dsRNA (**B**). The dsRNA is now used for replication/transcription into new RNA1 molecules (**C**), all this process takes place in association with outer mitochondrial membranes. Afterwards, a subgenomic RNA, namely RNA3, is synthesized from the 3' terminus of RNA1 (**D**). RNA3 encodes (and is translated into) the two smal proteins B1 and B2 (**E**) which show nuclear localization. In addition, RNA3, presumaly like in alfanodavirus, also regulates RNA2 synthesis (**F**) and it is downregulated at the onset of RNA2 replication/transcription. RNA2 translation yields the capsid protein (**G**) and, finally, nascent (+) RNA1 and (+) RNA2 molecules are packaged into progeny virions (**H**) (Modified from Bandin and Souto, 2020 using Biorender.com).

1.2.2. Control and prevention of NNV

When viral diseases are introduced in an aquaculture system, they are quite difficult to control, and NNV infections are especially complicated because of the natural structure of the viral particle. NNV resists a wide range of pH, temperature and salinity (Frerichs et al.,

2000), so its control is mainly reduced to good husbandry practices, selecting NVV-free broodstock, or the use of external disinfestation of eggs by ozonation or using inlet water UV treated (Samuelsen et al., 2006; Doan et al., 2017). The prevention is restricted to the use of vaccines against the RGNNV genotype, and only two inactivated formalin-killed vaccines are available at the moment in the aquaculture market (Bandin and Souto, 2020). Due to this, it is critical to understand in greater depth the response of the fish to an infection with nodavirus and learn the affected processes where we can act to obtain higher resistence against this disease.

1.3. TELEOST IMMUNE ANTIVIRAL SYSTEM

The immune system protects animals from threats by parasites, bacteria and viruses. This immune response involves a coordinated set of interactions among host cells and the protective molecules they produce to prevent dangerous incursions and then to restore homeostasis.

Bony fishes, arising about 300 million years ago, are the most primitive animal group with a complete immune system, consisting on unspecific or innate immunity and specific or adaptive immunity. Although it is usual to describe these two types of immune responses separately, there is increasing evidence that both complement each other to maintain the maximum level of host immunocompetence.

1.3.1. Innate antiviral immunity and nodavirus

The innate immune system is independent of a prior exposure to any particular microorganism. In fish, the innate immune response has been considered an essential component in fighting diseases (White, 2007). The innate immune response against virus is mainly mediated by cellular (cell-mediated cytotoxic activity) and humoral (antiviral proteins) mechanisms (Uribe et al., 2011).

At humoral level, a betanodavirus infection *in vivo* shows a modulation in the expression of several pro-inflammatory cytokines such as interleukin IL-1β and the tumor necrosis factor (TNF) or effector molecules involved in the antiviral interferon (IFN) pathway, such as the Mx protein (Poisa-Beiro et al., 2008; Scapigliati et al., 2010). A later upregulation of the *ifn* gene, also points to the existence

of an IFN-independent activation of type I IFN effectors, therefore, probably the sea bass immune response agains NNV may be mediated by both IFN-dependent and -independent mechanisms (Valero et al., 2018). The cytokine modulation, suggests a complex pattern of inflammatoy responses during the NNV infection which can explain the vacuolization and neuroinflammatory process in the CNS of infected fish (Poisa-Beiro et al., 2008). The synthesis of antimicrobial peptides (AMP) by fish has become very important in the fight against viruses (Chia et al., 2010; Wang et al., 2010; Zhang et al., 2014; Pereiro et al., 2016). In a sea bass NNV infection an upregulation of hepcidin, complement component 3 and dicentracin AMPs have been identified (Valero et al., 2015; Valero et al., 2018).

The cell-mediated cytotoxic activity is carried out by nonspecific cytotoxic cells (NCCs), natural killer-like cells (NK) and cytotoxic-T lymphocytes (CTL) (Nakanishi et al., 2002; Fischer et al., 2006). The role of other immune cells such as the phagocytes is also important in viral clearance, however, the phagocytic activity is not affected by NNV infection in sea bass or seabream, and there is no cellular infiltration in the CNS during a NNV infection in gilthead seabream (López-Muñóz et al., 2012). The reactive oxygen species (ROS) production is increased in seabream (a NNV-resistant fish species) and decreased in sea bass (a NNV-susceptible fish species), which suggests that ROS production could be important in fighting the virus (Chaves-Pozo et al., 2012).

The cellular and the humoral levels are also closely related. Chaves-Pozo suggests the potential correlation between the cell-mediated cytotoxic activity and Mx expression or whether the IFN pathway/Mx could increase this activity in NNV infected sea bass (Chaves-Pozo et al., 2012).

These examples of how the innate immune system of fish acts at various levels against a NNV infection, demonstrate that this first defense barrier, despite not being pathogen specific, is essential for host defense and requires our deeper research attention.

1.3.2. Adaptive immunity and nodavirus

The adaptive immunity is activated after a previous encounter with a specific stimulus in the host. This response, which improves with the successive encounter with the same pathogen, is highly specific for each particular pathogen (Du Pasquier, 2001). Adaptive immunity also involves humoral and cellular responses. Immunoglobulins (Igs) are critical factors on the humoral adaptive immunity, produced by B cells which can recognize pathogen antigens, neutralizing and eliminating them. T cells mediate the cell adaptive immunity, which promotes the destruction of infected cells (Flajnik and Kasahara, 2010).

In teleosts, there are three main Ig isotypes, the IgM, the IgD, and the IgT/Z. IgM is the most abundante Ig in the serum used to confirm the specific immune-response against pathogens (Sunger, 2012). The immunoprotection that IgD confers is not well known (Edholm et al., 2011), but its role in the protection of the gills has been hypothesized (Bengtén et al., 2006), as well its role in mucosal homeostasis (Xu et al., 2016; Kong et al., 2019; Yu et al., 2019). IgT is involved in mucosal immunity in bony fish, similar to IgA in mammals (Zhang et al., 2010) and was further characterized in sea bass (Buonocore et al., 2017). During a NNV infection *in vivo*, there is an induction of gene encoding T and B lymphocyte markers, TCRβ/CD8α and IgM, respectively, in gilthead seabream, an increased level of TCRβ/CD8α in Atlantic halibut (Overgard et al., 2012) and an increased expression level of the IgM gene in sea bass (Valero et al., 2018) suggesting that the adaptive immune responses are critical in the defence against NNV (Grove et al., 2006; López-Muñoz et al., 2012; Piazzon et al., 2016; Buonocore et al., 2017). A more in-depth study of the adaptive immune response of fish to viruses is needed for the development of effective vaccines.

1.4. NEXT-GENERATION SEQUENCING

Over the years, there have been important advances in describing the replication cycles of viruses and which organs they infect or how they spread throughout the different tissues, but it is also very important to know how the host reacts against infection and the different responses that exist between cells or organisms that are susceptible or resistant to the virus, finding the targets to develop an optimal therapeutic strategy.

Next-generation sequencing (NGS) techniques allow us a more in-depth knowledge of the interaction between the virus and the host, and the genomic or proteomic changes caused by the viral infection can inform about the responses that are important for viral survival and take advantage of them for antiviral purposes.

1.4.1. High-throughput RNA sequencing (RNA-Seq)

The RNA-Seq revolutionized transcriptomics by allowing RNA analysis through cDNA sequencing at massive scale. Compared to techniques used in past years such as microarrays, RNA-Seq allows greater coverage and better resolution of the transcriptome. The increasingly cheaper prices of NGS technologies allow the performance of studies in non-model species. Generation of a greater database enables a simple way to compare the response of different organisms to a virus or to several viruses, thus seek common and specific strategies for each virus-host interaction (Figure 1.5).

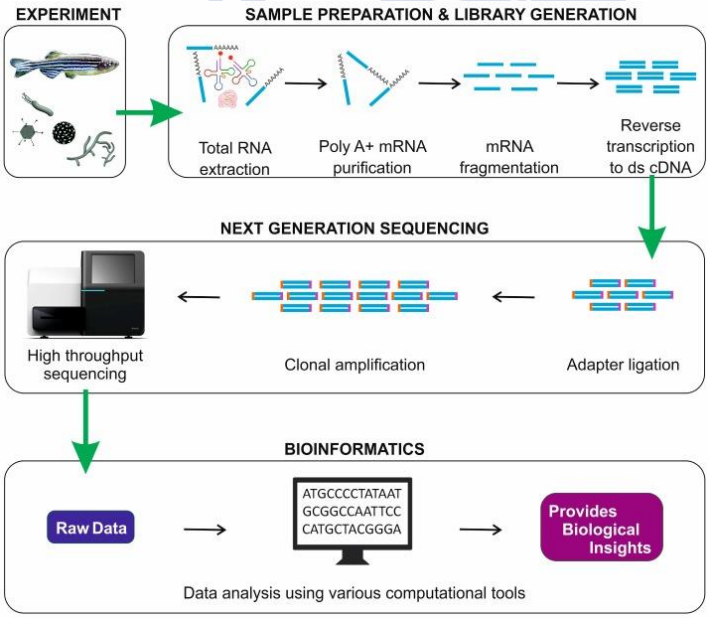

Figure 1.5. Illustration demonstrating the stepwise workflow of a conventional RNA-Seq based transcriptome analysis. Four major steps are involved: Experimental design, Sample preparation and library generation, Next-generation sequencing of the library, Bioinformatic analysis (Sudhagar et al., 2018).

Several studies have used RNA-Seq to understand the effects of NNV via the transcriptome profiling of *in vitro* infected cells and also *in vivo* infected organisms. Such investigations have been performed in grouper kidney cells (GK cell line) (Lu et al., 2012), Asian sea bass epithelial cells (SB cell line) (Liu et al., 2016), European sea bass leukocytes (Chaves-Pozo et al., 2017), striped snakehead fish cells (SSN-1 cell line) (Chen et al., 2017) and European sea bass brain cells (DLB-1 cell line) (Chaves-Pozo et al., 2019). The *in vivo* effect of NNV has also been analysed by RNA-Seq in the brain of sevenband grouper (Kim et al., 2017), pooled brain/eye and head kidney samples from *Senegalese sole* (Labella et al., 2018), the brain of Malabar grouper (Tso and Lu, 2018), and the liver, spleen and kidney of *Epinephelus moara* (Wang et al., 2019). However, the *in vivo* response of European sea bass remained almost completely unexplored by the use of NGS technology.

1.4.2. Long noncoding RNA (lncRNA)

Only a small proportion of the genome is transcribed into protein-coding mRNAs, there are numerous long noncoding RNAs (lncRNAs), functional RNA molecules that are generally not translated into proteins (Yao et al., 2019). The lncRNAs represent a subset of noncoding RNAs (ncRNAs) with a length over 200 nucleotides and transcribed in the same way as mRNA (Poting et al., 2009). However, lncRNAs are among the least well-understood ncRNAs. This is probably due to the variety of regulatory mechanisms that they could affect (Poting et al., 2009), but also to their rapid evolution, and consequently, to the absence of recognizable homologs for most of the lncRNAs even in evolutionarily close species (Hezroni et al., 2015; Perry and Ulitsky, 2016), and to the divergent subcellular location and function of certain conserved lncRNAs (Guo et al., 2020). LncRNAs regulate the expression of adjacent genes (*cis*-acting regulation) or genes located at other genomic locations, even on different chromosomes (*trans*-acting) (Poting et al., 2009) (Figure 1.6).

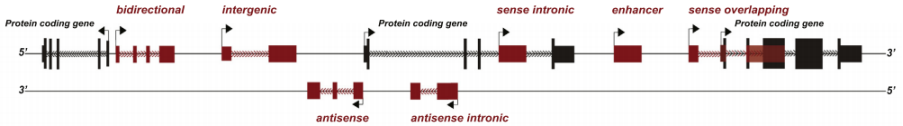

Figure 1.6. Classification of lncRNA. Positional classifications of lncRNAs based on their genomic location in respect to nearby protein coding genes: bidirectional, intergenic, antisense, antisense intronic, sense intronic, enhancer, sense-overlapping (Robinson et al., 2020).

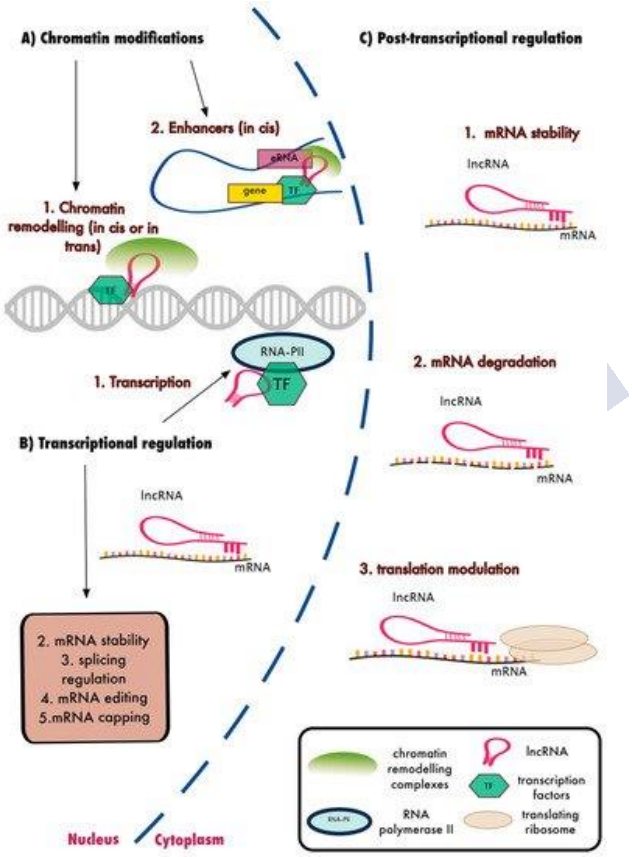

Figure 1.7. Biological functions of lncRNAs. LncRNAs were shown to interact with protein coding genes and their transcripts to regulate gene expression. **A** Nuclear lncRNAs interact with chromatin remodelling factors and transcription factors to regulate the expression of neighbouring or distal genes. **B** Nuclear lncRNAs also regulate transcription and several other transcriptional events of RNA processing. **C** Cytoplasmic lncRNAs were shown to interfere with post-transcriptional regulation such as mRNA stability and degradation as well as translational regulation of mRNAs (Hadjicharalambous and Lindsay, 2019).

The gene expression promotion or repression mediated by lncRNAs can be conducted through different mechanisms, including chromatin remodelling, promoter inactivation, transcription interference, activation and/or transport of transcription factors and epigenetic regulation (Poting et al., 2009) (Figure 1.7). This wide variety of potential regulatory mechanisms makes it difficult to establish concrete functions for specific lncRNAs. Nevertheless, lncRNAs have been demonstrated to be involved in immune system regulation in mammals (Aune and Spurlock, 2016; Elling et al., 2016). In fish, although functional studies remain highly limited, several publications reported the modulation of lncRNAs after different stimuli and/or conditions with a special focus on the immune system (Guo et al., 2020). Because lncRNAs can alter the expression of their adjacent genes, the functionality of those lncRNAs identified in fish is usually predicted based on the function of their neighbouring protein-coding genes (Wang et al., 2018).

1.5. REFERENCES

APROMAR, Asociación Empresarial de Acuicultura en España (2020) Informe de la acuicultura en España (online).

Aune TM, Spurlock CF (2016) Long non-coding RNAs in innate and adaptive immunity. *Virus Research* 212:146-160.

Bagni M (2015) Cultured aquatic species information programme, *Dicentrarchus labrax*. FAO *Fisheries Division* (online).

Bakopoulos V, Volpatti D, Adams A, Galeotti M, Richards R (1997) Qualitative differences in the immune response of rabbit, mouse and sea bass, *Dicentrarchus labrax* L., to *Photobacterium damsela* subsp *piscicida*, the causative agent of fish Pasteurelosis. *Fish and Shellfish Immunology* 7(3):161-174.

Bandín I, Souto S (2020) Betanodavirus and VER disease: A 30-year research review. *Pathogens* 9:106.

Bellance R, Gallet de Saint-Aurin D (1988) L'encéphalite virale du loup de mer. *Caraïbes Medical* 105-144.

Bengtén E, Quiniou S, Hikima J, Waldbieser G, Warr GW, Miller NW, Wilson M (2006) Structure of the catfish IGH locus: analysis of the region including the single functional IGHM gene. *Immunogenetics* 58(10):831-844.

Buonocore F, Stocchi V, Nunez-Ortiz N, Randelli E, Gerdol M, Pallavicini A, Facchiano A, Bernini C, Guera L, Scapigliati G, Picchietti S (2017) Immunoglobulin T from sea bass (*Dicentrarchus labrax* L.): molecular characterization, tissue localization and expression after nodavirus infection. *BMC Molecular Biology* 18:8.

Cammilleri G, CostaA, Graci S, Buscemi MD, Collura R, Vella A, Pulvirenti A, Cicero A, Giangrosso G, Schembri P, Ferrantelli V (2018) Presence of *Anisakis pegreffii* in farmed sea bass (*Dicentrarchus labrax* L.) Commercialized in Southern Italy: A first report. *Veterinary Parasitology* 259:13-16.

Chaves-Pozo E, Guardiola FA, Meseguer J, Esteban MA, Cuesta A (2012) Nodavirus infection induces a great innate cell-mediated cytotoxic activity in resistant, gilthead seabream, and susceptible, European sea bass, teleost fish. *Fish and Shellfish Immunology* 33(5):1159-1166.

Chaves-Pozo E, Valero Y, Esteve-Codina A, Gómez-Garrido J, Dabad M, Alioto T, Meseguer J, Esteban MA, Cuesta A (2017) Innate cell-mediated cytotoxic activity of European sea bass leucocytes against nodavirus infected cells: a functional and RNA-seq study. *Scientific Reports* 7(1):15396

Chaves-Pozo E, Bandín I, Olveira JG, Esteve-Codina A, Gómez-Garrido J, Dabad M, Alioto T, Esteban MÁ, Cuesta A (2019) European sea bass brain DLB-1 cell line is susceptible to nodavirus: a transcriptomic study. *Fish and Shellfish Immunology* 1:14–24

Chen SP, Wu JL, Su YC, Hong JR (2007) Anti-Bcl-2 family members, zfBcl-xL and zfMcl-1a, prevent cytochrome c release from cells undergoing betanodavirus-induced secondary necrotic cell death. *Apoptosis* 12(6):1043-4060.

Chen LJ, Su YC, Hong JR (2009) Betanodavirus non-structural protein B1: A novel anti-necrotic death factor that modulates cell death in early replication cycle in fish cells. *Virology* 385(2):444-454.

Chen W, Yi L, Feng S, Liu X, Asim M, Zhou Y, Lan J, Jiang S, Tu J, Lin L (2017) Transcriptomic profiles of striped snakehead fish cells (SSN-1) infected with red-spotted grouper nervous necrosis virus (RGNNV) with an emphasis on apoptosis pathway. *Fish and Shellfish Immunology* 60:346–354.

Chia RJ, Wu YC, Chen JY, Chi SC (2010) Antimicrobial peptides (AMP) with antiviral activity against fish nodavirus. *Fish and Shellfish Immunology* 28(3):434-439.

Dec C, Angelidis P, Baudin-Laurencin F (1990) Effects of oral vaccination against vibriosis in turbot, *Scophthalmus maximus* L., and sea bass *Dicentrarchus labrax* L. *Journal of Fish Diseases* 13(5):369-376.

Doan QK, Vandeputte M, Chatain B, Morin T, Allal F (2017) Viral encephalopathy and retinopathy in aquaculture: a review. *Journal of Fish Diseases* 40(5):717-742.

Dragesco A, Dragesco J, Coste F, Gasc C, Romestand B, Raymond JC, Bouix G (1995) *Philasterides dicentrarchi*, n. sp., (*Ciliophora*, *Scuticociliatida*), a histophagous opportunistic parasite of *Dicentrarchus labrax* (Linnaeus, 1758), a reared marine fish. *European Journal of Protistology*, 31(3):327-340.

Edholm ES, Bengten E, Wilson M (2011) Insights into the function of IgD. *Developmental and Comparative Immunology* 35(12):1309-1316.

Elling R, Chan J, Fitzgerald KA (2016) Emerging role of long noncoding RNAs as regulators of innate immune cell development and inflammatory gene expression. *European Journal of Immunology* 46(3):504-512

Fenner BJ, Thiagarajan R, Chua HK, Kwang J (2006) Betanodavirus B2 is an RNA interference antagonist that facilitates intracellular viral RNA accumulation. *Journal of Virology* 80:85-94.

Fischer U, Utke K, Somamoto T, Köllner B, Ototake M, Nakanishi T (2006) Cytotoxic activities of fish leucocytes. *Fish and Shellfish Immunology* 20(2):209-226.

Flajnik MF, Kasahara M (2010) Origin and evolution of the adaptive immune system. Genetic events and selective pressures. *Nature Reviews Genetics* 11:47-59.

Frerichs GN, Tweedie A, Starkey WG, Richards RH (2000) Temperature, pH and electrolyte sensitivity, and heat, UV and disinfectant inactivation of sea bass (*Dicentrarchus labrax*) neuropathy nodavirus. *Aquaculture* 185:13-24.

Glazebrook JS, Heasman PM, De Beer SW (1990) Picorna-like viral particles associated with mass mortalities in larval barramundi, *Lates calcarifer* Bloch. *Journal of Fish Diseases* 13(3):245-249.

Grove S, Johansen R, Reitan LJ, Press CM, Dannevig BH (2006) Quantitative investigation of antigen and immune response in nervous and lymphoid tissues of Atlantic halibut (*Hippoglossus hippoglossus*) challenged with nodavirus. *Fish and Shellfish Immunology* 218(5):525-539.

Guo CJ, Ma XK, Xing YH, Zheng CC, Xu YF, Shan L, Zhang J, Wang S, Wang Y, Carmichael GG, Yang L, Chen LL (2020) Distinct processing of lncRNAs contributes to non-conserved functions in stem cells. *Cell* 181(3):621-636

Guo YX, Dallmann K, Kwang J (2003a) Identification of nucleolus localization signal of betanodavirus GGNNV protein α. *Virology* 306(2):225-235.

Guo YX, Wei T, Dallmann K, Kwang J (2003b) Induction of caspase-dependent apoptosis by betanodaviruses GGNNV and demonstration of protein α as an apoptosis inducer. *Virology* 308:74-82.

Hadjicharalambous M, Lindsay MA (2019) Long non-coding RNAs and the innate immune response. *Non-coding RNA* 5(2):34.

Hezroni H, Koppstein D, Schwartz MG, Avrutin A, Bartel DP, Ulitsky I (2015) Principles of long noncoding RNA evolution derived from direct comparison of transcriptomes in 17 species. *Cell Reports* 11(7):1110-1122

Iwamoto T, Mise K, Takeda A, Okinaka Y, Mori KI, Arimoto M, Okuno T, Nakai T (2005) Characterization of striped jack nervous necrosis virus subgenomic RNA3 and biological activities of its encoded protein B2. *Journal of Genetic Virology* 86(10):2807-2816.

Johansen R, Needhan JR, Colquhoun DJ, Poppe TT, Smith AJ (2006) Guidelines for health and welfare monitoring of fish used in research. *Laboratory Animals* 40(4):323-340.

Kim JO, Kim JO, Kim WS, Oh MJ (2017) Characterization of the transcriptome and gene expression of brain tissue in Sevenband gouper (*Hyporthodus septemfasciatus*) in response to NNV infection. *Genes* 8(1):31

Kong WG, Yu YY, Dong S, Huang ZY, Ding LG, Cao JF, Dong F, Zhang XT, Liu X, Xu HY, Meng KF, Su JG, Xu Z (2019) Pharyngeal immunity in eartly vertebrates provides functional and evolutionary insight into mucosal homeostasis. *Journal of Immunology* 203(11):3054-3067.

Labella AM, Garcia-Rosado E, Bandín I, Dopazo CP, Castro D, Alonso MC, Borrego JJ (2018) Transcriptomic profiles of *Senegalese sole* infected with nervous necrosis virus reassortants presenting different degree of virulence. *Frontiers in Immunology* 9:1626

Liu P, Wang L, Kwang J, Yue GH, Wong SM (2016) Transcriptome analysis of genes responding to NNV infection in Asian seabass epithelial cells. *Fish and Shellfish Immunology* 54:342–352

López-Muñoz A, Sepulcre MP, García-Moreno D, Fuentes I, Béjar J, Manchado M, Álvarez MC, Meseguer J, Mulero V (2012) Viral nervous necrosis virus persistently replicates in the central nervous system of asymptomatic gilthead seabream and promotes a transient inflammatory response followed by the infiltration of IgM + B

lymphocytes. Developmental and Comparative Immunology 37(3-4):429-437.

Lu MW, Ngou FH, Chao YM, Lay YS, Chen NY, Lee FY, Chiou PP (2012) Transcriptome characterization and gene expression of *Ephinephelus spp* in endoplasmic reticulum stress-related pathway during betanodavirus infection in vitro. *BMC Genomics* 13:651

MAPAMA. Ministerio de Agricultura y Pesca, Alimentación y Medio Ambiente (2017) Informe del mercado de la lubina en España (online).

Munday BL, Kwang J, Moody N (2002) Betanodavirus infections of teleost fish: a review. *Journal of Fish Diseases* 25(3):127-142.

Nakanishi T, Fischer U, Dijkstra JM, Hasegawa S, Somamoto T, Okamoto N, Ototake M (2002) Cytotoxic T cell function in fish. *Developmetal and Compaprative Immunology* 26(2):137-139.

OIE, Office International des Epizooties, World Organization for Animal Health (1995) Diagnostic manual of aquatic animal diseases. *OIE Fish Disease Commission*, Paris.

Overgard AC, Nerland AH, Fiksdal IU, Patel S (2012) Atlantic halibut experimentally infected with nodavirus shows increased levels of T-cell marker and IFNγ transcripts. *Developmental and Comparative Immunology* 37(1):139-150.

Pereiro P, Romero A, Díaz-Rosales P, Figueras A, Novoa B (2016) Nk-lysin, an antimicrobial peptide expressed in fish erythrocytes is involved in antiviral defense. *Fish and Shellfish Immunology* 53:76.

Perry RBT, Ulitsky I (2016) The functions of long noncoding RNAs in development and stem cells. *Development* 143:3882-2894

Piazzon MC, Galindo-Villegas J, Pereiro P, Estensoro I, Calduch-Giner JA, Gómez-Casado E, Novoa B, Mulero V, Sitjá-Bobadilla A, Pérez-Sánchez J (2016) Differential modulation of IgT and IgM upon parassitic, bacterial, viral, and dietary challenges in a perciform fish. *Frontiers in Immunology* 7:637.

Poisa-Beiro L, Dios S, Montes A, Aranguren R, Figueras A, Novoa B (2008) Nodavirus increases the expression of Mx and inflammatory cytokines in fish brain. *Molecular Immunology* 45(1):218-225.

Poting CP, Oliver PL, Reik W (2009) Evolution and functions of long noncoding RNAs. *Cell* 136(4):629-641.

Robinon EK, Covarrubias S, Carpenter S (2020) The how and why of lncRNA function: An innate immune perspective. *BBA – Gene Regulatory Mechanisms* 1863:194419.

Samuelsen OB, Nerland AH, Jorgensen T, Bjorgan Schroder M, Svasand T, Bergh O (2006) Viral and bacterial diseases of Atlantic cod *Gadus morhua*, their prophylaxis and treatment: a review. *Disease of Aquatic Organisms* 71(3):239-254.

Scapigliati G, Buonocore F, Randelli E, Casani D, Meloni S, Zarletti G, Tiberi M, Pietretti D, Boschi I, Manchado M, Martín-Antonio B, Jimenez-Cantizano R, Bovo G, Borghesan F, Lorenzen N, Einer-Jensen K, Adams S, Thompson K, Alonso C, Bejar J, Cano I, Borrego JJ, Alvarez MC (2010) Cellular and molecular immune responses of the sea bass (*Dicentrarchus labrax*) experimentally infected with betanodavirus. *Fish and Shellfish Immunology* 28(2):303-311.

Schneemann A, Ball LA, Delsert C, Hohnson E, Nishizawa T (2005) Nodaviridae. In Virus Taxonomy, Eigth Report of the International Committee on Taxonomy of Viruses; Fauquet CM, Mayo MA, Maniloff J, Desselberger U, Ball LA, Eds.; Elsevier/Academic Press: London, UK.

Su YC, Wu JL, Hong JR (2009) Betanodavirus non-structural protein B2: A novel necrotic death factor that induces mitochondria-mediated cell death in fish cells. *Virology* 385(1):143-154.

Su YC, Reshi L, Chen LJ, Li WH, Chiu HW, Hong JR (2018) Nuclear targeting of the betanodavirus B1 protein via two arginine-rich domains induces G1/S cell cycle arrest mediated by upregulation of p53/p21. *Scientific Reports* 8:3079.

Sudhagar A, Kumar G, El-Matbouli M (2018) Transcriptome analysis based on RNA-Seq in understanding pathogenic mechanisms of diseases and the immune system of fish: A comprehensive review. *International Journal of Molecular Sciences* 19(1):245.

Sunyer JO (2012) Evolutionary and functional relationships of B cells from fish and mammals: insights into their novel roles in phagocytosis and presentation of particulate antigen. *Infectious Disorders - Drug Targets* 12(3):200-212.

Tso CH, Lu MW (2018) Transcriptome profiling analysis of grouper during nervous necrosis virus persistent infection. *Fish and Shellfish Immunol* 76:224-232.

Uribe C, Folch H, Enriquez R, Moran G (2011) Innate and adaptive immunity in teleost fish: a review. *Veterinarni Medicina* 56(10):486-503.

Valero Y, García-Alcázar A, Esteban MA, Cuesta A, Chaves-Pozo E (2015) Antimicrobial response is increased in the testis of European sea bass, but not in gilthead seabream, upon nodavirus infection. *Fish and Shellfish Immunology* 44(1):203-213.

Valero Y, Boughlala B, Arizcun M, Patel S, Fiksdal IU, Esteban MA, De Juan J, Meseguer J, Chaves-Pozo E, Cuesta A (2018) Genes related to cell-mediated cytotoxicity and interferon response are induced in the retina of European sea bass upon intravitreal infection with nodavirus. *Fish and Shellfish Immunology* 74:627-636.

Vandeputte M, Gagnaire PA, Allal F (2019) The European sea bass: a key marine fish model in the wild and in aquaculture. *Animal Genetics* 50(1):195-206.

Wang L, Tian Y, Cheng M, Li Z, Li S, Wu Y, Zhang J, Ma W, Li W, Pang Z, Zhai J (2019) Transcriptome comparative analysis of immune tissues from asymptomatic and diseased *Epinephelus moara* naturally infected with nervous necrosis virus. *Fish and Shellfish Immunolgy* 93:99–107.

Wang M, Jiang S, Wu W, Yu F, Chang W, Li P, Wang K (2018) Non-coding RNAs function as immune regulators in teleost fish. *Frontiers in Immunology* 9:2801

Wang YD, Kung CW, Chen JY (2010) Antiviral activity by fish antimicrobial peptides of epinecidin-1 and hepcidin 1-5 against nervous necrosis virus in medaka. *Peptides* 31(6):1026-1033.

Whyte SK (2007) The innate immune response of finfish - A review of current knowledge. *Fish and Shellfish Immunology* 23(6):1127-1151.

Wu H, Chiu C, Wu J, Gong H, Chen M, Lu M, Hong J (2008) Zebrafish anti-apoptotic protein zfBcl-xL can block betanodavirus protein α-induced mitochondria-mediated secondary necrosis cell death. *Fish and Shellfish Immunology* 24(4):436-449.

Xu Z, Takizawa F, Parra D, Gómez D, Jorgensen LG, LaPatra SE, Sunyer JO (2016) Mucosal immunoglobulins at respiratory surfaces mark an ancient association that predates the emergence of tetrapods. *Nature Communications* 7:10728.

Yao RW, Wang Y, Chen LL (2019) Cellular functions of long noncoding RNAs. *Nature Cell Biology* 21:542-551.

Yu YY, Kong WG, Xu HY, Huang ZY, Zhang XT, Ding LG, Dong S, Yin GM, Dong F, Yu W, Cao JF, Meng KF, Liu X, Fu Y, Zhang XZ, Zhang YZ, Sunyer JO, Xu Z (2019) Convergent evolution of mucosal immune responses at the buccal cavity of teleost fish. *iScience* 19:821-835.

Yoshikoki K, Inoue K (1990) Viral nervous necrosis in hatchery-reared larvae and juveniles of Japanese parrotfish, *Oplegnathus fasciatus* (Temminck & Schegel). *Journal of Fish Diseases* 13(1):69-77.

Zhang YA, Salinas I, Li J, Parra D, Bjork S, Xu Z, LaPatra SE, Barholomew J, Sunyer JO (2010) IgT, a primitive immunoglobulin class specialized in mucosal immunity. *Nature Immunology* 11(9):827-835.

Zhang M, Li M, Sun L (2014) NKLP27: a teleost NK-Lysin peptide that modulates immune response, induces degradation of bacterial DNA, and inhibits bacterial and viral infection. *PLoS One* 9(9):e106543.

Objectives

In the present Doctoral Thesis the following objectives are proposed:

1. To analyse the complete transcriptomic response of the European sea bass (*Dicentrarchus labrax*) after a nodavirus infection. The main target of this virus, the brain, was selected, as well as the head kidney for playing crucial roles in the organization of both immune and stress responses.

2. To identify non-coding regions of the genome that may be modulating in some way the transcriptomic response of sea bass to the virus in brain and head kidney.

3. To study of a new nodavirus vaccine as a search for alternatives to recombinant bacteria expressing viral antigens on their surface (known as spinycterins) and allow for greater safety and efficacy of the nodavirus vaccine.

4. To establish the nodavirus infection in zebrafish (*Danio rerio*) in order to get a new model of the nodavirus disease, exploring different routes of infection, the study of the behavior of larvae and the use of different transgenic fish lines to observe the immune response of fish and the distribution of the virus during infection.

USC
UNIVERSIDADE
DE SANTIAGO
DE COMPOSTELA

Chapter 2

RNA-Seq analysis of European sea bass (*Dicentrarchus labrax* L.) infected with nodavirus reveals powerful modulation stress response

Lama R[1]|, Pereiro P[1],[2], Valenzuela-Muñoz V[2], Gallardo-Escárate C[2], Tort L[3], Figueras A[1], Novoa B[1] (2020) RNA-Seq analysis of European sea bass (*Dicentrarchus labrax* L.) infected with nodavirus reveals powerful modulation of the stress response. Veterinary Research 51:64. doi: 10.1186/s13567-020-00784-y, ISSN: 1297-9716

[1]Institute of Marine Research (IIM), National Research Council (CSIC), Eduardo Cabello, 6, 36208 Vigo, Spain. [2]Laboratory of Biotechnology and Aquatic Genomics, Interdisciplinary Center for Aquaculture Research (INCAR), University of Concepción, P.O. Box 160, Concepción, Chile. [3]Department of Cell Biology, Physiology and Immunology, Autonomus University of Barcelona, 08193 Barcelona, Spain.

USC
UNIVERSIDADE
DE SANTIAGO
DE COMPOSTELA

2. RNA-Seq analysis of European sea bass (*Dicentrarchus labrax* L.) infected with nodavirus reveals powerful modulation stress response

2.1. INTRODUCTION

The causative agent of VER disease is the nervous necrosis virus (NNV), or nodavirus, belonging to family *Nodaviridae*, genus *Betanodavirus*. NNV is a naked, icosahedral, single-stranded, positive-sense RNA virus (Munday et al., 2002). Because of its neurotropic nature, NNV mainly affects the brain and retina of infected fish. When the nervous system of an individual is affected, it manifests very specific symptoms, such as erratic swimming in descending circles, which can cause curvature of the dorsal spine, resulting in a half-moon shaped fish until the time of death. Other described symptoms are exophthalmia, inflated abdomen and anorexia.

Bioinformatic tools allow the in-depth study of the interactions between an infected organism and its pathogen. Several studies have used high-throughput RNA sequencing (RNA-Seq) to understand the effects of NNV via the transcriptome profiling of *in vitro* infected cells (Lu et al., 2012; Liu et al., 2016; Chaves-Pozo et al., 2017; Chen et al., 2017; Chavez-Pozo et al., 2019) and also its *in vivo* effect (Kim et al., 2017; Labella et al., 2018; Tso and Lu, 2018; Wang et al., 2019). However, the *in vivo* response of European sea bass remains almost completely unexplored, and only a small number of publications have reported the modulation or involvement of immune factors in different tissues of *Dicentrarchus labrax* infected with NNV (Poisa-Beiro et al., 2008; Poisa-Beiro et al., 2009; Sarropoulou et al., 2009; Scapigliati et al., 2010; Buonocore et al., 2012; Chaves-Pozo et al., 2012; Novel et al., 2013; Valero et al., 2015; Buonocore et al., 2017). Therefore, the aim of this work was to analyse the complete transcriptome response of European sea bass to NNV infection. As the materials for this study, we

selected the main target organ of this virus, the brain, as well as the head kidney, because it plays crucial roles in the organization of both immune and stress responses. Samples were collected at 24 and 72 h post-infection (hpi), and the transcriptome profiles of the infected and uninfected animals were analysed. Interestingly, the induction of immune genes was practically undetectable, but we observed strong modulation of genes related to the hypothalamic-pituitary-interrenal (HPI) axis. This is the first time that RNA-Seq analysis has shown an interaction between neuroendocrine pathways and the immune system through the HPI axis during nodavirus infection.

2.2. MATERIALS AND METHODS

2.2.1. Fish infection and sampling for RNA-Seq

Healthy juvenile specimens of European sea bass (*Dicentrarchus labrax* L.) were obtained from the facilities of the Estación de Ciencias Mariñas de Toralla (ECIMAT, Universidad de Vigo, Spain) (average body weight of ~ 70 g) or from the Naturix Cantabria hatchery (Cantabria, Spain) (average body weight of ~ 10 g). Prior to the experiments, the fish were acclimatized to the laboratory conditions for 2 weeks; they were maintained in 500-litre fibreglass tanks with a re-circulating saline-water system (total salinity approximately 35 g/L) under a light-dark cycle of 12:12 h at 20-22 °C and were fed daily with a commercial diet. The animals were euthanized via an MS-222 overdose. All the experimental procedures were reviewed and approved by the CSIC National Committee on Bioethics under approval number ES360570202001/16/FUN01/PAT.05/tipoE/BNG.

The viral strain 475-9/99, belonging to the RGNNV genotype, was provided by the Institute Zooprofilattico delle Venize (Italy) after isolation from diseased sea bass (Bovo et al., 1999). The SSN-1 cell line (ECACC 96082808) was grown at 25 °C in Leibovitz's L15-medium (Gibco) supplemented with 10 % heat-inactivated foetal bovine serum (FBS) (Gibco), 1 % L-glutamine (Gibco) and a 1 % penicillin/streptomycin solution (Invitrogen). The virus was propagated in the SSN-1 cell line in the medium described above supplemented with 2 % FBS, with incubation at 25 °C until the cytopathic effect was extensive. The supernatants were harvested and centrifuged to eliminate

cell debris. Clarified supernatants were used in all infections. The viral titre, expressed as $TCID_{50}$/mL (tissue culture infectious dose infecting 50% of inoculated cultures), was determined in 96-well plates according to the endpoint titration procedure (Reed and Müench, 1938).

Sedated specimens of European sea bass (~70 g) were intramuscularly (i.m.) injected with 100 µl of SSN-1 culture medium (control) or with culture medium containing NNV at 10^6 $TCID_{50}$/mL (infected). A total of 9 fish per condition were sampled at 24 and 72 hpi. The same quantity of tissue from 3 animals was pooled, performing 3 biological replicates (3 fish/replicate) per tissue at each sampling point. The brain and head kidney were harvested under RNase-free conditions and stored at -80 °C until RNA isolation.

2.2.2. RNA isolation and high-throughput transcriptome sequencing

RNA extraction was performed with the Maxwell 16 LEV simply RNA tissue kit (Promega). The RNA concentration and purity were measured with a spectrophotometer (ND-1000, Nanodrop Technologies), and RNA integrity was analysed in an Agilent 2100 Bioanalyzer (Agilent Technologies Inc., Santa Clara, CA, USA) according to the manufacturer's instructions. All the samples showed an RIN over 8.0 and were therefore used for Illumina library preparation. Double-stranded cDNA libraries were constructed using the TruSeq RNA Sample Preparation Kit v2 (Illumina, San Diego, CA, USA), and sequencing was performed using Illumina HiSeq 4000 technology at Macrogen Inc., Korea (Seoul, Republic of Korea). The read sequences were deposited in the Sequence Read Archive (SRA) (http://www.ncbi.nlm.nih.gov/sra) under accession number PRJNA589774.

CLC Genomics Workbench v. 11.0.2 (CLC Bio, Aarhus, Denmark) was used for filtration and assembly and to perform the RNA-Seq and statistical analyses. Prior to assembly, the raw data from each sample were trimmed to remove adapter sequences and low-quality reads (quality score limit 0.05). All the high-quality reads were *de novo* assembled in a single file using default parameters (mismatch cost = 2, insert cost = 3, minimum contig length = 200 bp, and similarity = 0.8).

The contigs yielded by this assembly were annotated with the Blast2GO program against the UniProtKB/SwissProt database (http://UniProt.org) with a cutoff E-value of 1E-03.

2.2.3. RNA-Seq analysis

The transcriptome database generated for European sea bass was used as a reference for the various RNA-Seq analyses (mismatches = 2, length fraction = 0.8, similarity fraction = 0.8). Expression levels were calculated as transcripts per million (TPM) values. To determine statistically significant differences, a proportion-based statistical analysis was conducted using Baggerly's test and adjusting p-values by the false discovery rate (FDR) correction. Contigs showing a fold change (FC) > 2 in the absolute value in relation to the control group and an FDR < 0.05 were selected as differentially expressed genes (DEGs). Heat maps were constructed by plotting the $\log_2$ values of the normalized TPM values and were hierarchically clustered by estimating Manhattan distances with an average linkage criterion. Finally, functional annotation was performed at the online site DAVID 6.8 (https://david.ncifcrf.gov/) to conduct Gene Ontology (GO) enrichment and KEGG pathway analyses using the UniProtIDs of our DEG lists. For the GO and KEGG analyses, a p-value < 0.05 was employed.

2.2.4. NNV detection and RNA-Seq validation

cDNA synthesis from the sequenced samples was performed with the NZY First-Strand CDNA Synthesis Kit (NZYtech) using 0.1 µg of total RNA. The qPCR assays were performed using specific primers, and their efficiencies were previously tested according to the method described by Pfaffl (2001). Individual qPCR assays were conducted in a 25-µL reaction volume including 12.5 µL of SYBR GREEN PCR Master Mix (Applied Biosystems), 10.5 µL of ultrapure water (Sigma-Aldrich), 0.5 µL of each specific primer (10 µM) and 1 µL of cDNA template. All reactions were performed in technical triplicates in a 7300 Real-Time PCR System thermocycler (Applied Biosystems) with an initial denaturation step (95 °C, 10 min), followed by 40 cycles of a denaturation step (95 °C, 15 s) and a singly hybridization-elongation step (60 °C, 30 s). Relative gene expression was calculated via the Pfaffl

method and using *18S ribosomal RNA* (*18S*) as a reference gene. Fold units were calculated by dividing the normalized expression values of the different samples by the normalized expression values obtained in the controls.

To detect viral replication, a 203-bp PCR product from the NNV coat protein gene (RNA2) was chosen for its specificity and the absence of PCR artefacts or primer dimers (Kuo et al., 2011).

Twelve genes that were significantly modulated in the brain or head kidney were chosen for the validation of the RNA-Seq results. The sequences of the primers used for NNV detection and RNA-Seq validation are listed in Table 2.1. Additionally, a biological validation was conducted in an independent experiment. For this, ten sea bass (~ 50 g) were i.m. injected with 100 µL of SSN-1 culture medium (control) or with culture medium containing NNV at 10^6 $TCDI_{50}$/mL (infected). Five individual brain samples were taken at 24 and 72 hpi. Three genes that were significantly modulated in the RNA-Seq data were selected for qPCR analysis.

2.2.5. Cortisol implants and nodavirus challenge

A cortisol implant was prepared by dissolving cortisol in coconut oil (Sigma-Aldrich) at a final concentration of 50 µg cortisol/g body weight (Morgan and Iwama, 1996). Juvenile sea bass (~10 g) were anaesthetized, intraperitonealy (i.p.) injected with 100 µL of the cortisol implant or the vehicle alone (coconut oil), and then i.m. injected with 100 µL of an NNV suspension at 2 x 10^4 $TCID_{50}$/mL (infected) or the culture medium alone (control). The mortality of each group (two replicates of 20 fish each) was recorded.

In parallel, forty fish were divided into 4 tanks (10 fish/tank) and each group was inoculated as mentioned above for the survival experiment. Brain samples were collected at 24 and 72 hpi from each group (n = 5 individuals). The total brain was homogenized and half of the tissue was used for RNA isolation and the other half for protein extraction. RNA was used to analyse by qPCR the replication of the virus and the expression of two genes that were significantly modulated according to the RNA-Seq results: the immune gene encoding IgM (*ighm*), and the gene encoding the stress hormone prolactin (*prl*).

The remaining tissue was used for IgM detection via an enzyme-linked immunosorbent assay (ELISA). Frozen samples were homogenized in 400 µL of buffer containing 150 mM NaCl, 10 mM Tris-HCl, 1 mM EGTA, 1 mM EDTA (pH 7.4), 1 % Triton X-100, 0.5 % NP40-IGEPAL, 1x Halt phosphatase inhibitor cocktail (Sigma-Aldrich) and 1x protease inhibitor cocktail (Sigma-Aldrich). The tubes were kept on ice throughout the process to prevent protein denaturation. The homogenates were centrifuged at 1,000 *g* for 15 min at 4 °C, and the supernatants were centrifuged again at 20,000 *g* for 30 min at 4 °C. The resulting supernatants were recovered and stored at -80 °C. The concentration of protein in each sample was determined using a NanoDrop ND-1000 spectrophotometer. Protein extracts were diluted in 20 mM Tris-HCl (pH 4) at a proportion of 1 µg per 50 µL, and this volume was dispensed into each well of a 96-well flat-bottom high-binding plate (Costar), which was then incubated overnight (O/N) at 37 °C. A 100-µl volume of an 8 % non-fat dry milk solution in each well was used for blocking at room temperature (RT) for 4 h. Then, the wells were washed three times with distilled water. For the detection of the protein, 50 µl of a solution of the anti-IgM monoclonal antibody (Aquatic Diagnostics Ltd) diluted 1:33 in ELISA buffer (0.5 % BSA, 0.01 % Tween 20, 0.005 % phenol red and 10 % PBS in distilled water; pH 7) was added to the wells, followed by incubation for 2 h at RT and then washing three times with distilled water. The same volume of ELISA buffer alone at the same concentration was used as a negative control. A 50-µL volume per well of a goat anti-mouse IgG antibody labelled with horseradish peroxidase (HRP) (Sigma) diluted 1:500 in ELISA buffer was applied as the secondary antibody for the detection of the specific IgM-primary antibody interaction, followed by incubation for 45 min at RT. After three washes, 100 µL of the 1-Step Ultra TMB-ELISA solution (Thermo Scientific) was added to each well. The reaction was stopped with 2 N H_2SO_4, and the optical density was measured at 450 nm with a spectrophotometer (Labsystems iEMS Reader MF). The intensity of the control signal was subtracted from the intensity of the signal obtained with the anti-IgM antibody. These values were directly proportional to the amount of IgM protein present in each well.

Table 2.1. Sequence of the primer pairs used in this experiment.

Primer name	Direction	Primer sequence
B2 Bradykinin receptor (*bdkrb2*)	Forward	5'-AGA ACT GCC AGC ACC AGA GT-3'
	Reverse	5'-TTT TCA GCT TCA TCA TCC CC-3'
Leukocyte cell-derived chemotaxin-2 (*lect2*)	Forward	5'-ATT GCA GAG CTG ACC GAA CT-3'
	Reverse	5'-CCT CAG TGT GAC AGC AGG AA-3'
Prolactin (*prl*)	Forward	5'-TCC CCT CAG AGT CAA GCT GT-3'
	Reverse	5'-CAT CAG CCA GGA CAG GAT TT-3'
Fructose-bisphosphate aldolase A (*aldoa*)	Forward	5'-GGT GAA GGA CTT GCC ATC AT-3'
	Reverse	5'-CAC TGA GGA GAA CAG GAG GC-3'
Sacsin (*sacs*)	Forward	5'-GAA GCA GTT GAA GAC CCT CG-3'
	Reverse	5'-TCC ACA CGT CAA CAC CCT AA-3'
DNA damage-inducible transcript 4-like protein (*ddit4l*)	Forward	5'-CTT TCG TCC TCC GAC AAG AC-3'
	Reverse	5'-CAT GGA GCA AAC TCA GAC CA-3'
Cholesterol side-chain cleavage enzyme mitochondrial (*cyp11a1*)	Forward	5'-AGT GGT CCA TTT GTT CTG GC-3'
	Reverse	5'-TCA AAC CGT GTG ATC CTC AA-3'
Steroid 11-beta-hydroxylase (*cyp11b1*)	Forward	5'-CTG GTG CTC CAG CCT TAG AC-3'
	Reverse	5'-CAC CCC TCC TCT CCT CTA CC-3'
Steroid 17-alpha-hydroxylase/17.20 lyase (*cyp17a1*)	Forward	5'-AAA GAT TCA CCG ACG CAG AC-3'
	Reverse	5'-CCT GTT CAA CCC AGA TCG TT-3'
Steroid 21-hydroxylase (*cyp21*)	Forward	5'-CAC AGT CCA GTT CAG CCA GA-3'
	Reverse	5'-TCG CAA CAC AGA AGA TGG AG-3'
Steroidogenic acute regulatory protein mitochondrial (*StAR*)	Forward	5'-GAG GGA CGA GGA AAA ACA CA-3'
	Reverse	5'-GCT CGA CAG TGG AAG GAA AG-3'
Calreticulin (*calr*)	Forward	5'-GCC CTG GTT GTT GAA GTC AT-3'
	Reverse	5'-GGT GGA ATC CAA GCA CAA GT-3'
Immunoglobulin M (*igmh*)	Forward	5'-GAG CTG CAG AAG GAC AGT G-3'
	Reverse	5'-TCA GAC TGG CCT CAC AGC T-3'
Coat protein NNV	Forward	5'-GAC GCG CTT CAA GCA ACT C-3'
	Reverse	5'-CGA ACA CTC CAG CGA CAC AGC A-3'
18S sea bass	Forward	5'-GTT CCG ACC ATA AAC GAT GC-3'
	Reverse	5'-GAG GTT TCC CGT GTT GAG TC-3'

2.2.6. Respiratory burst activity determined by chemiluminescence assays

To verify the capacity of the infected cells to produce ROS, we analysed the burst activity of kidney leukocytes during *in vitro* and *in vivo* infections. For the *in vitro* assay, cell suspensions were collected under sterile conditions in L15 medium 1x and subjected to forced passage through a 100 µm nylon mesh. The obtained head kidney cell suspensions were layered over a 51 % Percoll (GE Healthcare) density gradient and centrifuged at 400 *g* for 30 min at 4 °C. After centrifugation, the band of leukocytes above the Percoll-medium interface was collected with a Pasteur pipette, washed twice with L15 and centrifuged at 400 *g* for 10 min at 4 °C. The cell pellet was resuspended in L15 supplemented as the SSN-1 medium. The cells were counted and adjusted to a concentration of 10^6 cells/mL. The cell suspensions were distributed in 96-well opaque white plates with a flat bottom and low evaporation lid (Falcon), and infected (or not) with NNV (10^4 $TCID_{50}$/mL) for 1, 24, 48 and 72 h before ROS production measurement. For the *in vivo* assay, animals (~10 g) were i.m. infected (or not) with NNV (10^4 $TCID_{50}$/mL), and at 1 and 5 days post-infection (dpi), head kidney samples were taken, and leukocytes were collected as described above, then plated in opaque white plates.

The emission of relative luminescence units (RLU) was determined after the stimulation of the cells with phorbol myristate acetate (PMA, Sigma-Aldrich) and amplified by the addition of 5-amino-2,3-dihydro-1,4-phthalazinedione (Luminol, Sigma-Aldrich). A stock solution of 0.1 M luminol was prepared in dimethyl sulfoxide (DMSO, Sigma-Aldrich) just before use. Luminol was diluted in PBS (Gibco) to obtain a working solution with a final concentration of 10-4 M. The PMA stock (1 mg/mL in DMSO) was also diluted in the luminol working solution to obtain a final concentration of 1 µg/mL. The working solutions of luminol either alone or in combination with PMA were added to the wells, and the generation of chemiluminescence was measured after 5 min in a luminometer (Fluoroskan Ascent, Labsystems). Four biological replicates and triplicate wells were assayed.

2.2.7. Inactivation of NNV using hydrogen peroxide

Hydrogen peroxide (H_2O_2) has been used to study the effect of ROS produced during viral infection on NNV replication. A 30 % stock solution of H_2O_2 (Perhydrol, Merck) was sterilized by filtration through a 22 µm-pore filter and kept in a dark sealed container. The viral suspension (10^4 $TCID_{50}$/mL) was treated with the H_2O_2 solution at a final concentration of 3 % and incubated for 5 or 24 h at 4 °C. To stop the reaction and remove residual H_2O_2, the viral suspensions were treated twice with 12.5 U/mL of catalase from bovine liver (Sigma-Aldrich) for 10 min at RT. Viral suspensions without H_2O_2 treatment were incubated under the same conditions and served as a control for the infection, and aliquots of H_2O_2-catalase treated medium were also included as a control for the treatment. Then, SSN-1 cells seeded in 24-well plates were inoculated with these suspensions (4 wells per condition) and incubated at 25 °C for 72 h. After this period, viral replication was analysed by qPCR.

2.2.8. Intracellular calcium measurement with FLUO-4 AM

For *in vitro* experiments, SSN-1 cells were distributed in 24-well plates, infected with NNV and incubated at 25 °C for 24, 72 and 96 h. Noninfected controls were also included. For *in vivo* experiments, fish were injected with NNV (10^4 $TCID_{50}$/mL) or culture medium, and at 1 and 5 dpi, primary cell cultures of the brain were obtained (4 biological replicates per condition and sampling point). The entire brain was sampled; the meninges were completely removed by dissection; and the brain was finally collected in Hanks' Balanced Salt Solution without calcium chloride or magnesium sulphate (HBSS, Sigma-Aldrich), washed three times and subjected to forced passage through an 80 µm nylon mesh. The obtained cell suspension was centrifuged at 300 g for 10 min at 4 °C. The cell pellet was resuspended in L15 supplemented as the SSN-1 medium. The brain cells were counted and adjusted to a concentration of 10^6 cells/mL.

For both experiments, cells were washed with PBS and loaded with 10 µL of FLUO-4 AM (Sigma-Aldrich) diluted in L15 without phenol red (Sigma-Aldrich) to avoid interfering with the fluorescence of the probe. After an incubation period of 2.5 h at 25 °C, the cells were

washed, followed by 45 min of de-esterification. The cells were then counted and resuspended at a concentration of 2×10^5 cells/mL in L15 without phenol red. The cell suspensions were distributed in 96-well plates (Cliniplate-Thermo Scientific) to measure changes in fluorescence with an excitation wavelength of 485 nm and emission wavelength of 538 nm (Fluoroskan Ascent, Labsystems). Each sample was measured in triplicate.

2.2.9. Cell treatment with calcium channel inhibitors and calcium chelators

We used different inhibitors of cellular calcium channels and calcium chelators to study the effect of cytoplasmic calcium on NNV replication and ROS production. As inhibitors of calcium channels, we used thapsigargin (Tg; Sigma-Aldrich), which causes calcium release from the endoplasmic reticulum; carboxyamidotriazole (CAI; Sigma-Aldrich), which is an inhibitor of non-voltage-dependent calcium entry and inhibits mitochondrial calcium import; nitrendipine (Sigma-Aldrich), a calcium entry blocker shown to inhibit the movement of calcium through L-type calcium channels; and verapamil hydrochloride (Sigma-Aldrich), which inhibits calcium movement across cell membranes, both inward and outward. As calcium chelators, we selected the intracellular calcium chelator BAPTA-AM (Sigma-Aldrich) and the extracellular calcium chelator EGTA (Sigma-Aldrich). The final concentrations used for the experiments were as follows: Tg (5 µM), CAI (0.5 µM), nitrendipine (0.5 µM), BAPTA-AM (50 µM), and EGTA (60 µM).

To analyse the effect of the changes in calcium homeostasis on NNV replication, SSN-1 cells were distributed in 24-well plates and pretreated for 2 h with the calcium chelators and pharmacological inhibitors, then washed twice with PBS and infected with NNV for 48 h at 25 °C. Viral replication was analysed by qPCR in 5 biological replicates per treatment.

To determine ROS production in the presence of the calcium chelators, primary cultures of head kidney leukocytes were pretreated for 2 h with the calcium chelators BAPTA-AM and EGTA, washed twice with PBS, and inoculated with NNV (infected) or control medium

(control). ROS production was measured as described above with 8 biological replicates and 3 technical replicates.

2.2.10. Statistical analysis

Kaplan-Meier survival curves were analysed with a log-rank (Mantel-Cox) test. The correlation between the RNA-Seq and qPCR data was analysed by using Pearson's correlation coefficient. For the remaining experiments, the results were represented graphically as the mean + standard error of the mean (SEM), and significant differences were determined using Student's t-test. For the comparisons among different sampling points the significant differences were stablished using one-way ANOVA (poshoc Tukey's multiple comparison test). Statistically significant differences were indicated as ***/### ($0.0001 < p < 0.001$), **/## ($0.001 < p < 0.01$) or */# ($0.01 < p < 0.05$).

2.3. RESULTS

2.3.1. Effects of NNV challenge in juvenile sea bass

European sea bass challenged with NNV began to manifest clinical signs of infection at 8 dpi; these signs mainly consisted of erratic swimming behaviours, such as spiral or whirling swimming, belly-up floating, and laying down at rest. After 12 days, the survival rate of the infected individuals was only 16.5 % (Figure 2.1A). In parallel to this mortality assay, we collected brain and head kidney samples from infected and uninfected animals at 24 and 72 hpi, which were used for RNA-Seq analyses. NNV replication was confirmed by qPCR in these samples, and a time-dependent increase in viral replication was observed in both tissues, whereas the uninfected control samples were negative for the detection of the virus (Figure 2.1B). As expected, higher replication levels were detected in the brain, which is the target tissue of NNV, after 72 h.

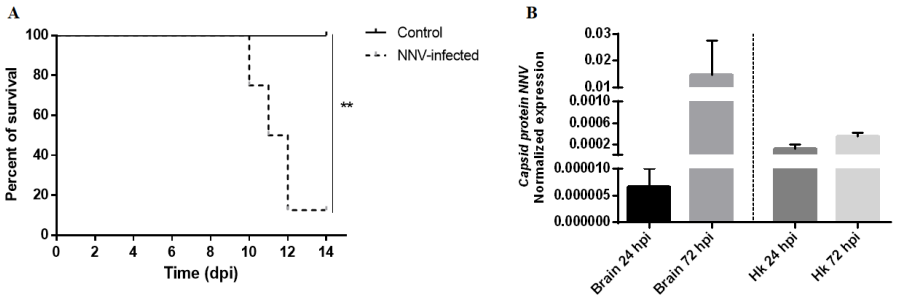

Figure 2.1. Effects of NNV intramuscular infection in juvenile *D. labrax*. **A** Kaplan-Meier survival of NNV-infected and uninfected fish. **B** Replication of NNV at 24 and 72 hpi in brain and head kidney samples. The level of viral replication was measured by qPCR amplification of the gene encoding the NNV capsid protein.

2.3.2. Transcriptome modulation in European sea bass after NNV infection

A summary of the average reads per sample, assembly data and contig annotation is provided in Table 2.2. After adapter trimming and quality filtering of the raw data, an average of 28,044,852.6 high-quality reads per sample were obtained, with a mean length of 101 bp. These reads were *de novo* assembled and yielded a total of 347,317 contigs. Among these contigs, 10.2 % were successfully annotated against the UniProtKB/Swiss-Prot database with an E-value cutoff of 1E-03.

Table 2.2. Summary of Illumina sequencing, assembly and annotation.

Description	Value
Raw data	
Reads per sample	28,044,852.60
Average lenght (bp)	101
Number of samples	24
***De novo* assembly**	
Number of contigs	347,317
Average length (bp)	723
N75 (bp)	453
N50 (bp)	1,088
N25 (bp)	2,851
UniprotKB/swiss-prot blast	
Succesfully annotated contigs (%)	10.2

RNA-Seq analyses were conducted to evaluate transcriptome modulation in the brain and head kidney during infection with nodavirus. Using the obtained data, DEGs between the infected and uninfected fish were identified according to an FC > |2| and FDR < 0.05. As expected, due to the neurotropic nature of the virus, a greater number of DEGs were registered in the brain, which showed 4,062 transcripts that were differentially regulated at 24 hpi and 1,478 at 72 hpi (Figure 2.2A; Supplementary information). On the other hand, only 32 and 76 DEGs were registered in the head kidney at 24 and 72 hpi, respectively (Figure 2.2D; Supplementary information). Both the stacked column chart (Figure 2.2A) and the corresponding heatmap (Figure 2.2B) showed that most of the transcripts that were significantly modulated in the brain at 24 hpi were inhibited by the viral challenge; however, the response seemed to be more equilibrated at 72 hpi (Figure 2.2A-C), which was also observed in the head kidney (Figure 2.2D-F).

GO enrichment analyses were carried out to explore the biological processes that were enriched during infection. In the brain, only four biological processes were significantly enriched at 24 hpi: "calcium ion transmembrane transport", "response to mechanical stimulus", "negative regulation of dendrite morphogenesis" and "positive regulation of plasminogen activation" (Figure 2.3A). However, although the number of DEGs in the brain was lower at 72 hpi, the number of enriched terms was 31 in this case, and many of them were related to ion transport and processes regulated by calcium or mediated by different neurotransmitters or their receptors (Figure 2.3B). In the case of the head kidney, enriched biological processes were only obtained at 24 hpi, with the terms "oxidation-reduction process", "glucocorticoid biosynthetic process" and "sterol metabolic process" being the most enriched (Figure 2.3C).

2.3.3. Modulation of immune-related genes after NNV infection

Whereas almost no typical immune genes seemed to be significantly modulated by viral challenge in the head kidney at the analysed sampling points, some of these genes were differentially expressed in the brain (Table 2.3). At 24 hpi, only 10 immune-related

contigs were modulated by the infection, including the overexpression of a c-type lectin, the chemotaxin *lect2* and the *nktr* receptor of natural killer cells. Interestingly, three relevant immune genes were downregulated at this sampling point: the *immunoglobulin mu chain C region secreted form* (*igmh*), the *stimulator of interferon genes protein* (*sting*) and the *NLR family CARD domain containing 3* (*nlrc3*). After 72 h, the number of immune genes that were modulated by the infection was also low, with the only overexpressed genes being *pentraxin 4* (*ptx4*), *viperin* or *radical S-adenosyl methionine domain-containing protein 2* (*rsad*), *complement component c3* (*c3o*) and *complement c1q tumour necrosis factor-related protein 1* (*c1qt1*) (Table 2.3).

Table 2.3. Immune-related genes significantly modulated in the brain after NNV challenge.

Gene Name	24 hpi	72 hpi
Leukocyte cell-derived chemotaxin 2 (LECT2)	*3.54*	***-4.89***
C-type lectin (TENT)	*3.85*	
T-cell leukemia homeobox protein 3 (TLX3)	*2.47*	
Platelet-derived growth factor receptor (PGFR)	*2.35*	*2.15*
NK-tumor recognition protein (NKTR)	*2.14*	
Eomesodermin (EOMES)	*2.06*	
Probable ATP-dependent RNA helicase DDX17 (DDX17)	*2.01*	
Ig mu chain C region secreted form (IGHM)	***-2.91***	
Stimulator of interferon genes protein (STING)	***-4.13***	
NLR family CARD domain containing 3 (NLRC3)	***-8.7***	
Pentraxin-4 (PTX4)		*13.24*
Radical S-adenosyl methionine domain-containing protein 2 (RSAD2)		*6.25*
Complement component C3 (CO3)		*5.66*
Complement C1q tumor necrosis factor-related protein 1 (C1QT1)		*2.15*
B-cell lymphoma/leukemia 11A (BC11A)		***-2.09***
Semaphorin-4C (SEM4C)		***-2.12***
Nitric oxide synthase, brain (NOS1)		***-2.39***
E3 ubiquitin-protein ligase TRIM39 (TRIM39)		***-2.66***
Platelet glycoprotein V (GPV)		***-3.52***
Leukocyte cell-derived chemotaxin 1 (CNMD)		***-4.88***

Numbers in bold correspond to negative values.

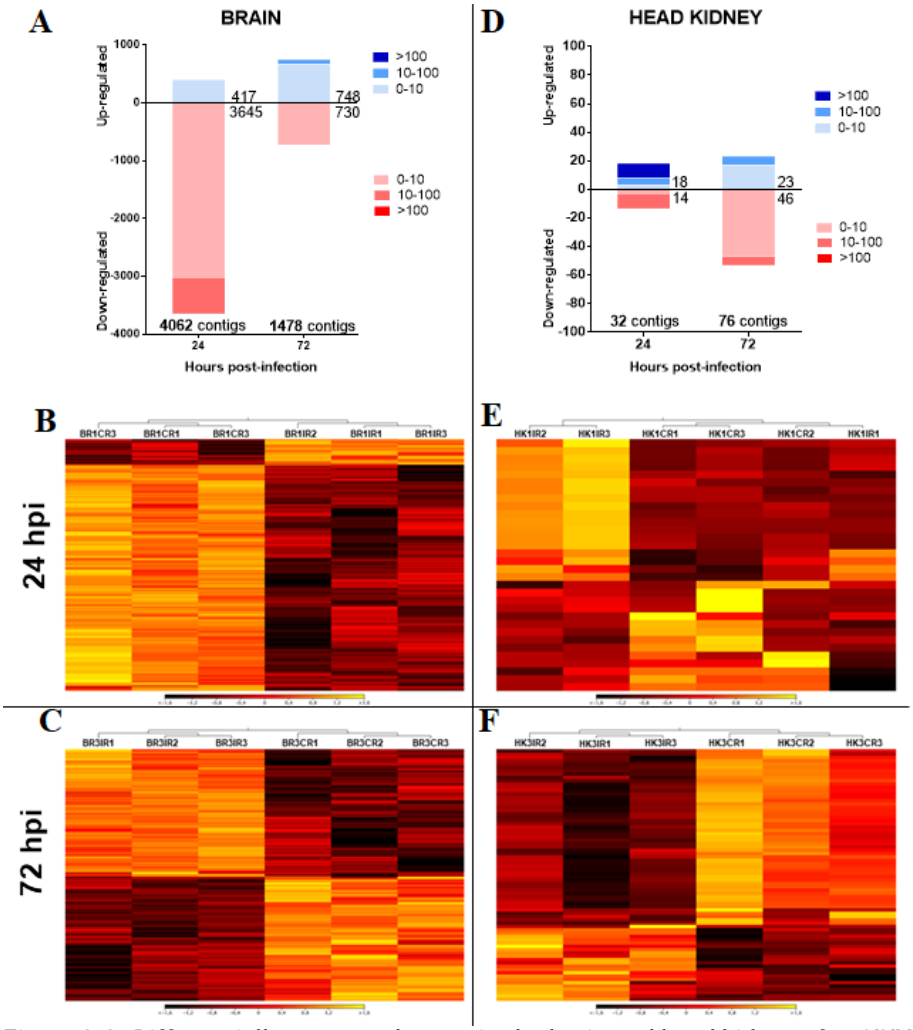

Figure 2.2. Differentially expressed genes in the brain and head kidney after NNV challenge. Stacked column charts reflect the number and intensity of the DEGs identified in the brain **A** and head kidney **D** at 24 and 72 hpi (FC > |2|; FDR < 0.05). Heat maps representing the log_2-transformed TPM expression values of the DEGs at 24 and 72 hpi for the brain **B**, **C** and head kidney **E**, **F**. Colors represent transcript expression ranging from black (less expressed) to yellow (more expressed).

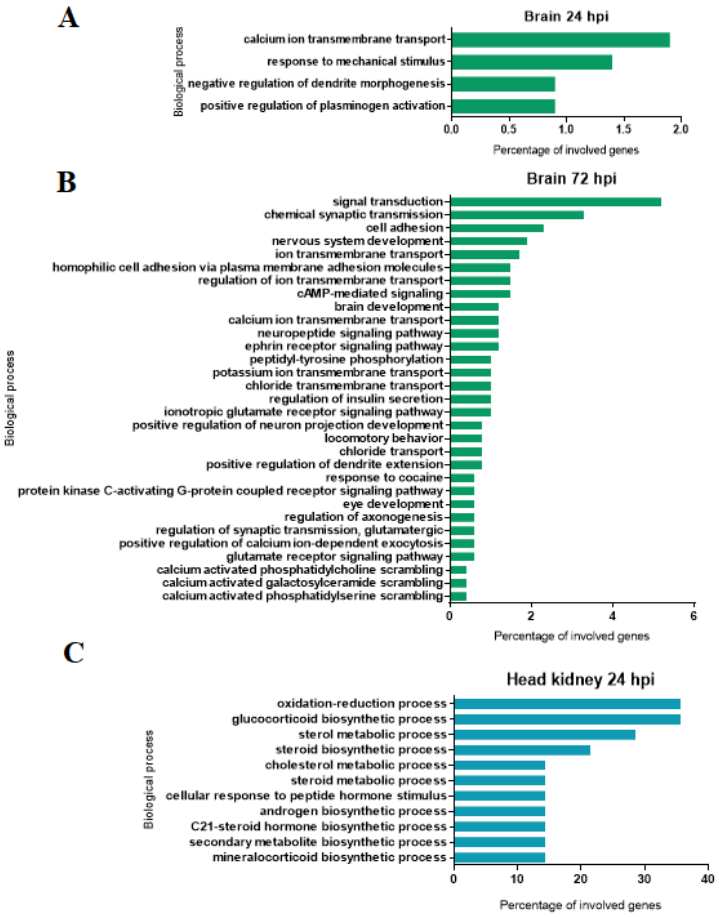

Figure 2.3. GO biological processes enriched in the brain at 24 **A** and 72 hpi **B** and in the head kidney at 24 hpi **C**. No enriched terms were observed for the head kidney at 72 hpi.

2.3.4. Nodavirus induces alterations in the HPI axis

HPI axis modulation in the brain

As reflected in the top 25 modulated contigs identified in the brain (Table 2.4), numerous genes encoding hormones involved in the HPI axis were greatly modulated after NNV infection. These genes corresponded to the pituitary hormones *prolactin* (*prl*), *somatolactin* (*sl*), *somatotropin* (*soma*) or *growth hormone* (*gh*), *gonadotropin* (*glha*), *thyrotropin* (*tsh*) and *pro-opiomelanocortin* (*pomc*), the last of

which encodes the precursor protein of adrenocorticotropic hormone (ACTH). Interestingly, a Venn diagram of the DEGs identified in the brain at 24 and 72 hpi revealed that among the 47 DEGs that were commonly modulated at both sampling points, there were 16 contigs that switched from being downregulated at 24 hpi to upregulated at 72 hpi (Figure 2.4A). These genes included those encoding the pituitary hormones *prl*, *gh*, *glh*, *tsh* and *pomc* (Figure 2.4B). Therefore, from 24 to 72 hpi, there was a complete shift in the expression of these HPI-related genes. On the other hand, only 2 common DEGs between 24 and 72 hpi showed a changed from being upregulated at 24 to downregulated at 72 hpi, which corresponded to *leukocyte cell-derived chemotaxin-2* (*lect2*) and the *glutamate receptor ionotropic nmde2* gene, encoding the neurotransmitter receptor Nmde2 (Figure 2.4C).

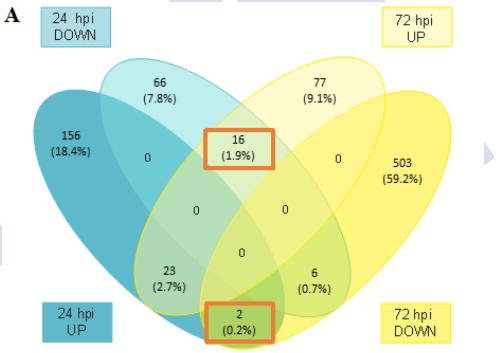

B

	FC 24 hpi	FC 72 hpi
Prolactin (PRL)	-101144.45	4713.60
Somatotropin (SOMA) – Growth hormone (GH)	-2711.84	1332.49
Pro-opiomelanocortin (POMC)	-349.84	13.23
Thyrotropin subunit beta (TSHB)	-172.68	27.90
Gonadotropin alpha chain (GLHA)	-71.08	19.53
Regulator of rDNA transcription protein 15 (RRT15)	-7.20	2.32
LINE-1 retrotransposable element ORF2 protein (LORF2)	-3.75	2.76
Serine protease 48 (PRS48)	-3.61	9.97
Protein quaking-A (QKIA)	-3.51	5.57
Synembryn-A (RIC8A)	-3.19	3.24
LINE-1 retrotransposable element ORF2 protein (LORF2)	-2.97	5.02
WD repeat-containing protein on Y chromosome (WDY)	-2.96	4.43
Receptor-type tyrosine-protein phosphatase F (PTPRF)	-2.92	5.75
LINE-1 retrotransposable element ORF2 protein (LORF2)	-2.70	10.99
Transmembrane protease serine 11F (TM11F)	-2.52	4.03
Transposable element Tcb1 transposase (TCB1)	-2.34	2.57

C

	FC 24 hpi	FC 72 hpi
Leukocyte cell-derived chemotaxin-2 (LECT2)	3.55	-4.89
Glutamate receptor ionotropic, NMDA 2B (NMDE2)	2.65	-3.36

Figure 2.4. Venn diagram of the up- and downregulated DEGs identified in the brain at 24 and 72 hpi. Some contigs showed a reversal of their modulation from upregulated to downregulated, or vice versa, between 24 and 72 hpi.

Table 2.4. Top 25 up- and downregulated DEGs in the brain at 24 and 72 hpi.

Up		Down	
UniProt/SwissProt description	**FC**	**UniProt/SwissProt description**	**FC**
24 hpi			
Hydroxytryptamine receptor 3E (5HT3E5)	51.82	Prolactin (PRL)	-101144.4
Bile acid-CoA:amino acid N-acyltransferase (BAAT)	13.07	Somatolactin (SL)	-13670.06
Actin-related protein 2/3 complex subunit 1A(ARC1A)	12.76	Growth hormone (GH) - Somatotropin (SOMA)	-2711.84
Collagen alpha-1(X) chain (COAA1)	10.87	Gonadotropin subunit beta-2 (GTHB2)	-1896.99
B2 bradykinin receptor (BKRB2)	7.36	O-acyltransferase like protein (OACYL)	-377.22
Deoxyribonuclease-1 (DNAS1)	6.95	Pro-opiomelanocortin (POMC)	-349.84
Deoxyribonuclease-1 (DNAS1)	6.48	Serotransferrin-1 (STF)	-240.04
Alkaline phosphatase, tissue-nonspecific isozyme (PPBT)	6.20	Thyrotropin subunit beta (TSHB)	-172.68
Proline-rich basic protein 1 (PROB1)	4.78	Gonadotropin alpha chain (GLHA)	-71.08
Probable cysteine--tRNA ligase, mitochondrial (SYCM)	4.68	Transmembrane protein 130 (TM130)	-27.42
MAGUK p55 subfamily member 4 (MPP4)	4.34	LINE-1 type transposase domain-containing protein 1 (LITD1)	-18.39
Acidic repeat-containing protein (ACRC)	4.20	Pituitary-specific positive transcription factor 1 (PIT1)	-16.88
Gag-Pol polyprotein (POL)	4.14	Troponin T, fast skeletal muscle isoforms (TNNT3)	-16.50
MICAL-like protein 2 (MILK2)	4.12	Transcription factor COE1 (COE1)	-16.04
Leucine-rich repeat and coiled-coil domain-containing protein 1 (LRCC1)	4.07	Methylmalonyl-CoA mutase, mitochondrial (MUTA)	-15.94
Tetranectin (TETN)	3.86	Gonadotropin subunit beta-1 (GTHB1)	-12.59
ATP-binding cassette sub-family A member 1 (ABCA1)	3.81	LINE-1 reverse transcriptase homolog (LIN1)	-10.49
Oxysterol-binding protein-related protein 11 (OSB11)	3.78	Pituitary homeobox 3 (PITX3)	-10.15

Table 2.4. (continued)

Up		Down	
UniProt/SwissProt description	**FC**	**UniProt/SwissProt description**	**FC**
DNA replication complex GINS protein PSF3 (PSF3)	3.58	Myosin regulatory light chain 2, skeletal muscle isoform type 2 (MLRS)	-9.10
Filamin-C (FLNC)	3.57	NLR family CARD domain containing 3 (NLRC3)	-8.70
Leukocyte cell-derived chemotaxin-2 (LECT2)	3.55	LINE-1 retrotransposable element ORF2 protein (LORF2)	-8.66
Deoxynucleoside triphosphate triphosphohydrolase SAMHD1 (SAMH1)	3.50	UPF0577 protein KIAA1324 (K1324)	-8.58
Protein Largen (LARGN)	3.41	NADH dehydrogenase (NDUFA1)	-7.48
High affinity choline transporter 1 (SC5A7)	3.37	Regulator of rDNA transcription protein 15 (RRT15)	-7.20
Cathepsin D (CATD)	3.36	Fructose-bisphosphate aldolase A (ALDOA)	-6.90
72 hpi			
Prolactin (PRL)	4713.6	Myosin regulatory light chain 2, skeletal muscle isoform type 2 (MLRS)	-47.94
Somatotropin (SOMA)	1332.4	Collagen alpha-1(II) chain (CO2A1)	-34.45
Thyrotropin subunit beta (TSHB)	27.90	Transposon Ty3-I Gag-Pol polyprotein (YI31B)	-30.32
Probable cysteine--tRNA ligase, mitochondrial (SYCM)	25.81	Fructose-bisphosphate aldolase A (ALDOA)	-19.98
Gonadotropin alpha chain (GLHA)	19.53	Troponin T, fast skeletal muscle isoforms (TNNT3)	-18.43
Pentraxin-4 (PTX4)	13.24	Sodium channel protein type 4 subunit alpha B (SC4AB)	-14.00
Pro-opiomelanocortin (POMC)	13.23	Sarcoplasmic/endoplasmic reticulum calcium ATPase 1 (AT2A1)	-13.68
LINE-1 retrotransposable element ORF2 protein (LORF2)	10.99	Creatine kinase M-type (KCRM)	-12.46
Serine protease 48 (PRS48)	9.97	Actin, alpha skeletal muscle 2 (ACT2)	-11.73

Table 2.4. (continued)

Up		Down	
UniProt/SwissProt description	**FC**	**UniProt/SwissProt description**	**FC**
Probable E3 ubiquitin-protein ligase HERC4 (HERC4)	8.55	Keratin, type I cytoskeletal 17 (K1C17)	-11.31
Sacsin (SACS)	7.07	Parvalbumin alpha (PRVA)	-10.45
C-X-C motif chemokine 9 (CXCL9)	7.07	Collagen alpha-1(II) chain (CO2A1)	-9.10
Radical S-adenosyl methionine domain-containing protein 2 (RSAD2)	6.63	Keratin, type I cytoskeletal 13 (K1C13)	-8.06
Sacsin (SACS)	6.37	DNA damage-inducible transcript 4-like protein (DDT4L)	-5.60
Receptor-transporting protein 3 (RTP3)	5.81	Receptor-type tyrosine-protein phosphatase F (PTPRF)	-5.58
Receptor-type tyrosine-protein phosphatase F (PTPRF)	5.75	Metabotropic glutamate receptor 8 (GRM8)	-5.54
Complement component C3 (CO3)	5.66	Alpha-1B adrenergic receptor (ADA1B)	-5.46
Protein quaking-A (QKIA)	5.57	Sodium channel protein type 4 subunit alpha B (SC4AB)	-5.30
Inter-alpha-trypsin inhibitor heavy chain H2 (ITIH2)	5.03	Amiloride-sensitive amine oxidase (AOC1)	-5.15
LINE-1 retrotransposable element ORF2 protein (LORF2)	5.02	DNA damage-inducible transcript 4-like protein (DDT4L)	-5.03
Dynein heavy chain 8, axonemal (DYH8)	4.99	Bifunctional heparan sulfate N-deacetylase/N-sulfotransferase 3 (NDST3)	-5.02
Retrovirus-related Pol polyprotein from transposon 412 (POL4)	4.73	Leukocyte cell-derived chemotaxin-2 (LECT2)	-4.89
Inter-alpha-trypsin inhibitor heavy chain H5 (ITIH5)	4.50	Leukocyte cell-derived chemotaxin 1 (CNMD)	-4.89
WD repeat-containing protein on Y chromosome (WDY)	4.43	Feline leukemia virus subgroup C receptor-related protein 2 (FLVC2)	-4.83
Filamin-C (FLNC)	4.37	Sulfotransferase family cytosolic 2B member 1 (ST2B1)	-4.79

Neurotransmitters and their receptors are also involved in the activation and/or deactivation of the HPI axis. Indeed, we observed that a large number and various types of neurotransmitter receptors were modulated during infection with NNV (Table 2.5). In general, although with some exceptions, we observed overexpression of some neurotransmitter receptors at 24 hpi but downregulation at 72 hpi (Table 2.5). Those neurotransmitter receptors that were overexpressed at 24 hpi corresponded to serotonin and glutamate receptors, whereas at 72 h, serotonin and glutamate receptors were mainly inhibited, as were acetylcholine and adrenergic receptors. Although some GABA receptors were slightly inhibited after 72 h, *gbrb1* was overexpressed (FC = 4.26), and it was the most differentially modulated GABA receptor. Among all the modulated receptors, the highest fold change was observed for the serotonin receptor *5-hydroxytryptamine receptor 3E* (*5ht3e*) at 24 hpi, which was overexpressed in infected animals by 52-fold compared to control fish.

Among the enriched GO terms associated with the brain during NNV infection, we also found high representation of terms related to calcium homeostasis (Figure 2.3A, B). Excessive stimulation by neurotransmitters can cause excitotoxicity by increasing the massive influx of calcium ions into cells (Dong et al., 2009). Therefore, a similar pattern to that observed for the neurotransmitters could be expected for the genes encoding calcium transporters. When the DEGs included among the enriched biological processes related to calcium were represented in a heat map, we generally observed the overexpression of the calcium-related genes at 24 hpi (Figure 2.5A), but most of these genes were downregulated at 72 hpi (Figure 2.5B). Based on the KEGG pathway analysis of calcium signaling, we identified the main cellular calcium regulators affected by infection with NNV at both sampling points (Figure 2.5C, D). As expected based on previous observations, at 24 hpi, the changes in gene expression seemed to favour higher levels of calcium in the cytoplasm (overexpression of several calcium import channels), whereas at 72 hpi, the opposite response was observed (downregulation of calcium importers).

Therefore, NNV infection induced strong modulation of genes related to the HPI axis in the brain by affecting the expression of the

genes encoding neurotransmitter receptors, calcium transporters and pituitary hormones. However, the tendencies were mainly opposite between the two sampling points.

Table 2.5. Genes encoding neurotransmitter receptors significantly modulated in the brain after NNV infection.

Type of neutrotransmitter receptor	Receptor or related protein	24 hpi	72 hpi
Serotonin receptors	5-hydroxytryptamine receptor 3E (5HT3E)	51.82	
	5-hydroxytyptamine receptor 5A (5HT5A)		**-3.19**
	5-hydroxytyptamine receptor 1F (5HT1F)		**-2.74**
Glutamate receptors	N-methyl-D-aspartate (NMDA) NMDA1		**-2.35**
	N-methyl-D-aspartate (NMDA) NMDA 2A		**-2.77**
	N-methyl-D-aspartate (NMDA) NMDA 2B	2.65	**-3.36**
	N-methyl-D-aspartate (NMDA) NMDA 2C		2.22
	N-methyl-D-aspartate (NMDA) NMDA 2D		**-2.38**
	A-amino-3-hydroxy-5-methyl-4-isoazolepropionic acid (AMPA) AMPA1 (GluR-1)		**-2.32**
	A-amino-3-hydroxy-5-methyl-4-isoazolepropionic acid (AMPA) AMPA2 (GluR-2)	2.05	
	A-amino-3-hydroxy-5-methyl-4-isoazolepropionic acid (AMPA) AMPA3 (GluR-3)		**-2.68**
	A-amino-3-hydroxy-5-methyl-4-isoazolepropionic acid (AMPA) AMPA4 (GluR-4)		**-2.06**
	2-carboxy-3-carboxymethyl-4-isopropenylpyrrolide (kainate) 5 (GluK5)		**-2.04**
	Metabotropic glutamate receptor 1 (mGluR1)	2.12	
	Metabotropic glutamate receptor 4 (mGluR4)		**-2.14**
	Metabotropic glutamate receptor 5 (mGluR5)		**-3.28**

Table 2.5. (continued)

Type of neutrotransmitter receptor	Receptor or related protein	24 hpi	72 hpi
Glutamate receptors	Metabotropic glutamate receptor 8 (mGluR8)		**-5.54**
	Vesicular glutamate transporter 1 (VGluT1)	2.03	
	Vesicular glutamate transporter 2.1 (VGL2A)		**-2.24**
	AMPA receptor-interacting protein 1 (GRIP1)		2.10
	Glutamate receptor-interacting protein 2 (GRIP2)	2.01	2.01 & **-2.05**
	Kainate-binding protein. Glutamate receptor U1 (GLRK)	2.06	
	Sodium-dependent glutamate/aspartate transporter 1 (EAA1, GLAST-1)	2.51	**-2.39**
GABA receptors	GABA(A) receptor subunit alpha-2 (GBRA2)		**-2.85**
	GABA(A) receptor subunit alpha-5 (GBRA5)		**-2.63**
	GABA(A) receptor subunit beta-1 (GBRB1)		4.26
	GABA(A) receptor subunit beta-3 (GBRB3)		**-3.07**
	GABA(A) receptor subunit beta-4 (GBRB4)		**-2.41**
	GABA(A) receptor subunit pi (GBRP)		**-2.43**
Acetylcholine receptors	Muscarinic acetylcholine receptor M2 (ACM2)		**-2.14**
	Neuronal acetylcholine receptor subunit alpha-3 (ACHA3)		**-3.14 & -2.70**
	Neuronal acetylcholine receptor subunit alpha-7 (ACHA7)		**-3.24**
Adrenergic receptors	Alpha-1B adrenergic receptor (ADA1B)		**-5.46**
	Alpha-2B adrenergic receptor (ADA2B)		**-2.01**
	Alpha-1Db adrenergic receptor (AA2DB)		**-2.70**

Numbers in bold correspond to negative values.

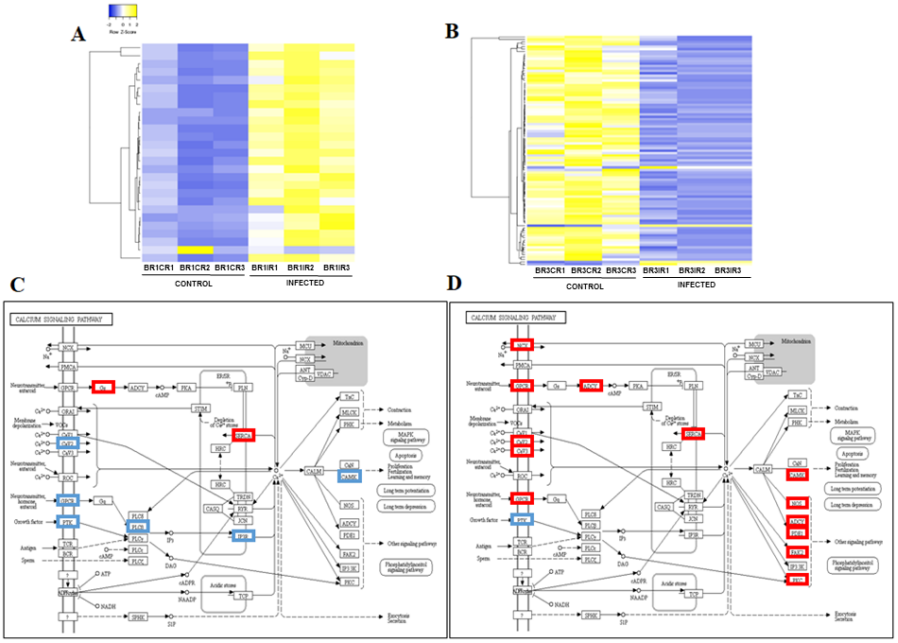

Figure 2.5. Modulation of DEGs related to calcium transport and homeostasis in the brain at 24 and 72 hpi. Heat maps representing the log_2-transformed TPM expression values of the calcium-related contigs at 24 **A** and 72 hpi **B**. Colors represent transcript expression ranging from blue (less expressed) to yellow (more expressed). Representation of the modulation of the calcium signaling KEGG pahtway components according to the RNA-Seq results at 24 **C** and 72 hpi **D**.

HPI axis modulation in the head kidney

ACTH stimulates the production of cortisol, the main stress hormone, by the interrenal cells of the head kidney. When we analysed the effect of NNV in head kidney samples, we found that there were only 17 annotated DEGs at 24 hpi, and most of the upregulated genes encoded enzymes involved in the final steps of the steroid hormone biosynthesis pathway, specifically related to the transformation of cholesterol into cortisol (Table 2.6; Figure 2.6): *cytochrome p450* 11b, *mitochondrial* (*cyp11b1*), *steroidogenic acute regulatory protein, mitochondrial* (*star*), *steroid 21-hydroxylase* (*cyp21a*), *cytochrome p450 17a1* (*cyp17a1*), *3 beta-hydroxysteroid dehydrogenase* (*3bhsd*) and *cholesterol side-chain cleavage enzyme, mitochondrial* (*cyp11a1*). None of these genes were significantly modulated after 72 h.

Table 2.6. Top 25 up- and downregulated DEGs in the head kidney at 24 and 72 hpi.

Up		Down	
UniProt/SwissProt description	**FC**	**UniProt/SwissProt description**	**FC**
24 hpi			
Cytochrome P450 11B, mitochondrial (CP11B)	7007.72	Transcription cofactor vestigial-like protein 4 (VGLL4)	-88.03
Steroidogenic acute regulatory protein, mitochondrial (STAR)	1423.20	Keratin, type I cytoskeletal 13 (K1C13)	-71.73
Cytochrome P450 11B, mitochondrial (CP11B)	453.32	NLR family CARD domain-containing protein 3 (NLRC3)	-64.71
Steroid 21-hydroxylase (CP21A)	349.77	Keratin, type II cytoskeletal 8 (K2C8)	-60.16
Steroid 21-hydroxylase (CP21A)	326.02	Translocase of chloroplast 34 homolog, chloroplastic (TOC34)	-15.80
Steroid 17-alpha-hydroxylase/17,20 lyase (CP17A)	307.93	Carbonic anhydrase 1 (CAH1)	-5.18
Steroid 17-alpha-hydroxylase/17,20 lyase (CP17A)	95.58		
3 beta-hydroxysteroid dehydrogenase/Delta 5 -> 4-isomerase type 1 (3BHSD)	61.79		
Nuclear receptor subfamily 5 group A member 2 (NRSA2)	43.00		
Chemokine-like receptor 1 (CML1)	17.97		
Cholesterol side-chain cleavage enzyme, mitochondrial (CP11A)	4.37		
72 hpi			
Acidic mammalian chitinase (CHIA)	32.07	Contactin-associated protein-like 5 (CNTP5)	-39.47
Transposon Ty3-I Gag-Pol polyprotein (YI31B)	10.35	Elongation factor 1-gamma (EF1G)	-32.60
Myosin-binding protein C, fast-type (MYPC2)	6.51	Phosphoserine aminotransferase (PSAT)	-6.24
Fructose-bisphosphate aldolase A (ALDOA)	5.12	Lanosterol 14-alpha demethylase (CP51A)	-6.08

Table 2.6. (continued)

Up		Down	
UniProt/SwissProt description	**FC**	**UniProt/SwissProt description**	**FC**
Neuronal acetylcholine receptor subunit beta-4 (ACHB4)	2.84	D-3-phosphoglycerate dehydrogenase (3-PGDH)	-5.03
Glyceraldehyde-3-phosphate dehydrogenase (G3P)	2.75	Calreticulin (CALR)	-4.42
Rieske domain-containing protein (RFESD)	2.08	Protein FAM111A (F111A)	-4.16
		Calreticulin (CALR)	-3.74
		Mitochondrial glutamate carrier 1 (GHC1)	-3.43
		Arachidonate 12-lipoxygenase, 12R-type (LX12B)	-3.20
		Ubiquitin carboxyl-terminal hydrolase isozyme L3 (UCHL3)	-3.06
		Fibronectin (FINC)	-3.05
		Argininousuccinate synthase (ASSY)	-3.04
		Quinone oxidoreductase PIG3 (QORX)	-2.88
		Calreticulin (CALR)	-2.76
		Stromal cell-derived factor 2-like protein 1 (SDF2L)	-2.75
		Endoplasmic reticulum chaperone BiP (BiP)	-2.71
		Inositol-3-phosphate synthase 1-A (INO1A)	-2.69
		Protein disulfide-isomerase A6 (PDIA6)	-2.63
		Spermidine synthase (SPEE)	-2.62
		Nuclear mitotic apparatus protein 1 (NUMA1)	-2.49
		Protein disulfide-isomerase A4 (PDIA4)	-2.47
		Rac GTPase-activating protein 1 (RGAP1)	-2.45
		L-lactate dehydrogenase A chain (Ldha)	-2.40
		Histone chaperone asf1b-B (AS1BB)	-2.36

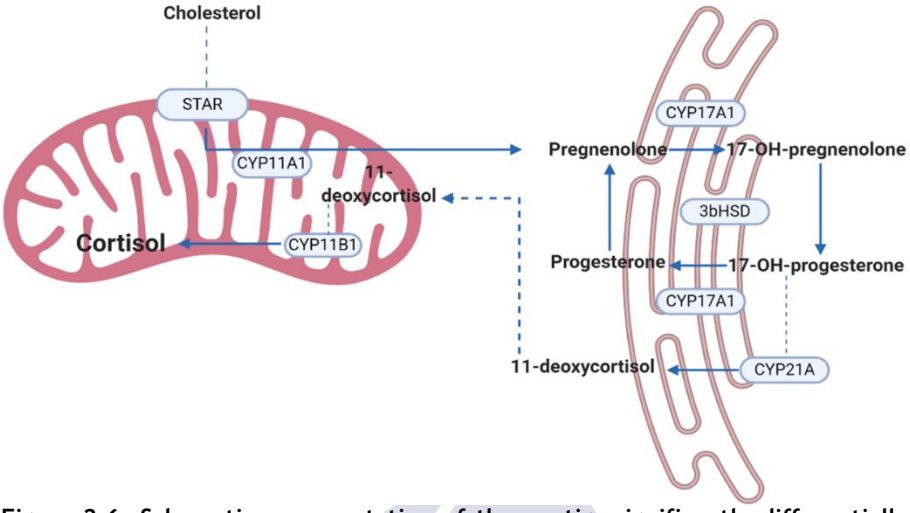

Figure 2.6. Schematic representation of the contigs significantly differentially modulated in the head kidney at 24 hpi with NNV. These DEGs mainly consisted of the genes encoding those enzymes involved in the last steps of cortisol synthesis.

2.3.5. Effect of cortisol on defence against NNV

The modest modulation of immune genes contrasted with the broad, intense changes in the expression of the genes involved in the HPI axis. The individuals carrying the cortisol implant showed a lower survival rate (5.3 %) compared to those inoculated with the vehicle alone (62.9 %) (Figure 2.7A), which was associated with a higher NNV level detected by qPCR at 72 hpi (Figure 2.7B).

Interestingly, cortisol did not significantly affect the expression of the *ighm* gene in the absence or presence of NNV infection (Figure 2.7C). Surprisingly, when the IgM protein content was analysed, higher levels of IgM were detected at 72 hpi in the animals infected with NNV and carrying cortisol implants compared to those infected but injected with the vehicle (Figure 2.7D). Therefore, although our results showed an increase in sea bass susceptibility to NNV with cortisol overload, it seems that this lower resistance was not mediated by IgM synthesis suppression. We also observed higher expression of *prl* associated with the combination of cortisol overload and NNV infection after 72 hpi compared to those animals inoculated with the vehicle and infected with NNV, although due to the high deviation among the samples, differences were not statistically significant (Figure 2.7E).

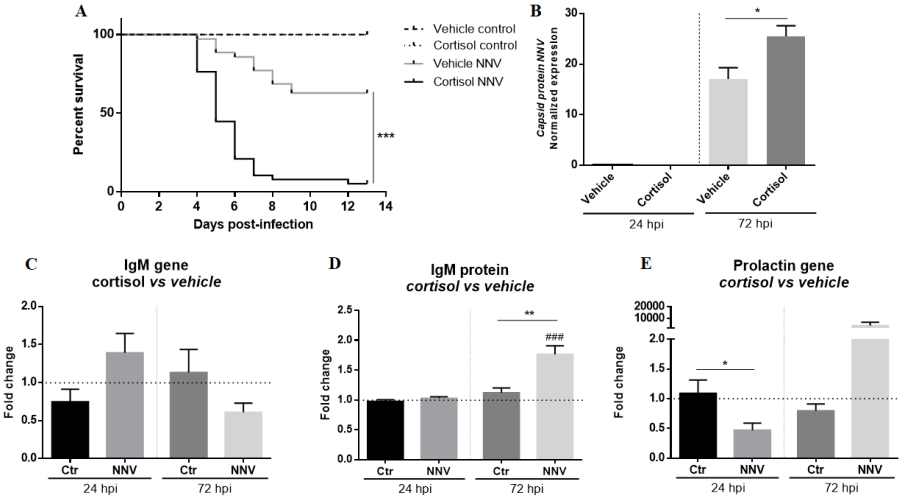

Figure 2.7. Cortisol effects during NNV infection A Kaplan-Meier survival curve representing the higher NNV susceptibility of sea bass carrying intraperitoneal slow-release cortisol implants compared to those inoculated with the vehicle alone. **B** NNV replication in the brain of sea bass carrying the cortisol implants or the vehicle alone (n = 5 individual samples). Viral replication was detected by qPCR amplification of the gene encoding the NNV capsid. **C** Expression of the *ighm* gene in NNV-infected or uninfected fish in the absence or presence of cortisol overload. The data are represented as fold change expression level in those animals carrying cortisol implants compared to those inoculated with the vehicle. **D** Detection of the IgM protein by ELISA in NNV-infected or uninfected fish carrying cortisol implants or the vehicle alone (n = 5 individual samples). The data are represented as fold change of protein abundance in those animals carrying cortisol implants compared to those inoculated with the vehicle. **E** Expression of the *prl* gene in NNV-infected or uninfected fish in the absence or presence of cortisol overload. The data are represented as fold change expression level in those animals carrying cortisol implants compared to those inoculated with the vehicle.

2.3.6. ROS production modulation during NNV infection

Cortisol synthesis involves the production of ROS due to the activity of the steroidogenic cytochrome P450 enzymes (Quinn and Payne, 1984, 1985; Hornsby, 1987). However, at 72 hpi, we observed the downregulation of some genes encoding enzymes implicated in ROS production in the head kidney, including *ero1-like protein alpha* (*ero1a*), *hypoxia-upregulated protein 1* (*hyou1*), *protein disulphide-isomerase a4* (*pdia4*) and *quinone oxidoreductase pig3* (*qorx*). Therefore, we can assume that there was a shift in ROS generation in

the head kidney from 24 to 72 hpi. To better understand the effect of NNV on the production of ROS, we conducted the *in vitro* infection of head kidney cells and measured ROS production at different times post-infection. The results showed that at 1 hpi, there was a significantly higher ROS level in the infected cells (Figure 2.8A). However, after 24 h, ROS production was lower in the infected cells, and this pattern was maintained at 48 and 72 hpi (Figure 2.8A). These data could be explained by the downregulation of *ero1* in the late stages of infection, as the product of this gene is the largest producer of H_2O_2 in the ER (Mennerich et al., 2019). When we analysed the modulation of ROS production *in vivo* at 1 and 5 dpi, we found that ROS production in head kidney cells decreased with the time of infection, showing significant inhibition at 5 dpi compared to the uninfected fish (Figure 2.8B).

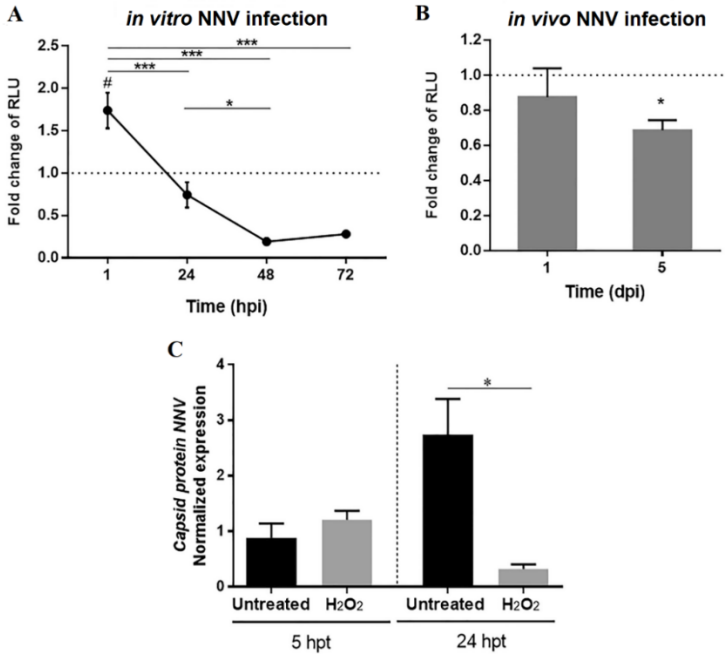

Figure 2.8. Effect of NNV on cellular ROS production and the antiviral activity of oxygen radicals A ROS production by head kidney leukocytes during *in vitro* infection with NNV. The data are represented as the fold change relative luminescence units (RLUs) in the infected samples compared to those of the uninfected cells at each sampling point. Statistically significant differences between NNV-infected and control cells were represented with #, whereas differences along time for the

infected cells were represented with *. **B** ROS detection in head kidney leukocytes at 1 and 5 dpi after *in vivo* infection with NNV. The data are represented as the fold change of the RLUs in the infected fish compared to those measured for the uninfected animals. **C** Replication levels of NNV after treatment with H_2O_2 measured by qPCR amplification of the gene encoding the NNV capsid. hpt: hours post-treatment.

To investigate how the levels of ROS could affect the replication of NNV, we further evaluated the antiviral effects of these radicals by using H_2O_2. We found that when the virus was incubated with H_2O_2 for 5 h, there was no appreciable effect on NNV replication in SNN-1 cells (Figure 2.8C). However, when the treatment was maintained for 24 h, viral replication was significantly reduced compared to that of the non-treated virus (Figure 2.8C).

2.3.7. Calcium modifications interfere with ROS production and NNV replication

We analysed the calcium load within SSN-1 cells during NNV infection by using the fluorescent probe FLUO-4 AM, which is used to measure calcium (Ca^{2+}) concentrations inside living cells. As shown in Figure 2.9A, NNV-infected cells showed a lower Ca^{2+} concentration than uninfected cells at all tested times post-infection (24, 72 and 96 hpi). To further confirm the effect of the modulation of the genes encoding calcium transporters in the brain after NNV challenge, we also infected European sea bass *in vivo*; at 1 and 5 dpi, the brain was sampled, and the tissue was disintegrated to measure the Ca^{2+} concentration. As observed for the SNN-1 cells, the intracellular Ca^{2+}concentration decreased with the time of infection (Figure 2.9B).

We further evaluated how these changes in the cellular Ca^{2+} content in the infected cells could affect ROS production and NNV replication. For this purpose, we treated a primary culture of head kidney cells with BAPTA-AM or EGTA. We observed a significant decrease in ROS production when cells were treated with BAPTA-AM but not with EGTA, indicating that the sequestration of intracellular free Ca^{2+} influences the production of ROS by cells (Figure 2.9C).

If infected cells show alterations in their Ca^{2+} load and in the expression of different Ca^{2+} channels (which in turn affect the production of ROS), the modulation of Ca^{2+} could influence the

replication of the virus. To better understand this effect, we tested different Ca^{2+} channel blockers and Ca^{2+} chelators. When SNN-1 cells were pretreated for 2 h with the channel blocker CAI, thapsigargin and the intracellular Ca^{2+}chelator BAPTA-AM and then infected for 48 h, a significant reduction in the replication of NNV was observed compared to the untreated but infected cells (Figure 2.9D). These results demonstrate that although Ca^{2+} overload could negatively impact NNV replication, the virus requires Ca^{2+} availability.

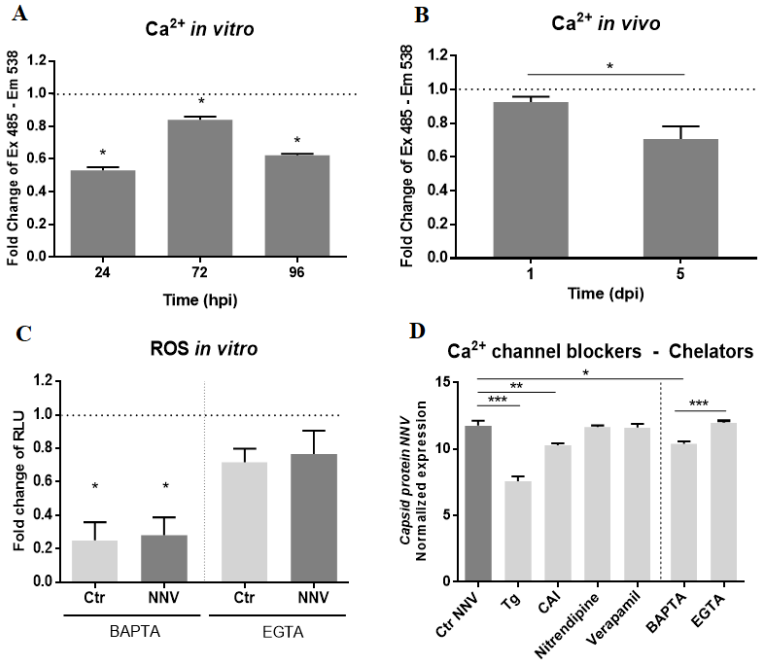

Figure 2.9. Modulation of the intracellular calcium content by NNV infection and the effect of cytoplasmic calcium availability on ROS production and NNV replication. A Intracellular Ca^{2+} measurement with the fluorescent probe FLUO-4 AM in SSN-1 cells during infection with NNV. Values are the fold change of the fluorescence value obtained for the infected cells compared to the uninfected ones. **B** Ca^{2+} content measurement with FLUO-4 AM in brain cells isolated from *in vivo* NNV-infected sea bass and represented as the fold change value compared to the uninfected fish. **C** ROS production detection in head kidney leukocytes after *in vitro* pretreatment with the Ca^{2+} chelators BAPTA-AM and EGTA and with or without NNV infection for 1 h. The data are represented as the fold change compared to untreated and uninfected cells. **D** Replication of NNV in SSN-1 cells after pretreatment with Ca^{2+} channel blockers and chelators and infection with NNV for 48 h. Viral replication was detected by qPCR amplification of the gene encoding the NNV capsid.

2.3.8. Validation of the RNA-Seq results

For the validation of the RNA-Seq results, some of the most differentially regulated genes in each tissue were selected and analysed by qPCR. For the validation of the brain data, *bdkrb2*, *lect2*, *prl*, *aldoa*, *sacs* and *ddit4l* genes were chosen (Figure 2.10A). For validation of the head kidney results, *cyp11a1*, *cyp11b1*, *cyp17a1*, *cyp21a*, *star* and *calr* genes were chosen (Figure 2.10B). The Pearson's correlation coefficient between the RNA-Seq and qPCR data was r = 0.903 (Figure 2.10C). Additionally, the expression of three genes significantly modulated in brain at 24 and 72 hpi (*lect2*, *prl* and *aldoa*) was analysed in an independent experiment composed by 5 individual biological replicates. For this experiment, the Pearson's correlation coefficient between the RNA-Seq and qPCR data was r = 0.835 (Figure 2.10D).

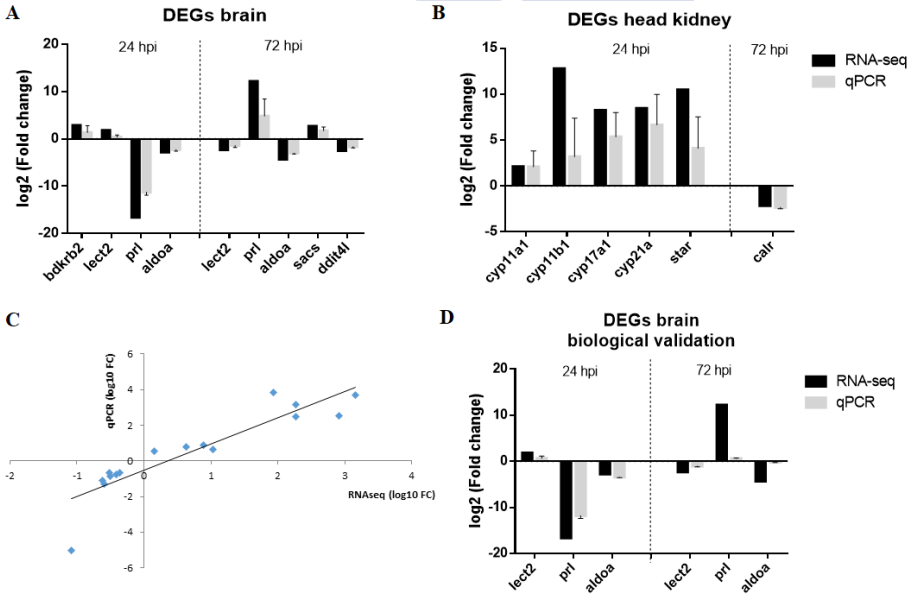

Figure 2.10. Validation of the RNA-Seq results by qPCR. A Comparison of RNA-Seq and qPCR data for genes significantly modulated in brain. **B** Comparison of RNA-Seq and qPCR data for genes significantly modulated in head kidney. C Correlation between the RNA-Seq and qPCR data. **D** Validation of three genes significantly modulated in brain at 24 and 72 hpi in an independent experiment.

2.4. DISCUSSION

NNV exhibits a neurotropic nature and causes damage to the nervous system (brain, retina and spinal cord) of infected fish (Munday et al., 2002). For this reason, understanding how the brain responds to its first contact with the virus is critical for elucidating the antiviral strategies of this immune-privileged organ. The immune-privileged tissue concept suggests the existence of different conditions that help to control the access of pathogens to the CNS but also the exacerbation of inflammation (Forrester et al., 2018). This is why both pro-inflammatory and anti-inflammatory cytokines are overexpressed after stimulation by several types of stressors, including pathogens and vaccines (Khansari et al., 2017). These responses are thought to be an evolutionary adaptation to protect indispensable organs with limited regeneration capacities from uncontrolled inflammation (Benhar et al., 2012). However, some pathogens, such as NNV, can overcome these physiological and immunological barriers and reach the CNS, but circulating immune cells can also migrate to the CNS and, together with resident immune cells, generate a response against the pathogen. A powerful immune response in the brain could lead to severe damage as a consequence of the activated pro-inflammatory mechanisms, whereas the absence of response could allow the persistence and spreading of the pathogen. This situation generates interesting interplay between "fighting" and "tolerance".

Here, we sought to study the response of *D. labrax* to an infection by NNV, one of the most threatening pathogens in the culture of this important commercial fish species. Some previous studies have revealed the overexpression of certain immune genes after *in vivo* or *in vitro* infection with NNV in both European sea bass (Dios et al., 2007; Poisa-Beiro et al., 2008; Poisa-Beiro et al., 2009; Sarropoulou et al., 2009; Scapigliati et al., 2010; Buonocore et al., 2012; Chaves-Pozo et al., 2012; Novel et al., 2013; Valero et al., 2015; Buonocore et al., 2017) and other fish species (Lu et al., 2012; Valero et al., 2015; Liu et al., 2016; Chen et al., 2017; Kim et al., 2017; Tso and Lu, 2018; Wang et al., 2019; Wang et al., 2019) , but the present study is the first to conduct RNA-Seq in *D. labrax* after *in vivo* infection with NNV.

Among the most differentially modulated genes in the brain, we observed high representation of pituitary hormones involved in the HPI axis, which is equivalent to the hypothalamic-pituitary-adrenal (HPA) axis of mammals. The HPI axis is activated under stress conditions and culminates in the secretion of cortisol by interrenal cells (Gorissen and Flik, 2016). Cortisol is the main active corticosteroid in fish (Barton and Iwama, 1991), and its secretion is induced by the release of the ACTH by the pituitary gland. The released ACTH activates the steroidogenic signalling pathway, leading to cortisol secretion as the final product of HPI axis activation (Gorissen and Flik, 2016).

Based on our transcriptome data, this stress response seemed to be activated at 24 hpi but attenuated after 72 h (Figure 2.11). At the earlier sampling point, we found overexpression of the serotonin and glutamate receptors in the brain, both of which are activators of the HPA axis by increasing corticotropin-releasing hormone (CRH) signalling systems (Heisler et al., 2007; Levy and Tasker, 2012). However, we did not observe changes in *crh* gene expression after NNV infection, and even the genes encoding pituitary hormones were downregulated at this point, including *pomc* and, consequently, ACTH levels. The only genes that were differentially modulated in the head kidney were those encoding enzymes involved in the synthesis of cortisol from cholesterol, which is indicative of HPI axis activation (Figure 2.11). Indeed, the downregulation of pituitary hormones could be explained by the negative feedback established between cortisol release and the recurrent synthesis of hypothalamic and pituitary hormones (Gorissen and Flik, 2016). Similar results were observed in the rainbow trout head kidney after treatment with *Vibrio* bacterin (Khansari et al., 2017). Moreover, our results are supported by a recent paper on the effects of vaccine exposure in seabream (*Sparus aurata*). Thus, the gene expression responsiveness of the brain and pituitary to biotic stressors is low compared to the response induced by a physical stressor such as air exposure, meaning that acute abiotic stressors generate a significant neuroendocrine reaction, whereas biotic stressor reactions are modulated in the brain and pituitary (Liu et al., 2019).

The effect of stressors in animals involves a significant allostatic load, i.e., a sudden requirement for energy and resources. This means

that most of the immediately available resources are diverted to stress response mechanisms to cope with the stressor, particularly those related to the initial rapid fight and flight responses (cardiovascular, respiratory, tissue perfusion; see Schreck and Tort, 2016), while more routine metabolic and growth processes are downregulated. Therefore, responses that require a significant amount of energy and take some time, such as some immune responses, are delayed or postponed. This could explain the lack of response of immune genes observed at early time points (24 h) in the present work, as found for the Ig genes. When a stressor lasts longer, regulatory and feedback mechanisms allow other responses to the situation, as occurred after 72 h. This explains why genes related to growth and energetics, such as those encoding prolactin, somatolactin and somatotropin (Table 2.4), were severely downregulated at 24 h but upregulated at 72 h.

Cortisol modulates the immune response by provoking immunosuppression (Yada and Nakanishi, 2002; Tort, 2011). Consequently, we observed the nearly total absence of an immune response at 24 hpi, and some immune-related genes were even downregulated at that time (including the gene encoding IgM), which could also be explained by high cortisol levels. In previous works based on qPCR analysis, overexpression of inflammation and antiviral immune genes was observed both in head kidney and brain from *D. labrax* infected with NNV (Poisa-Beiro et al., 2009; Scapigliati et al., 2010; Chaves-Pozo et al., 2012; Novel et al., 2013). One of the most commonly analysed genes is the type I interferon-stimulated gene *myxovirus resistance gene* (*mx*) (Poisa-Beiro et al., 2009; Scapigliati et al., 2010; Chaves-Pozo et al., 2012; Novel et al., 2013), suggesting the activation of the main antiviral pathway, the type I interferon response. The absence of this response in our RNA-Seq results could be directly conditioned by the high stress response reached in the animals, which at the same time could influence the survival. Pijanowski et al. observed that those common carp (*Cyprinus carpio*) lines more susceptible to bacterial and parasite infection also showed a higher ability to respond to stress, whereas the highly resistant lines showed modest modulation of stress-related factors, revealing a certain potential correlation between stress response and infectious disease susceptibility

(Pijanowski et al., 2015). Based on this, the genetic background of the animals could be conditioning both the stress and the immune response.

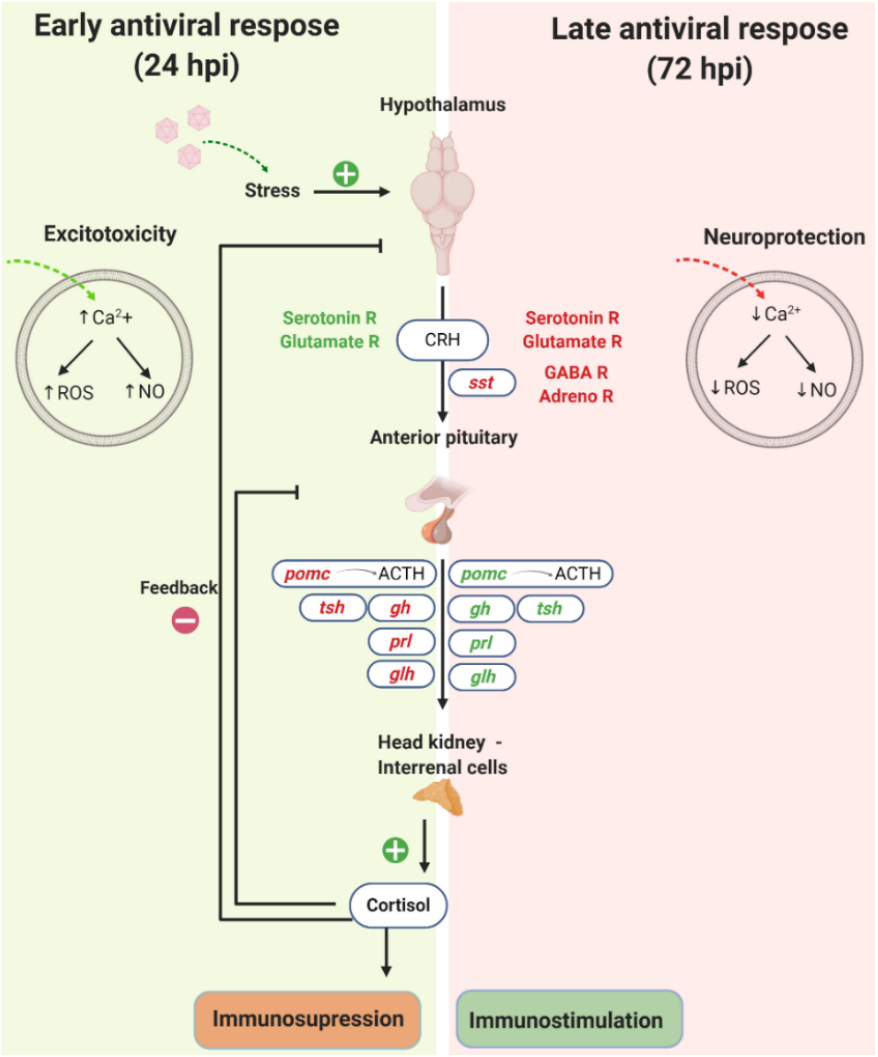

Figure 2.11. Schematic representation of the predicted alterations of the hypothalamic-pituitary-interrenal (HPI) axis after NNV infection and its associated effects based on the transcriptome data. Green indicates genes upregulated according to the RNA-Seq data; red indicates genes downregulated according to the RNA-Seq data (using Biorender.com).

It has been previously suggested that the adaptive immune response is critical in the defence against NNV, even at early times post-infection (Grove et al., 2006; López-Muñoz et al., 2012; Piazzon et al., 2016; Buonocore et al., 2017). Considering this suggestion and the observed overexpression of the genes involved in cortisol synthesis in the head kidney, we further investigated whether cortisol overload increases the susceptibility of European sea bass to NNV. However, although the administration of cortisol implants in the peritoneum increased the susceptibility of European sea bass to NNV, they did not negatively affect the synthesis of IgM. Although, in general terms, stressful conditions or cortisol administration decreased the IgM levels in different teleost species, some exceptions were observed (see Parra et al., 2015). Based on our results and the conclusions by Parra et al., it seems that the regulation of the immune system by the neuroendocrine machinery is more complex than the interaction of cortisol with its receptors, and other components could be involved in the control of the immune response. Indeed, in the present work we observed that at 72 hpi higher IgM levels were found in those animals infected with NNV and carrying the cortisol implants compared to those infected but inoculated with the vehicle, suggesting that the synergy of the two stimuli may have increased IgM synthesis. High prolactin levels have been previously related to IgM synthesis in rainbow trout (*Oncorhynchus mykiss*) (Yada et al., 1999), and we confirmed that *prl* gene expression was also elevated at 72 hpi in the presence of the combination of the cortisol implant+NNV. How the combination of cortisol and NNV infection potentiates the expression of *prl* remains to be elucidated.

The hyperactivation of neurotransmitter receptors, especially glutamate receptors, generates excitotoxicity, which is defined as cell death resulting from the toxic effects of excitatory amino acids (Dong et al., 2009) Prolonged exposure to glutamate generates an excessive influx of Ca^{2+} into neurons, which is highly neurotoxic and results in neuronal degeneration by increasing the production of nitric oxide (NO) and ROS, among other mechanisms (Dong et al., 2009). Indeed, at 24 hpi, the expression of genes involved in Ca^{2+} transport and cellular homeostasis seemed to be directed toward increasing Ca^{2+} levels into

the cytoplasm, and some genes involved in ROS production, such as *ecto-NOX disulphide-thiol exchanger 1* (*enox1*), were also overexpressed (Figure 2.11). As a consequence, the host response at this early point could favour neuronal damage as well as an immunosuppressive status. The high ROS production associated with increased intracellular Ca^{2+} would be harmful to NNV, as shown in the present work. Indeed, whereas physiological levels of intracellular Ca^{2+} are necessary for efficient NNV replication, an excess of Ca^{2+} would be pernicious. Ca^{2+} ions are required for the efficient virion assembly and infectivity of betanodaviruses (Chen et al., 2015). As we also observed in this work, the NNV was able to modulate the ROS production, and this seems to be highly dependent on Ca^{2+} availability. However, ROS production tended to decrease with time. The transcriptome response also completely changed at 72 hpi, most likely as a response to protect neurons from the damage caused by excitotoxicity or to overcome the immunosuppressive effect of cortisol (Figure 2.11). The overexpression of serotonin and glutamate receptors practically disappeared, and some of these receptors were even downregulated at this sampling point. Moreover, the *immunoglobulin superfamily member 11* (*igsf11*) gene, encoding an adhesion molecule implicated in the synaptic stabilization of glutamate receptors (Jang et al., 2016), was inhibited, as was the *glucocorticoid modulatory element-binding protein 1* (*gmeb1*) gene, which produces a protein that increases sensitivity to glucocorticoids (Chen et al., 2002). Interestingly, the most upregulated neurotransmitter receptor in the present study was *gbrb1*, which inhibits HPA axis activation (Chen et al., 2002). Accordingly, three adrenergic receptors that mainly play an excitatory role in the regulation of the HPA axis (Plotsky et al., 1987) were downregulated. As expected, the modulation of cellular Ca^{2+} regulators completely changed after 72 h, and most of the genes encoding Ca^{2+} importers were downregulated. Consequently, the genes encoding the enzymes involved in NO and ROS production were not induced, and even the nitric oxide synthase gene *nos1* was downregulated. It has been previously demonstrated that the inhibition of neuronal nitric oxide synthase protects against excitotoxicity (Schulz et al., 1995).

The genes encoding the hypothalamic hormone *somatostatin* (*sst*) and *somatostatin receptor type 2* (*sstr2*) were inhibited at 72 hpi, which probably led to the overexpression of the pituitary hormone repertoire (Figure 2.11), due to its inhibitory activity in the pituitary gland (Schonbrunn and Koch, 1987). Among the pituitary hormones, prolactin plays a critical stimulatory role in the proliferation of immune cells and the synthesis of immune factors (Constanza et al., 2015) but also acts as a neuroprotective factor by reducing the Ca^{2+} overload induced by an excess of glutamate (Rivero-Segura et al., 2017). As a consequence, the production of NO is inhibited by prolactin (Gonzalez et al., 2004). Additionally, the *pomc* gene is overexpressed at this time point, based on which we might expect an upregulation of the genes involved in the synthesis of cortisol, which were not found to be significantly affected. At the same time, cortisol establishes negative feedback towards pituitary hormones, including ACTH, to control the magnitude of glucocorticoid release (Gorissen and Flick, 2016), which could explain the downregulation of *pomc* at 24 hpi but its higher expression after 72 h. As a consequence of all these modulations, the antiviral response might be more active at this time point, but although some relevant immune genes were overexpressed after 72 hpi of NNV infection, the response was still very discrete. At later sampling points, the antiviral response would most likely be more pronounced. Indeed, in the experiment involving cortisol implants, NNV induced the expression of *ighm* at 72 hpi, but this probably depends on the intensity of infection.

Alterations in the HPA axis have been observed in association with neurotropic and non-neurotropic virus and bacterial infections in mammals and even in association with viral and bacterial components (Webster and Sternberg, 2004; Silverman et al., 2005). However, this is the first time that the modulation of the HPI axis has been described under teleost neurotropic virus infection. Although some of the processes described in this work need to be studied in a more detailed way, it seems that the initial boundless stress response is counteracted by the host. This could be a strategy to reduce the neural damage associated with excitotoxicity and a mechanism for increasing the immune response. Nevertheless, a higher immune response would

increase inflammation due to the activity of pro-inflammatory cytokines, which could be the reason for the high susceptibility of European sea bass to NNV: an equilibrium between the neuroprotective environment and efficient immune response is difficult to achieve. The study of this response in fish species resistant to NNV, such as gilthead seabream (*Sparus aurata*) (Castric et al., 2001), could help to better elucidate this complex interplay.

Supplementary information accompanies this Chapter 2 at https://doi.org/10.1186/s13567-020-00784-y.

Availability of data and materials. The read sequences were deposited in the NCBI Sequence Read Archive (SRA) under accesion number PRJNA589774.

2.5. REFERENCES

Barton BA, Iwama GK (1991) Physiological changes in fish from stress in aquaculture with emphasis on the response and effects of corticosteroids. *Annual Review of Fish Diseases* 1:13-26.

Benhar I, London A, Schwartz M (2012) The privileged immunity of immune privileged organs: the case of the eye. *Frontiers in Immunology* 3:296.

Bovo G, Nishizawa T, Maltese C, Borghesan F, Mutinelli F, Montesi F, De Mas S (1999) Viral encephalopathy and retinopathy of farmed marine fish species in Italy. *Virus Research* 63(1-2):143-146.

Buonocore F, Randelli E, Tranfa P, Scapigliati G (2012) A CD83-like molecule in sea bass (*Dicentrarchus labrax*): molecular characterization and modulation by viral and bacterial infection. *Fish and Shellfish Immunology* 32(6):1179-1184.

Buonocore F, Stocchi V, Nunez-Ortiz N, Randelli E, Gerdol M, Pallavicini A, Facchiano A, Bernini C, Guerra L, Scapigliati G, Picchietti S (2017) Immunoglobulin T from sea bass (*Dicentrarchus*

labrax L.): molecular characterization, tissue localization and expression after nodavirus infection. *BMC Molecular Biology* 18:8.

Castric J, Thiéry R, Jeffroy J, de Kinkelin P, Raymond J (2001) Sea bream *Sparus aurata*, an asymptomatic contagious fish host for nodavirus. *Disease of Aquatic Organisms* 47(1):33-38.

Chaves-Pozo E, Guardiola FA, Meseguer J, Esteban MA, Cuesta A (2012) Nodavirus infection induces a great innate cell-mediated cytotoxic activity in resistant, gilthead seabream, and susceptible, European sea bass, teleost fish. *Fish and Shellfish Immunology* 33:1159-1166.

Chaves-Pozo E, Valero Y, Esteve-Codina A, Gómez-Garrido J, Dabad M, Alioto T, Meseguer J, Esteban MA, Cuesta A (2017) Innate cell-mediated cytotoxic activity of European sea bass leucocytes against nodavirus infected cells: a functional and RNA-seq study. *Scientific Reports* 7:15396.

Chaves-Pozo E, Bandín I, Olveira JG, Esteve-Codina A, Gómez-Garrido J, Dabad M, Alioto T, Esteban MÁ, Cuesta A (2019) European sea bass brain DLB-1 cell line is susceptible to nodavirus: a transcriptomic study. *Fish and Shellfish Immunology* 1:14-24.

Chen J, Kaul S, Simons SS Jr (2002) Structure/activity elements of the multifunctional protein, GMEB-1. Characterization of domains relevant for the modulation of glucocorticoid receptor transactivation properties. *Journal of Biology Chemistry* 277(24):22053-22062.

Chen NC, Yoshimura M, Guan HH, Wang TY, Misumi Y, Lin CC, Chuankhayan P, Nakagawa A, Chan SI, Tsukihara T, Chen TY, Chen CJ (2015) Crystal structures of a piscine betanodavirus: mechanisms of capsid assembly and viral infection. *PLoS Pathogens* 11:e1005203.

Chen W, Yi L, Feng S, Liu X, Asim M, Zhou Y, Lan J, Jiang S, Tu J, Lin L (2017) Transcriptomic profiles of striped snakehead fish cells (SSN-1) infected with red-spotted grouper nervous necrosis virus

(RGNNV) with an emphasis on apoptosis pathway. *Fish and Shellfish Immunology* 60:346-354.

Costanza M, Binart N, Steinman L, Pedotti R (2015) Prolactin: a versatile regulator of inflammation and autoimmune pathology. *Autoimmunity Reviews* 14(3):223-230.

Dios S, Poisa-Beiro L, Figueras A, Novoa B (2007) Suppression subtraction hybridization (SSH) and macroarray techniques reveal differential gene expression profiles in brain of sea bream infected with nodavirus. *Molecular Immunology* 44(9):2195-2204.

Dong XX, Wang Y, Qin ZH (2009) Molecular mechanisms of excitotoxicity and their relevance to pathogenesis of neurodegenerative diseases. *Acta Pharmacologica Sinica* 30(4):379-387.

Forrester JV, McMenamin PG, Dando SJ (2018) CNS infection and immune privilege. *Nature Reviews Neuroscience* 19:655-671.

Gonzalez C, Corbacho AM, Eiserich JP, Garcia C, Lopez-Barrera F, Morales-Tlalpan V, Barajas-Espinosa A, Diaz-Muñoz M, Rubio R, Lin SH, Martinez de la Escalera G, Clapp C (2004) 16K-prolactin inhibits activation of endothelial nitric oxide synthase, intracellular calcium mobilization, and endothelium-dependent vasorelaxation. *Endocrinology* 145(12):5714-5722.

Gorissen M, Flik G (2016) The endocrinology of the stress response in fish: an adaptation-physiological view. *Biology of stress in fish-fish physiology* 35:75-11.

Grove S, Johansen R, Reitan LJ, Press CM, Dannevig BH (2006) Quantitative investigation of antigen and immune response in nervous and lymphoid tissues of Atlantic halibut (*Hippoglossus hippoglossus*) challenged with nodavirus. *Fish and Shellfish Immunology* 21(5):525-539.

Heisler LK, Pronchuk N, Nonogaki K, Zhou L, Raber J, Tung L, Yeo GS, O'Rahilly S, Colmers WF, Elmquist JK, Tecott LH (2007)

Serotonin activates the hypothalamic-pituitary-adrenal axis via serotonin 2C receptor stimulation. *Journal of Neuroscience* 27(26):6956-6964.

Jang S, Oh D, Lee Y, Hosy E, Shin H, van Riesen C, Whitcomb D, Warburton JM, Jo J, Kim D, Kim SG, Um SM, Kwon SK, Kim MH, Roh JD, Woo J, Jun H, Lee D, Mah W, Kim H, Kaang BK, Cho K, Rhee JS, Choquet D, Kim E (2016) Synaptic adhesion molecule IgSF11 regulates synaptic transmission and plasticity. *Nature Neuroscience* 19(1):84-93.

Khansari AR, Parra D, Reyes-López FE, Tort L (2017) Modulatory in vitro effect of stress hormones on the cytokine response of rainbow trout and gilthead sea bream head kidney stimulated with *Vibrio anguillarum* bacterin. *Fish and Shellfish Immunology* 70:736-749.

Kim JO, Kim JO, Kim WS, Oh MJ (2017) Characterization of the transcriptome and gene expression of brain tissue in Sevenband gouper (*Hyporthodus septemfasciatus*) in response to NNV infection. *Genes* 8(1):31.

Kuo HC, Wang TY, Chen PP, Chen YM, Chuang HC, Chen TY (2011) Real-time quantitative PCR assay for monitoring of nervous necrosis virus infection in grouper aquaculture. *Journal of Clinical Microbiology* 49(3):1090-1096.

Labella AM, Garcia-Rosado E, Bandín I, Dopazo CP, Castro D, Alonso MC, Borrego JJ (2018) Transcriptomic profiles of *Senegalese sole* infected with nervous necrosis virus reassortants presenting different degree of virulence. *Frontiers in Immunology* 9:1626.

Levy BH, Tasker JG (2012) Synaptic regulation of the hypothalamic-pituitary-adrenal axis and its modulation by glucocorticoids and stress. *Frontiers in Cellular Neuroscience* 6:24.

Liu P, Wang L, Kwang J, Yue GH, Wong SM (2016) Transcriptome analysis of genes responding to NNV infection in Asian seabass epithelial cells. *Fish and Shellfish Immunology* 54:342-352.

Liu X, Khansari A, Teles M, Martínez-Rodríguez G, Zhang Y, Mancera JM, Reyes-López FE, Tort L (2019) Brain and pituitary response to vaccination in gilthead seabream (*Sparus aurata* L.). *Frontiers in Physiology* 10:717.

López-Muñoz A, Sepulcre MP, García-Moreno D, Fuentes I, Béjar J, Manchado M, Álvarez MC, Meseguer J, Mulero V (2012) Viral nervous necrosis virus persistently replicates in the central nervous system of asymptomatic gilthead seabream and promotes a transient inflammatory response followed by the infiltration of IgM + B lymphocytes. *Developmental and Comparative Immunology* 37(3-4):429-437.

Lu MW, Ngou FH, Chao YM, Lay YS, Chen NY, Lee FY, Chiou PP (2012) Transcriptome characterization and gene expression of *Ephinephelus spp* in endoplasmic reticulum stress-related pathway during betanodavirus infection *in vitro*. *BMC Genomics* 13:651.

Mennerich D, Kelokumpu S, Kietzmann T (2019) Hypoxia and reactive oxygen species as modulators of endoplasmic reticulum and Golgy homeostasis. *Antioxidants and Redox Signal* 30(1):113-137.

Morgan JD, Iwama GK (1996) Cortisol-induced changes in oxygen consumption and ionic regulation in coastal cutthroat trout (*Oncorhynchus clarki clarki*) parr. *Fish Physiology and Biochemisty* 15(5):385-394.

Munday BL, Kwang J, Moody N (2002) Betanodavirus infections of teleost fish: a review. *Journal of Fish Diseases* 25(3):127-142.

Novel P, Fernandez-Trujillo MA, Gallardo-Galvez JB, Cano I, Manchado M, Buonocore F, Randelli E, Scapigliati G, Alvarez MC, Bejar J (2013) Two Mx genes identified in European sea bass

(*Dicentrarchus labrax*) respond differently to VNNV infection. *Veterinary Immunology and Immunopathology* 153(3-4):240-248.

Parra D, Reyes-Lopez FE, Tort L (2015) Mucosal immunity and B cells in teleosts: effect of vaccination and stress. *Frontiers in Immunology* 6:354

Pfaffl MW (2001) A new mathematical model for relative quantification in real-time RT-PCR. *Nucleic Acids Research* 29(9):45.

Piazzon MC, Galindo-Villegas J, Pereiro P, Estensoro I, Calduch-Giner JA, Gómez-Casado E, Novoa B, Mulero V, Sitjà-Bobadilla A, Pérez-Sánchez J (2016) Differential modulation of IgT and IgM upon parasitic, bacterial, viral, and dietary challenges in a perciform fish. *Frontiers in Immunology* 7:637.

Pijanowski L, Jurecka P, Irnazarow I, Kepka M, Szwejser E, Verburg-van Kemenade BML, Chadzinska M (2015) Activity of the hypothalamus-pituitary-interrenal axis (HPI axis) and immune response in carp lines with different susceptibility to disease. *Fish Physiology and Biochemistry* 41(5):1261-1278.

Plotsky PM, Otto S, Sutton S (1987) Neurotransmitter modulation of corticotropin releasing factor secretion into the hypophysial-portal circulation. *Life Sciences* 41(10):1311-1317.

Poisa-Beiro L, Dios S, Montes A, Aranguren R, Figueras A, Novoa B (2008) Nodavirus increases the expression of Mx and inflammatory cytokines in fish brain. *Molecular Immunology* 45(1):218-225.

Poisa-Beiro L, Dios S, Ahmed H, Vasta GR, Martínez-López A, Estepa A, Alonso-Gutiérrez J, Figueras A, Novoa B (2009) Nodavirus infection of sea bass (*Dicentrarchus labrax*) induces up-regulation of galectin-1 expression with potential anti-inflammatory activity. *Journal of Immunology* 183(10):6600-6611.

Reed LJ, Müench H (1938) A simple method of estimating fifty per cent endpoints. *American Journal of Epidemiology* 27(3):493-497.

Rivero-Segura NA, Flores-Soto E, García de la Cadena S, Coronado-Mares I, Gomez-Verjan JC, Ferreira DG, Cabrera-Reyes EA, Lopes LV, Massieu L, Cerbón M (2017) Prolactin-induced neuroprotection against glutamate excitotoxicity is mediated by the reduction of $[Ca^{2+}]i$ overload and NF-κB activation. *PLoS One* 12(5):e0176910.

Sarropoulou E, Sepulcre P, Poisa-Beiro L, Mulero V, Meseguer J, Figueras A, Novoa B, Terzoglou V, Reinhardt R, Magoulas A, Kotoulas G (2009) Profiling of infection specific mRNA transcripts of the European seabass *Dicentrarchus labrax*. *BMC Genomics* 10:157.

Scapigliati G, Buonocore F, Randelli E, Casani D, Meloni S, Zarletti G, Tiberi M, Pietretti D, Boschi I, Manchado M, Martin-Antonio B, Jimenez-Cantizano R, Bovo G, Borghesan F, Lorenzen N, Einer-Jensen K, Adams S, Thompson K, Alonso C, Bejar J, Cano I, Borrego JJ, Alvarez MC (2010) Cellular and molecular immune responses of the sea bass (*Dicentrarchus labrax*) experimentally infected with betanodavirus. *Fish and Shellfish Immunology* 28(2):303-311.

Schreck CB, Tort L (2016) The concept of stress in fish. *Biology of stress in fish-fish physiology* 35:1-34.

Schonbrunn A., Koch B.D. (1987) Mechanisms by which Somatostatin Inhibits Pituitary Hormone Release. In: Reichlin S. (eds) *Somatostatin*. Serono Symposia, USA. Springer, Boston, MA.

Schulz JB, Matthews RT, Jenkins BG, Ferrante RJ, Siwek D, Henshaw DR, Cipolloni PB, Mecocci P, Kowall NW, Rosen BR (1995) Blockade of neuronal nitric oxide synthase protects against excitotoxicity *in vivo*. *Journal of Neuroscience* 15(12):8419-8429.

Silverman MN, Pearce BD, Biron CA, Miller AH (2005) Immune modulation of the hypothalamic-pituitary-adrenal (HPA) axis during viral infection. *Viral Immunology* 18(1):41-78.

Tort L (2011) Stress and immune modulation in fish. *Developmental and Comparative Immunology* 35(12):1366-1375.

Tso CH, Lu MW (2018) Transcriptome profiling analysis of grouper during nervous necrosis virus persistent infection. *Fish and Shellfish Immunology* 76:224-232.

Valero Y, Morcillo P, Meseguer J, Buonocore F, Esteban MA, Chaves-Pozo E, Cuesta A (2015) Characterization of the IFN pathway in the teleost fish gonad against the vertically transmitted nervous necrosis virus. *Journal of General Virology* 96:2176-2187.

Wang L, Tian Y, Cheng M, Li Z, Li S, Wu Y, Zhang J, Ma W, Li W, Pang Z, Zhai J (2019) Transcriptome comparative analysis of immune tissues from asymptomatic and diseased *Epinephelus moara* naturally infected with nervous necrosis virus. *Fish and Shellfish Immunology* 93:99-107.

Webster JI, Sternberg EM (2004) Role of the hypothalamic-pituitary-adrenal axis, glucocorticoids and glucocorticoid receptors in toxic sequelae of exposure to bacterial and viral products. *Journal of Endocrinology* 181(2):207-221.

Yada T, Nagae M, Moriyama S, Azuma T (1999) Effects of prolactin and growth hormone on plasma immunoglobulin M levels of hypophysectomized rainbow trout, *Oncorhynchus mykiss*. *General and Comparative Endocrinology* 115(1):46-52.

Yada T, Nakanishi T (2002) Interaction between endocrine and immune systems in fish. *International Review of Cytology* 220:35-92.

USC
UNIVERSIDADE
DE SANTIAGO
DE COMPOSTELA

Chapter 3

Potential involvement of lncRNAs in the modulation of the transcriptome response to nodavirus challenge in European sea bass (*Dicentrarchus labrax* L.)

Pereiro P[1,2], **Lama R[1]**, Moreira R[1], Valenzuela-Muñoz V[2], Gallardo-Escárate C[2], Novoa B[1], Figueras A[1] (2020) Potential involvement of lncRNAs in the modulation of the transcriptome response to nodavirus challenge in European sea bass (*Dicentrarchus labrax* L.). Biology 9:165. doi: 10.3390/biology9070165, ISSN 2079-7737

[1]Institute of Marine Research (IIM), National Research Council (CSIC), Eduardo Cabello, 6, 36208 Vigo, Spain. [2]Laboratory of Biotechnology and Aquatic Genomics, Interdisciplinary Center for Aquaculture Research (INCAR), University of Concepción, P.O. Box 160, Concepción, Chile.

USC
UNIVERSIDADE
DE SANTIAGO
DE COMPOSTELA

3. Potential involvement of lncRNAs in the modulation of the transcriptome response to nodavirus challenge in European sea bass (*Dicentrarchus labrax* L.)

3.1. INTRODUCTION

In recent years, some publications have reported the involvement of numerous immune factors in the defense against nodavirus in different tissues from *D. labrax* (Poisa-Beiro et al., 2008; Poisa-Beiro et al., 2009; Sarropoulou et al., 2009; Scapigliati et al., 2010; Buonocore et al., 2012; Chaves-Pozo et al., 2012; Novel et al., 2013; Valero et al., 2015; Buonocore et al., 2017). The development of NGS technologies also enabled us to analyse the complete transcriptome response after NNV infection both *in vitro* (Chaves-Pozo et al., 2017; Chaves-Pozo et al., 2019) and, more recently, *in vivo* (Lama et al., 2020). Nevertheless, the potential role of ncRNAs in the modulation of the response to NNV infection in *D. labrax* has not been determined.

The non-coding regions of the genome remained largely unexplored until the last decade. The lncRNAs represent a subset of ncRNAs with a length over 200 nucleotides and transcribed in the same way as mRNA (Poting et al., 2009). However, lncRNAs are among least well-understood ncRNAs. LncRNAs regulate the expression of adjacent genes (*cis*-acting regulation) or genes located at other genomic locations, even on different chromosomes (*trans*-acting) (Poting et al., 2009). In fish, although functional studies remain highly limited, several publications reported the modulation of lncRNAs after different stimuli and/or conditions with a special focus on the immune system (Guo et al., 2020). Because lncRNAs can alter the expression of their adjacent genes, the functionality of those lncRNAs identified in fish is usually predicted based on the function of their neighbouring protein-coding genes (Wang et al., 2018).

In this work, we identified the lncRNA repertoire in the head kidney and brain from European sea bass. We selected these tissues because the head kidney is the main immune and hematopoietic organ in fish and the brain is a target tissue for NNV. Our results showed the existence of tissue-specific lncRNAs, with a specialised role in the maintenance of the basic functions of each tissue, as well as a broad modulation of the lncRNAs after NNV challenge. The functionality of these infection-induced lncRNAs was predicted based on the analysis of their nearby coding genes, revealing a variety of processes in which they could be involved. Because samples were taken at 24 and 72 hpi, we also observed a highly variable lncRNA profile depending on the sampling point, which could be indicative of the fine-tuned gene regulation mediated by these lncRNAs.

3.2. MATERIALS AND METHODS

3.2.1. Fish infection and sampling

Juvenile *D. labrax* (average weight 70 g) were obtained from the Estación de Ciencias Mariñas de Toralla (ECIMAT, Universidad de Vigo, Spain) facilities. Prior to experiments, fish were acclimatized to the laboratory conditions for 2 weeks and maintained in 500 l fiberglass tanks with a re-circulating saline-water system (total salinity approximately 35 g/L) with a light-dark cycle of 12:12 h at 20-22 ˚C and fed daily with a commercial diet. Animals were euthanized via MS-222 (Sigma-Aldrich) overdose (500 mg/L). All the experimental procedures were reviewed and approved by the CSIC National Committee on Bioethics under approval number ES360570202001/20/FUN.01/INM06/BNG01. The nodavirus RGNNV (strain 475-9/99) was propagated at 25 ˚C in the SSN-1 cell line (ECACC 96082808) cultured in L-15 medium (Gibco) supplemented with 2 mM glutamine (Gibco), 2 % FBS (Gibco) and 1 % penicillin/streptomycin solution (Invitrogen). The virus stock was titrated into 96-well plates according to established protocols (Reed and Muench, 1938), and aliquots were stored at -80 ˚C until use.

A total of 18 sea bass were intramuscularly injected with 100 µL of a NNV suspension (10^6 $TCID_{50}$/mL), whereas the same number of fish served as the control and were inoculated with the same volume of

medium (L-15 + glutamine + 2 % FBS + penicillin/streptomycin). Head kidney and brain samples were taken from nine fish at 24 and 72 h post-challenge. The same quantity of tissue from three animals was pooled, obtaining three biological replicates (three fish/replicate) per tissue at each sampling point. For this challenge experiment, mortality data and viral replication analysis in head kidney and brain from infected fish were previously provided (Lama et al., 2020).

3.2.2. RNA isolation and high-throughput transcriptome sequencing

Total RNA from the different samples was extracted using the Maxwell 16 LEV simplyRNA Tissue kit (Promega, Madison, WI, USA) with the automated Maxwell 16 Instrument in accordance with instructions provided by the manufacturer. The quantity and purity of the total RNA was measured in a NanoDrop ND-1000 (NanoDrop Technologies), and RNA integrity was analysed in the Agilent 2100 Bioanalyzer (Agilent Technologies) according to the manufacturer's instructions. All the samples showed an RIN over 8.0; therefore, they were used for Illumina library preparation. Double-stranded cDNA libraries were constructed using the TruSeq RNA Sample Preparation Kit v2 (Illumina, San Diego, CA, USA), and sequencing was performed using Illumina HiSeq™ 4000 technology at Macrogen Inc. Korea (Seoul, Republic of Korea). The read sequences were deposited in the Sequence Read Archive (SRA) (http://www.ncbi.nlm.nih.gov/sra) under the accession number PRJNA589774.

3.2.3. Sequence assembly and lncRNA mining

CLC Genomics Workbench, v. 11.0.2 (CLC Bio) was used to filter, assemble and perform the RNA-Seq and statistical analyses. Raw reads were trimmed to remove adaptor sequences and low-quality reads (quality score limit 0.05). A reference transcriptome was constructed by *de novo* assembly using all the samples with an overlap criterion of 70 % and a similarity of 0.9 to exclude paralogous sequence variants. The settings used were a mismatch cost = 2, deletion cost = 3, insert cost = 3 and minimum contig length = 200 base pairs. From the *de novo* assembly, the selection of the lncRNAs was conducted following the

pipeline previously described (Tarifeño et al., 2017) but with some modifications. Briefly, the contigs were annotated using Blastx (E-value < 1E-5) against the proteins for all the bony fish species included in the NCBI GenBank and UniProt/Swiss-Prot databases. All the annotated contigs were deleted from the assembly, as well as all the contigs with an average coverage < 50. The potential open reading frames (ORFs) were predicted for the remaining contigs, and those with a potential ORF > 200 bp were discarded. After this step, the Coding Potential Assessment Tool (CPAT) (Wang et al., 2013) was used to discard sequences with coding potential. The contigs that passed all the filters were considered putative lncRNAs and retained for further analyses.

3.2.4. Differential expression analysis

RNA-Seq analysis of the putative lncRNAs were conducted with the following settings: mismatches = 2, length fraction = 0.8, similarity fraction = 0.8. The expression values were set as TPM. To identify and quantify the directions of variability in the data, a principal component analysis (PCA) plot was constructed by using the original expression values. Finally, Baggerley's statistical analysis test was used to compare gene expression levels and to identify differentially expressed lncRNAs. Transcripts with absolute FC values > 2 and FDR < 0.05 were retained for further analysis. Those significantly modulated lncRNAs were selected, and the average TMP value of the three biological replicates is represented in heat maps. To this end, the distance metric was calculated by Pearson's method, and lncRNAs were hierarchically clustered by average linkage. Venn diagrams were constructed with the Venny 2.1 tool (http://bioinfogp.cnb.csic.es/tools/venny/).

3.2.5. Genome mapping and identification of lncRNA neighbouring coding genes

To position the putative lncRNAs on the genome, the *D. labrax* genome (Tine et al., 2014), composed of 25 scaffolds, was uploaded into the CLC Genomics Workbench. These scaffolds were constructed based on linkage/radiation hybrid groups (LG1A - LGx), in which approximately 83 % of the contigs were located (Tine et al., 2014). The

remaining unanchored scaffolds were concatenated into a virtual chromosome ('UN') (Tine et al., 2014).

LncRNAs were mapped using the following parameters: length fraction = 0.8, similarity fraction = 0.8, mismatch cost = 2, insertion cost = 3 and deletion cost = 3. The correlation between the chromosome length and the number of mapped lncRNAs per chromosome was calculated with IBM SPSS Statistics V25.0 by using Pearson's correlation coeffcient (r). The coding genes flanking up to 10 kb upstream and downstream from the mapped and differentially expressed lncRNAs for each comparison were identified and selected for Gene Ontology (GO).

3.2.6. GO enrichment analyses

For the significantly differentially expressed lncRNAs in each comparison (Brain 24 h infected vs. Brain 24 h control; Brain 72 h infected vs. Brain 72 h control; HK 24 h infected vs. HK 24 h control; HK 72 h infected vs. HK 72 h control), the lncRNAs-neighbouring coding-genes were extracted for GO enrichment analyses using Blast2GO software (Conesa et al., 2005). For the GO enrichments, Fisher's exact test was run with default settings, a p-value cut-off of 0.01 was applied, and the enriched list was reduced to the most specific GO terms. The most enriched biological processes among the protein coding genes proximal to lncRNAs were represented. When the number of significantly enriched GO terms exceeded 30, only the 30 most significant terms were represented.

3.2.7. Correlation analyses between lncRNAs and coding genes

Correlations in the expression of lncRNAs and their neighbouring genes were calculated by using Pearson's correlation coeffcient and Spearman's rank correlation coeffcient with IBM SPSS Statistics V25.0. Correlations were considered to be significant when p-values were < 0.01. To illustrate the expression correlations, heat maps were illustrated with the free software Heatmapper (Babicki et al., 2016) and the average TPM values of the different experimental conditions and sampling points were normalised by row. The protein–protein

interaction networks were constructed with String 11.0 (https://string-db.org) (Szklarczyk et al., 2019).

3.2.8. qPCR validation of lncRNA expression

cDNA synthesis of the samples was conducted with the NZY First-Strand cDNA Synthesis kit (NZYTech, Lisbon, Portugal) using 0.5 g of total RNA. A total of 12 lncRNAs were used to validate the RNA-Seq results. Specific qPCR primers for the selected lncRNAs were designed using Primer 3 software (Rozen and Skaletsky, 2000), and their amplification effciency was calculated with the threshold cycle (CT) slope method (Pffafl, 2001). Primer sequences are listed in Table 3.1. Individual qPCR reactions were carried out in a 25 µL reaction volume containing 12.5 µL of SYBR GREEN PCR Master Mix (Applied Biosystems), 10.5 µL of ultrapure water, 0.5 µL of each specific primer (10 µM) and 1 µL of two-fold diluted cDNA template in MicroAmp optical 96-well reaction plates (Applied Biosystems). Reactions were conducted using technical triplicates in a 7300 Real-Time PCR System thermocycler (Applied Biosystems). qPCR conditions consisted of an initial denaturation step (95 ˚C, 10 min) followed by 40 cycles of a denaturation step (95 ˚C, 15 s) and one hybridization-elongation step (60 ˚C, 1 min). The relative expression level of the lncRNAs was normalised following the Pfaffl method (Pffafl, 2001) and using *18S ribosomal RNA* (*18S*) as a reference gene.

3.3. RESULTS

3.3.1. Assembly, annotation and lncRNA mining

A summary of the reads, assembly data, contig annotation and lncRNA information is included in Table 3.2. Approximately 680 million reads were obtained from the different samples of European sea bass with an average of 28 million per sample, and over 99 % of raw reads met the quality control standards. From the *de novo* assembly, a total of 347,317 contigs were obtained with an average length of 723 bp. A total of 69 % of the contigs (240,274) were successfully annotated against the bony fish sequences. From the non-annotated contigs (107,043), a total of 12,158 passed all the filters to be considered potential lncRNAs (Supplementary information). The length of these

selected contigs ranged from 200 to 6,829 bp with an average length of 667 bp (Figure 3.1A). The GC content of the predicted lncRNAs ranged from 11 to 80 % with an average value of 38 % (Figure 3.1B).

Table 3.1. Primer pairs used to validate the lncRNA differential expression analysis.

LncRNA	Forward	Reverse
lnc_contig0068337	TTTTCCTGTTGCTCCGTCTT	AGAAACTCCCGCCCATTAGT
lnc_contig0093031	GGGATTTTCCAGAGGAGAGG	ACCACCACAGGTCACAGGTT
lnc_contig0005556	CTCCTGTTCCCTGTCAGCTC	TCACTCTACAGCCGTCACGA
lnc_contig0012669	TGTCACCATTTCAGGCTTCA	GCCACTCCGAAGTGACAAA
lnc_contig0082064	GTGGGGACCCTGTCAAGATA	GTGCTTGAGGAGATTCCAGC
lnc_contig0073426	CAAAGCTGGAACAAAATCTCC	TACACACACGCAGGTATCGG
lnc_contig0066190	GCACGCTGTGTTTTCTTTGA	CAGAGGCTATGCACTGGTCA
lnc_contig0018835	CAGCATCGCTGTCAGATTGT	GATTGGCTGAGGAGATTGGA
lnc_contig0016989	ATCTGACCCAACCCTTCACA	GCCCTTAATTCCATGTTTGC
lnc_contig0024843	CAACAGTGCTGGACTGGCTA	TGTTGGGAATCTTTGCTCCT
lnc_contig0052951	AGCTGATTGGGATGGAAATG	CTTAGGGAGGGCAGTGTCTG
lnc_contig0065271	CGCACAGACTGCAACAGAGT	CAGGAAAGGGGGTAGAGAGG

Table 3.2. Summary of the Illumina sequencing, assembly, annotation and lncRNA identification.

Description	Value
Reads	
Reads per sample	28,044,852.60
***De novo* assembly**	
Number of contigs	347,317
Minimum length (bp)	200
Maximum length (bp)	26,142
Average length (bp)	723
N50 (bp)	1,088
Total assembled reads	215,126,479
Annotation	
Annotated contigs	240,274 (69 %)
Non-annotated contigs	107,043
LncRNAs	
Potential lncRNAs	12,158
Minimum length (bp)	200
Maximum length (bp)	6,829
Average length (bp)	667
LncRNAs mapped on genome	11,667 (95.96 %)

From the 12,158 putative lncRNAs, 95.96% (11,667) were successfully mapped to the *D. labrax* genome (Figure 3.1C). The scaffold with a higher number of lncRNAs was the virtual chromosome 'UN' (2,004 lncRNAs). This finding is most likely due to the greater length of this virtual chromosome compared to the true ones. Indeed, a strong positive correlation (Pearson's r = 0.99) existed between the chromosome length and the number of predicted lncRNAs per chromosome (Figure 3.1D), reflecting that there is no enrichment in lncRNA abundance in any particular chromosome.

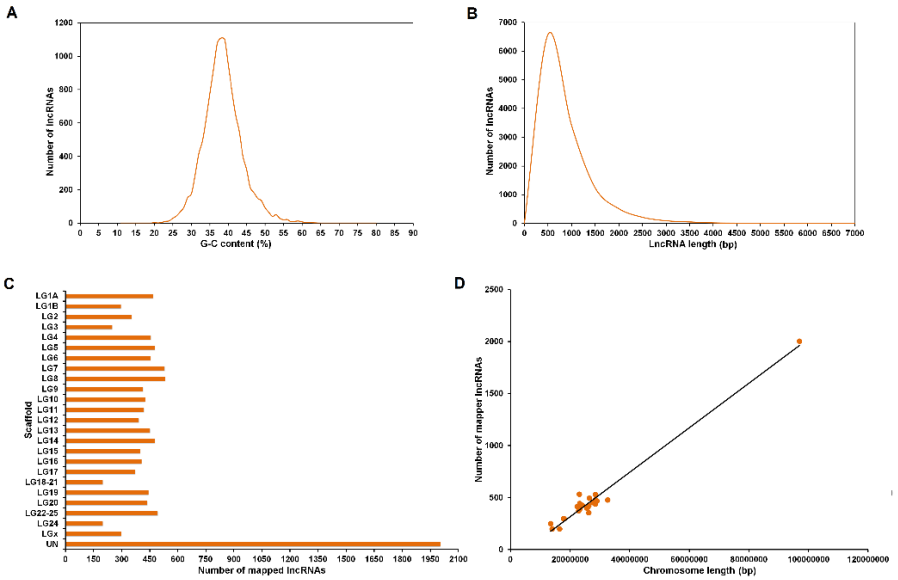

Figure 3.1. Features of predicted lncRNAs in *D. labrax*. **A** Guanine-cytosine (GC) content and **B** length distribution of the 12,158 predicted lncRNAs. **C** LncRNA abundance and localization per chromosome. **D** Correlation between chromosome length and lncRNA abundance.

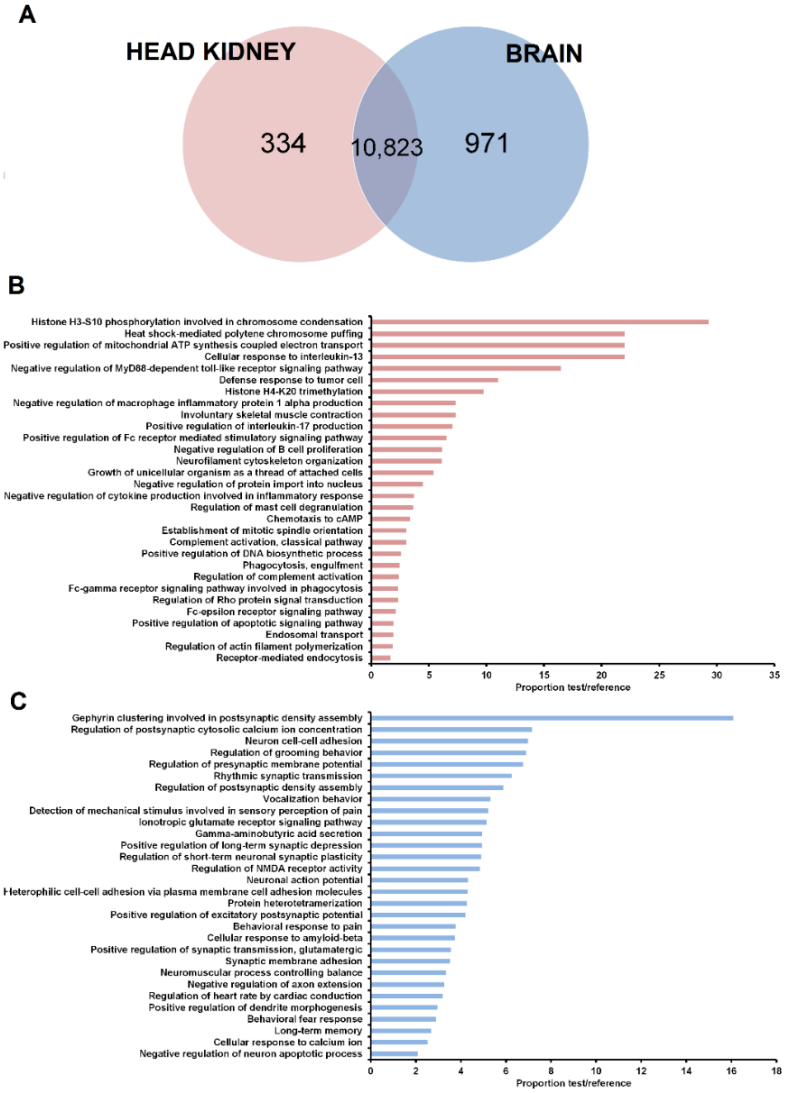

Figure 3.2. LncRNAs identified per tissue. A Venn diagram reflecting the number of lncRNAs with a trasncripts per million (TPM) value in at least one of the samples from each tissue. Most of the predicted lncRNAs were detected in both the head kidney and brain. In contrast, a total of 30 predicted lncRNAs obtained a TPM value of 0 in all the samples. **B, C** The neighbouring coding genes of the lncRNAs expressed in the head kidney but not in the brain **B** and vice versa **C** were analysed by GO enrichment analyses (biological processes). Only the 30 most significant terms were represented.

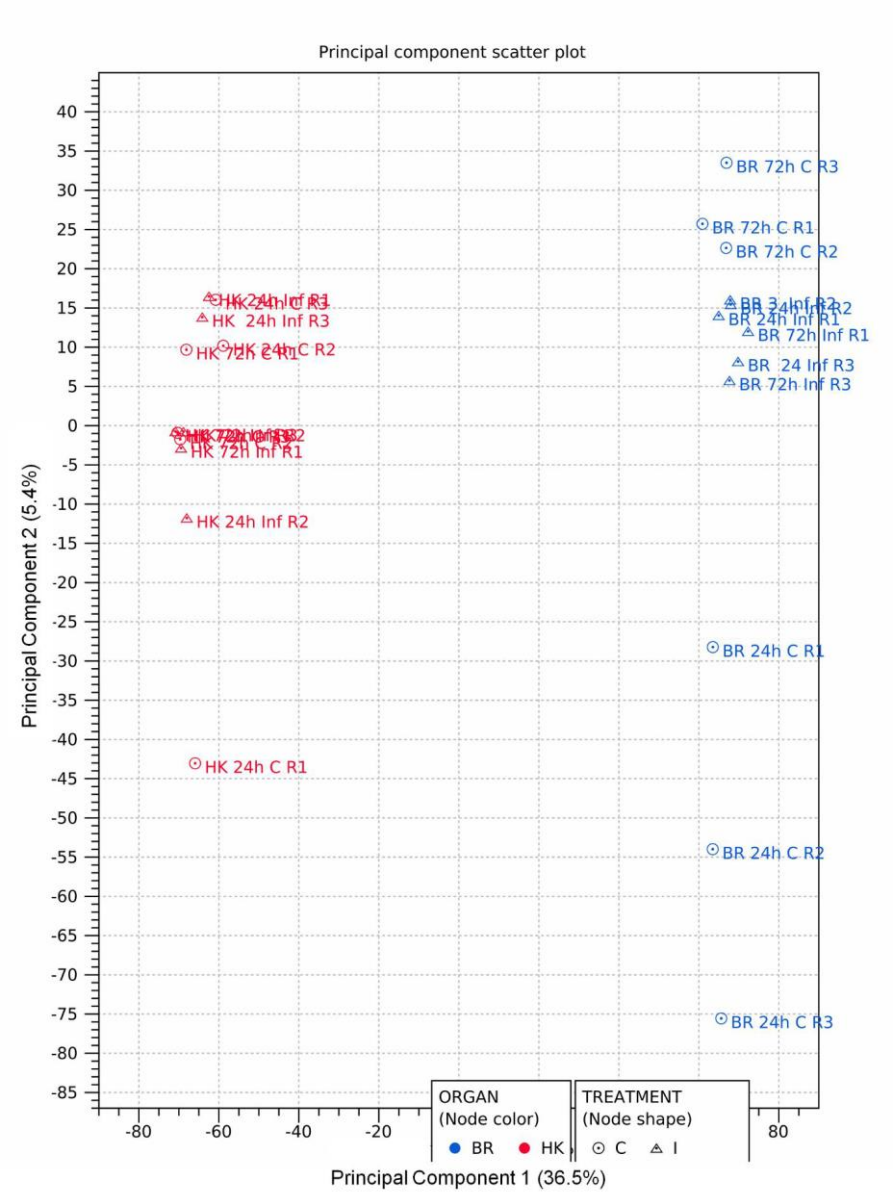

Figure 3.3. Principal component analysis (PCA) of the lncRNAs in the different samples. Each point represents a biological replicate, and different colours represent the different tissues. Samples were mainly clustered according to the tissue (head kidney or brain) with independence of the NNV infection.

3.3.2. Tissue distribution of the lncRNAs

To identify lncRNAs expressed in head kidney but not in brain and vice versa, only those lncRNAs with a TPM value of 0 in all the samples from the same tissue (12 samples) were considered absent in the corresponding tissue. A Venn diagram of the lncRNAs detected in the head kidney and brain was constructed (Figure 3.2A). While 30 lncRNAs did not show a TPM value in any of the samples both in head kidney and brain, most of the lncRNAs were detected in both tissues (10,823). A total of 971 lncRNAs were expressed in the brain but not in the head kidney, whereas 334 lncRNAs were only found in the head kidney. As expected, GO enrichment analysis of the lncRNAs expressed only in one of the tissues revealed biological processes directly related to specific aspects of the functionality of each organ (Figure 3.2B, C). In the head kidney, numerous immune terms were enriched, which were mainly related to the production of cytokines, Toll-like receptor signaling, inflammation, leukocyte activation and proliferation, complement pathway and phagocytosis (Figure 3.2B). On the other hand, neighboring genes of those lncRNAs expressed only in the brain showed enrichment in terms directly related to the nervous system (Figure 3.2C). To illustrate the relevance of the tissue and of the infection in the lncRNA profile, a PCA score plot was constructed (Figure 3.3). Interestingly, all the head kidney samples clustered separately from the brain samples, reflecting the higher weight of the tissue compared to the NNV infection.

3.3.3. Differential expression of lncRNAs after NNV challenge

The differential expression analysis (FC > |2|, FDR < 0.05) for each tissue and sampling point is provided in Supplementary information. A total of 204 and 93 lncRNAs were significantly modulated in the head kidney at 24 and 72 h after NNV infection, respectively (Figure 3.4A). In the brain, 931 and 342 lncRNAs were affected at these sampling points (Figure 3.4A). In both tissues, the number of upregulated lncRNAs was higher than that of downregulated lncRNAs at 24 h post-challenge, but these differences were substantially reduced after 72 h.

A Venn diagram was constructed to illustrate the shared and unshared lncRNAs modulated in both tissues at different days post-

challenge (Figure 3.4B). Most of the differentially expressed lncRNAs were only modulated in one of the tissues and their expression pattern also completely changed in the same tissue depending on the day after infection (Figure 3.4B).

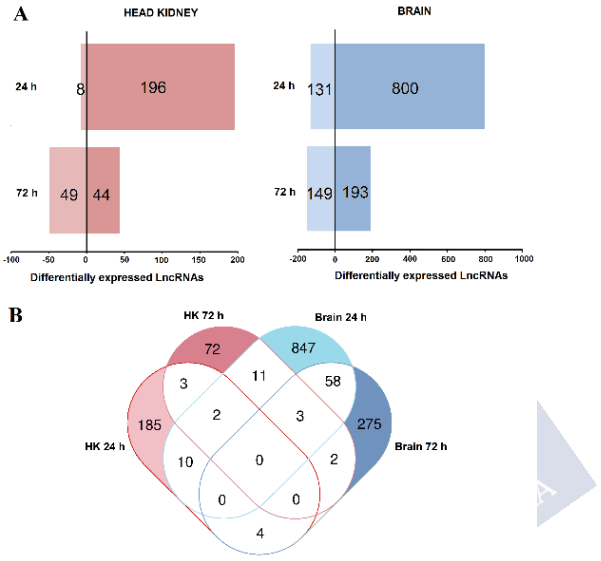

Figure 3.4. Temporal expression of the predicted lncRNAs after nodavirus infection in head kidney and brain. A Number of lncRNAs up- and downregulated in each tissue at 24 and 72 hpi with NNV. **B** Venn diagram representing the shared and unshared lncRNAs modulated after NNV challenge in both tissues at the different sampling points.

Indeed, by analysing the lncRNAs affected by the infection per tissue, we observed that in the head kidney, only 5 lncRNAs were commonly modulated at both 24 and 72 h post-challenge, representing 1.7 % of the total lncRNAs affected by the infection in this tissue (Figure 3.5A). In the brain, the number of shared lncRNAs between both sampling points was 61, representing 5 % of the total (Figure 3.5B). This almost complete switch in the lncRNA profile over time is also reflected in the corresponding heat maps (Figure 3.5A, B). Interestingly, in both tissues, the pattern of the analysed lncRNAs showed a notably different profile between the control at 24 h and at 72 h (Figure 3.5A, B). This highlights the importance of including the

corresponding controls for each sampling point, especially in the case of a very stressful manipulation for the challenge (anesthesia and intramuscular injection). However, the absence of a time 0 control did not allow to determine the basal lncRNA expression profile in the analysed tissues, which could be also an interesting question. In general terms, for both HK and the brain, four main clusters of lncRNAs were observed. For HK, cluster 1 included lncRNAs mainly downregulated at 72 hpi, cluster 2 grouped lncRNAs induced at 24 h by nodavirus, cluster 3 included lncRNAs induced at both 24 and 72 h after infection and cluster 4 included lncRNAs downregulated at both sampling points (Figure 3.5A). In the brain, cluster 1 was mainly composed of lncRNAs overexpressed at 72 h post-challenge, cluster 2 included those lncRNAs induced both at 24 and 72 h, cluster 3 included lncRNAs highly expressed in controls at 72 h and finally, cluster 4 included the lncRNAs highly represented in the control at 24 h (Figure 3.5B).

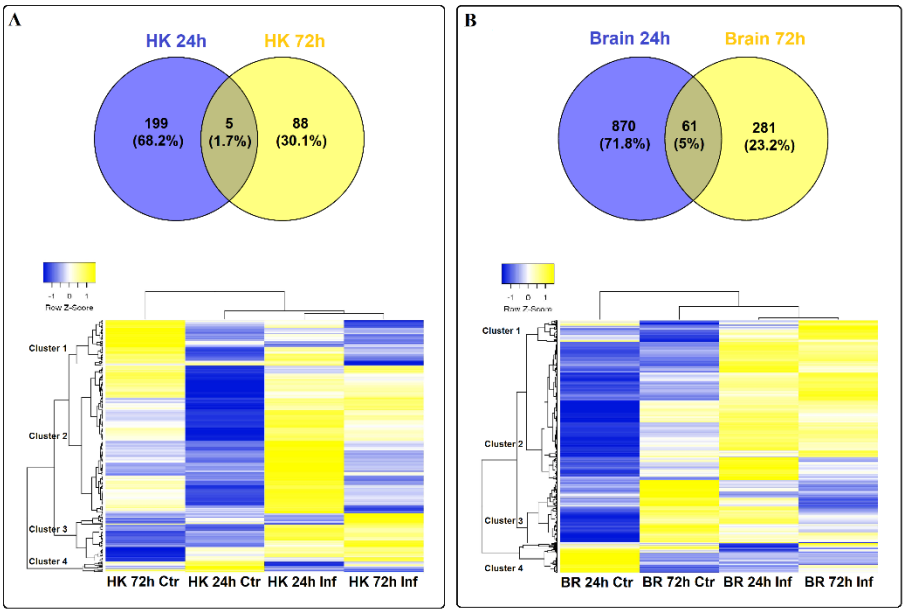

Figure 3.5. Modulation of lncRNAs in A head kidney and B brain after nodavirus challenge. Venn diagrams represent the number of shared and unshared lncRNAs significantly modulated at each sampling point (FC > |2|, FDR < 0.05). Heat maps of the lncRNAs significantly affected by the infection in each tissue and hierarchical clustering of the different samples constructed with the TPM values.

3.3.4. GO enrichment of the lncRNA neighbouring coding genes

The coding genes flanking the differentially expressed lncRNAs were extracted (Supplementariy information) for GO enrichment analysis. The 30 most significantly enriched biological processes are represented in Figures 3.6 and 3.7 for head kidney and brain samples, respectively.

For head kidney samples (Figure 3.6), numerous biological process terms directly involved in immunity were found to be enriched at 24 h post-challenge ('negative regulation of mast cell activation', 'positive regulation of immunoglobulin production', 'positive regulation of B cell proliferation', 'antigen processing and presentation of exogenous peptide antigen via MHC class II', and 'neutrophil mediated immunity'). Nevertheless, this immune representation seemed to be diluted at 72 h, although the immune-related term 'leukotriene production involved in inflammatory response' also appeared to be enriched. In this tissue, some biological process terms suggesting DNA damage and cell cycle arrest were observed both at 24 h ('signal transduction involved in G2 DNA damage checkpoint', 'signal transduction involved in mitotic DNA damage checkpoint') and 72 h post-challenge ('DNA damage induced protein phosphorylation', 'cell cycle arrest'). At this sampling point, the term 'positive regulation of endoplasmic reticulum stress-induced intrinsic apoptotic signaling pathway' was also significantly represented.

In brain samples, the enriched terms were almost completely different from those observed in head kidney (Figure 3.7). In this case, although a biological process immune term was also found at 24 h ('positive regulation of isotype switching to IgA isotypes'), the representation of immune processes was lower compared to head kidney. As also occurred in the head kidney, some DNA damage terms were also observed ('nucleotide-excision repair, DNA gap filling', 'nucleotide-excision repair, pre-incision complex assembly', 'regulation of double-strand break repair via homologous recombination'), as well as numerous de-ubiquitination-related processes. Moreover, two biological processes related to calcium homeostasis were also represented ('induction of synaptic vesicle

exocytosis by positive regulation of presynaptic cytosolic calcium ion concentration' and 'positive regulation of high voltage-gated calcium channel activity'). After 72 h, the representation of immune terms increased in this tissue, with the biological process enriched terms 'regulation of toll-like receptor 9 signalling pathway', 'negative regulation of antigen receptor-mediated signalling pathway' and 'B cell differentiation'. Two stress-related biological processes were represented ('positive regulation of translation in response to stress' and 'response to isolation stress'), and as was observed in head kidney, an ER stress term ('regulation of response to endoplasmic reticulum stress'). The representation of immune biological processes in both tissues could be directly related to the NNV replication level, since the detection of the virus was higher in the head kidney at 24 hpi compared to the brain, but it remained practically unaltered after 72 h (Lama et al., 2020). On the other hand, the NNV detection enormously increased in the brain at 72 hpi (Lama et al., 2020), which could explain the higher representation of immune-related terms at this sampling point in the brain.

3.3.5. Expression correlation of lncRNAs and coding genes

To compare the magnitude of the modulation after NNV infection, we constructed scatter dot plots with the FC values of the DEGs and the lncRNAs in the different samples (FC > |2|, FDR > 0.05) (Figure 3.8). For the DEGs, only those that were successfully annotated were included (Lama et al., 2020). In general terms, the FC variations of the DEGs were considerably more pronounced compared to those observed for the lncRNAs (Figure 3.8).

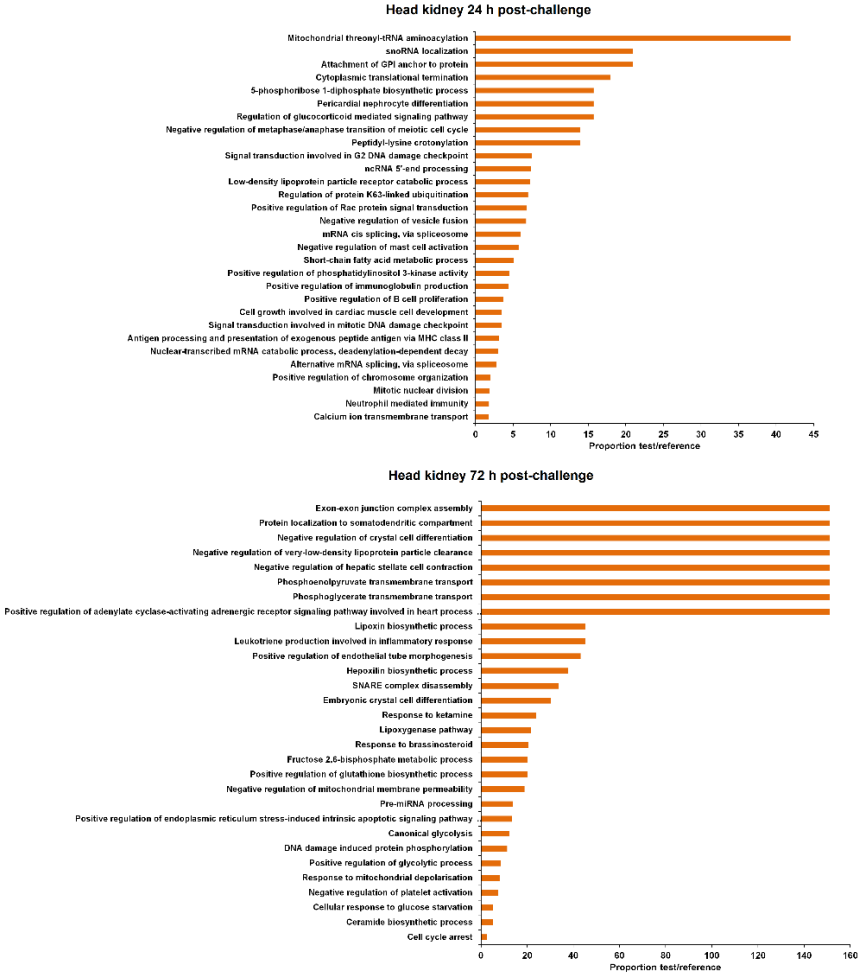

Figure 3.6. GO enrichment analysis (biological processes) of the neighboring coding genes of the differentially modulated lncRNAs (FC > |2|, FDR < 0.05) **in head kidney after viral challenge.** Only the 30 most significant terms were represented.

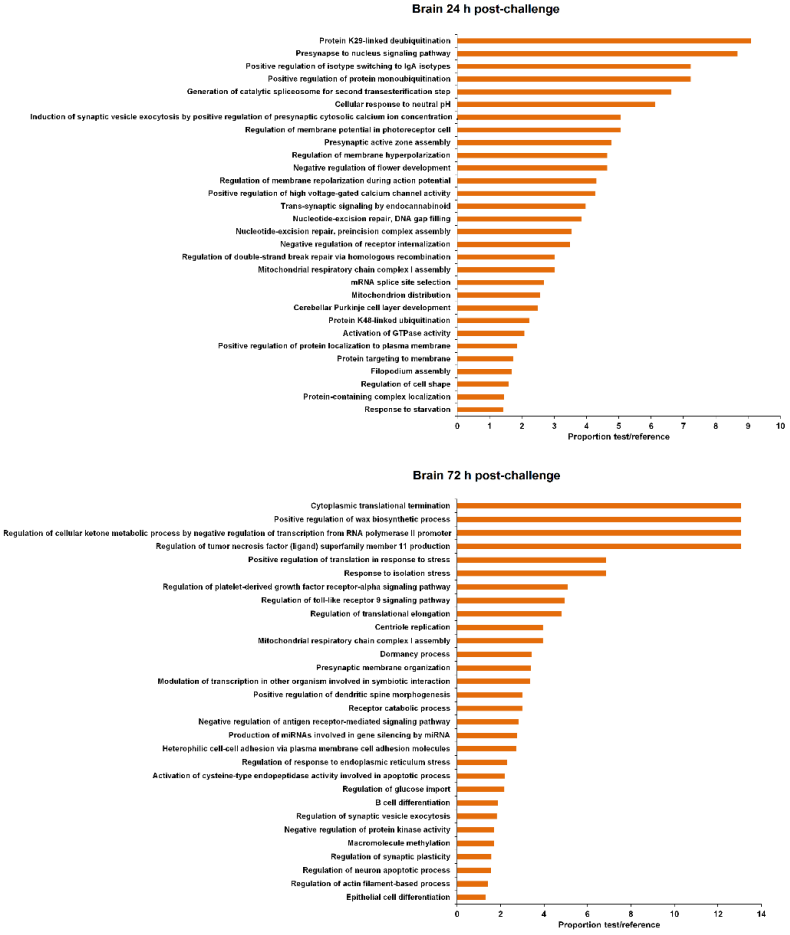

Figure 3.7. GO enrichment analysis (biological processes of the neighboring coding genes of the differentially modulated lncRNAs (FC > |2|, FDR < 0.05) **in the brain after viral challenge.** Only the 30 most significant terms were represented.

To correlate the expression of the lncRNAs and their flanking coding genes, we randomly selected four DEGs after NNV infection (Lama et al., 2020) with at least one adjacent lncRNA significantly modulated after the viral challenge. The *complement component C3* (*c3*), *NK-tumour recognition protein* (*nktr*), *cerebellin 1* (*cbln1*) and *beta-1,4-galactosyltransferase 1* (*b4galt1*), which were overexpressed in the brain after infection, were represented together with all the

predicted lncRNAs flanking and/or overlapping those genes. The TPM values were used to construct the heat maps (Figure 3.9A) and to calculate the correlation values (Figure 3.9B). Only one potential lncRNA (Lnc_contig0102476) was found near the *c3* gene, which was significantly upregulated (FC = 3.66) in the brain at 24 hpi. The expression of *c3* and the corresponding lncRNA were strongly correlated, since both were overexpressed in the brain after viral challenge (Figure 3.9A, B). For *nktr*, four lncRNAs were predicted to be located in the vicinity of the gene (Lnc_contig0004499, Lnc_contig0006737, Lnc_contig0002850, Lnc_contig0029684), and three of them were significantly upregulated in the brain at 24 and/or 72 h after infection. In this case, all the lncRNAs showed the same tendency as that observed for the *nktr* gene (Figure 3.9A, B). In the case of *cbln1*, four neighbouring lncRNAs were also identified (Lnc_contig0006952, Lnc_contig0221449, Lnc_contig0041997, Lnc_contig0114726), and whereas three of them showed the same pattern as *cbln1*, the expression of Lnc_contig0221449 was inversely correlated with gene expression (Figure 3.9A, B). Finally, the lncRNA predicted to be positioned near *b4galt1* (Lnc_contig0036634) was significantly overexpressed in the brain both at 24 and 72 h after NNV infection, and a notably high correlation with gene expression was observed (Figure 3.9A, B).

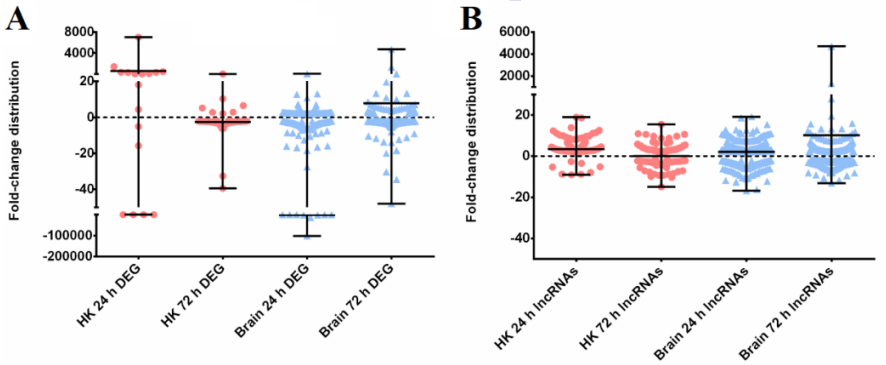

Figure 3.8. Magnitude of transcriptome modulation in the head kidney and brain after NNV infection. A Fold-change values (FC > |2|, FDR < 0.05) of the differentially expressed coding genes. **B** Fold-change values of the differentially expressed lncRNAs (FC > |2|, FDR < 0.05). Graphs represent the individual FC values, the mean and the range.

A

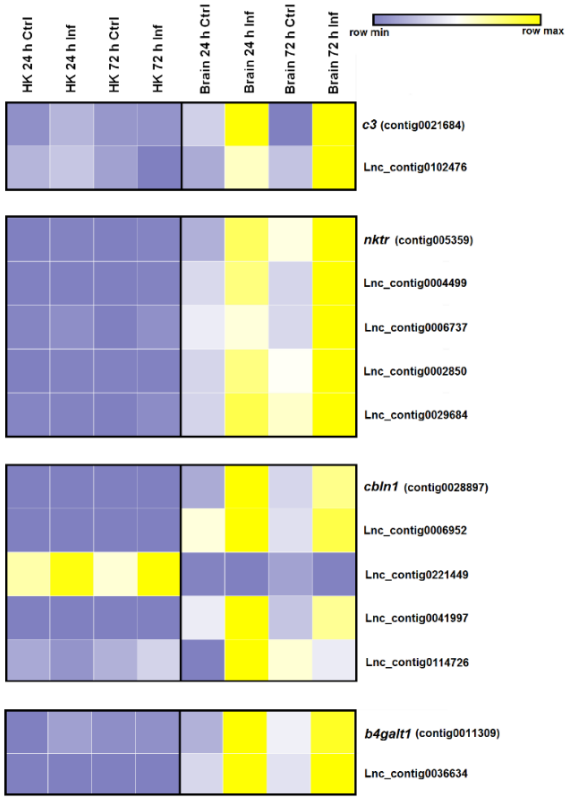

B

Gene	lncRNA	Pearson	Spearman
c3 (contig0021684)	Lnc_contig0102476	0.89 *	0.55^{ns}
nktr (contig0005359)	Lnc_contig0004499	0.97 *	0.95 *
	Lnc_contig0006737	0.93*	0.95 *
	Lnc_contig0002850	0.99 *	0.98 *
	Lnc_contig0029684	0.99 *	0.93 *
cbln1 (contig0028897)	Lnc_contig0006952	0.94 *	0.94*
	Lnc_contig0221449	-0.76 *	-0.85 *
	Lnc_contig0041997	0.97 *	0.94 *
	Lnc_contig0114726	0.83 *	0.56^{ns}
b4galt1 (contig0011309)	Lnc_contig0036634	0.98 *	0.91 *

Figure 3.9. Correlation between differentially modulated coding genes after NNV infection and their flanking lncRNAs. A Heat map representing the TPM values of four genes and their neighboring lncRNAs across the different head kidney and brain samples. Expression levels are represented as row-normalised values on a blue-yellow color scale. **B** Correlation values (Pearson's correlation coefficient and Spearman's rank correlation coefficient) between the lncRNAs and their nearby coding genes. * representes significant correlation and ^{ns} non-significant correlation.

3.3.6. LncRNAs could mediate calcium homeostasis

In a previous analysis of the coding transcriptome, we found a strong regulation of genes involved in Ca^{2+} homeostasis in the brain, and the concentration of this cation seems to be highly altered during NNV infection and is crucial for infectivity (Lama et al., 2020). In this work, the biological process terms 'induction of synaptic vesicle exocytosis by positive regulation of presynaptic cytosolic calcium ion concentration' and 'positive regulation of high voltage-gated calcium channel activity' were also enriched in the brain at 24 hpi (Figure 3.7), as well as other calcium-related terms not included in the 30 most significantly enriched GO terms but significantly enriched at 24 h and/or at 72 h post-challenge. To illustrate the connections among the different lncRNA neighbouring coding genes involved in Ca^{2+} homeostasis, a protein–protein network interaction was constructed only for the neighbouring genes of those lncRNAs significantly modulated after viral infection (Figure 3.10A). Most of the proteins encoded by these genes were interconnected, and the main function of these genes is to directly mediate Ca^{2+} transport across the cellular, mitochondrial and ER membranes. Among the molecules represented, *sarcoplasmic endoplasmic reticulum calcium atpase 1-like* (*atp2a1* or *serca1*) was the most modulated gene in the coding-transcriptome analysis (Lama et al., 2020). On the other hand, the *regulator of g-protein signalling 6-like* (*rgs6*) was slightly modulated (Lama et al., 2020). To exemplify the potential involvement of lncRNAs in the modulation of Ca^{2+} homeostasis-related genes, these two genes were selected, and their expression was correlated to that observed for their neighbouring lncRNAs (Figure 3.10B). Positive or negative correlations between each coding gene and the corresponding lncRNAs were observed, and these correlations were significant for the *atp21a* gene and the lncRNA Lnc_contig0024843 and for the *rgs6* gene and Lnc_contig0052951. The three lncRNAs were included in the validation of the RNA-Seq results by qPCR.

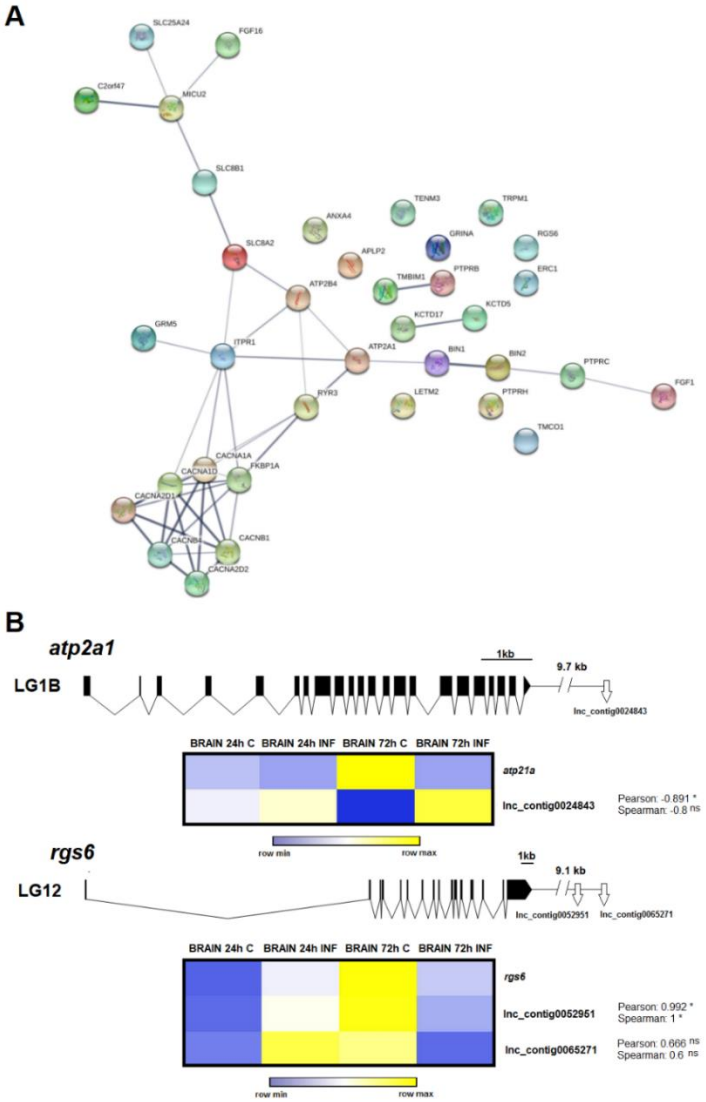

Figure 3.10. Calcium homeostasis-related genes and their relationship with lncRNAs. A Protein-protein interaction network of the lncRNAs neighbouring coding genes involved in calcium homeostasis. Numerous lncRNAs significantly modulated in the brain after NNV infection were flanked by genes directly related to calcium homeostasis. **B** Gene representation of two genes mediating cellular calcium concentration after NNV challenge and genomic location of their neighbouring lncRNAs. Heat maps represented the TPM values of the different contigs. Expression levels are represented as row-normalised values on a blue-yellow colour scale. * represents significant correlation and ^{ns} non-significant correlation.

3.3.7. qPCR validation of lncRNA expression

RNA-Seq results were validated by qPCR by analysing the expression of 12 putative lncRNAs significantly modulated in the RNA-Seq results (10 for brain and 2 for head kidney). Although in general terms the magnitude of the modulation was higher in the RNA-Seq data, the qPCR FCs followed the same tendency (Figure 3.11). Indeed, a positive correlation was obtained between the RNA-Seq and qPCR FC values by using Pearson's correlation coefficient (r = 0.84).

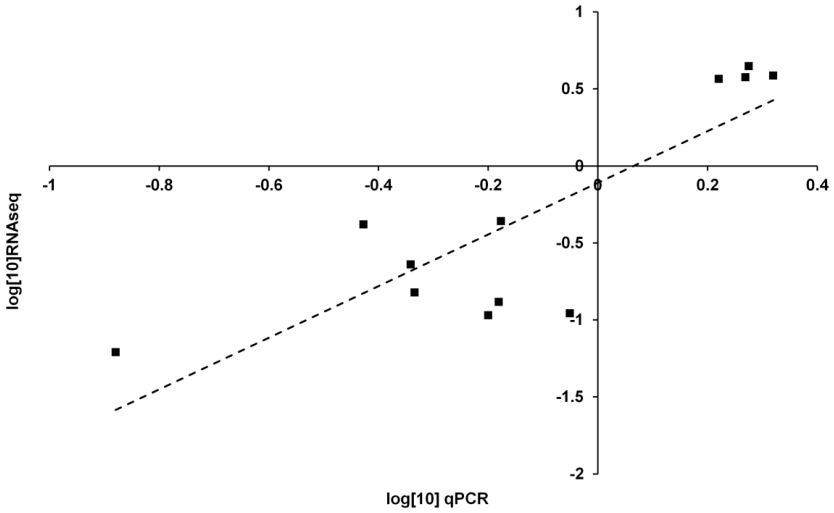

Figure 3.11. Validation of differentially expressed lncRNAs through qPCR. Twelve potential lncRNAs were validated. Pearson's correlation test showed a value of 0.84.

3.4. DISCUSSION

In mammals, lncRNAs have been linked to a variety of immune processes, including inflammation (Carpenter et al., 2013; Rapicavoli et al., 2013), T cell development, differentiation and migration (Hu et al., 2013), B cell maturation (Agirre et al., 2019), interferon response (Kambara et al., 2014), dendritic cell differentiation (Wang et al., 2014) and granulocyte maturation (Zhang et al., 2009). The lncRNA profile has been shown to be modulated after different viral infections in several species (Peng et al., 2010; Zhang et al., 2016; Zhao et al., 2018; Hudson et al., 2019). Moreover, for several lncRNAs, their specific

function in viral infection has been elucidated (Fortes and Morris, 2016).

Massive analysis of zebrafish (*Danio rerio*) lncRNAs enabled the identification of numerous conserved zebrafish lncRNAs with a putative orthologue in mammals (Chen et al., 2018), which could be indicative of functional conservation. This analysis of the lncRNA repertoire in zebrafish has derived in the creation of a refined database (Hu et al., 2018), which could help to facilitate the functional analyses in this model species. However, to the best of our knowledge, only one publication has reported the specific immune function of a lncRNA in fish. In that work, the authors found that the PU.1 gene, which is involved in the expression of adaptive immune genes, is negatively regulated by its antisense lncRNA (Wei et al., 2014). In the case of zebrafish, the existence of numerous mutant lines could facilitate the identification of lncRNAs related to specific functions. This finding was observed for the heterozygous rag1$^{+/-}$ zebrafish, which is partially deficient in the Rag1 protein, an endonuclease involved in the assembly of immunoglobulins and T cell receptor (TCR) genes (Bassing et al., 2002). When wild-type and rag1$^{+/-}$ zebrafish were infected with the spring viremia of carp virus (SVCV), those animals partially deficient in Rag1 showed a modulation of lncRNAs surrounded by genes involved in adaptive immunity, which was not observed in wild-type fish (Valenzuela-Muñoz et al., 2019). A plausible explanation is that those animals deficient in adaptive mechanisms potentiated this response to combat the infection compared to the full competent animals (Valenzuela-Muñoz et al., 2019).

In the past several years, some publications have reported the identification and modulation of lncRNAs in aquacultured fish against a variety of pathogens, especially in salmonids (Boltaña et al., 2016; Elling et al., 2016; Paneru et al., 2016; Valenzuela-Miranda et al., 2016; Valenzuela-Muñoz et al., 2018). However, to date, no lncRNA analyses have been conducted in European sea bass. We first investigated the modulation of the coding transcripts in head kidney and brain from *D. labrax* infected intramuscularly with nodavirus. In that work, we observed a strong modulation of the stress axis during infection with

the virus but a slight regulation of immune-related genes (Lama et al., 2020).

From the Illumina sequencing of the *D. labrax* transcriptome and *de novo* assembly (Lama et al., 2020), we selected those contigs that passed all the filters to be considered potential lncRNAs. We obtained a contig list of 12,158 lncRNAs, and 95.96 % of them mapped to the genome. Analysis of the lncRNA abundance per chromosome revealed a homogeneous distribution with a strong positive correlation between the number of putative lncRNAs and chromosome length.

RNA-Seq analysis of these contigs in the different samples showed that some lncRNAs were tissue-specific. This tissue specificity was previously reported for different vertebrate species (Ward et al., 2015; Kern et al., 2018), including zebrafish (Kaushik et al., 2013) and other teleost species (Boltaña et al., 2016). Most lncRNAs influence the expression of their nearby genes, acting as local regulators; therefore, lncRNA expression is often correlated with the expression of their adjacent coding genes (Ponting et al., 2009). These tissue-specific lncRNAs were flanked by protein-coding genes involved in biological processes closely linked to the functionality of that tissue. Because the head kidney is a major hematopoietic and immune tissue in fish (Zapata et al., 2006), numerous immune-related GO terms were only enriched in this organ. In the brain, almost all the enriched GO terms were directly related to the maintenance of neuronal functions and homeostasis, neurotransmitters and behavior.

NNV infection significantly modulated the expression of different lncRNAs in both the head kidney and brain. The brain showed a higher number of modulated lncRNAs (931 and 342 at 24 and 72 hpi, respectively) compared to the head kidney (204 and 93), probably because of the neurotropic nature of the virus. As was also reported for *Salmo salar* after infectious salmon anaemia virus (ISAV) infection (Boltaña et al., 2016) or *Caligus rogercresseyi* infestation (Valenzuela-Muñoz et al., 2018), lncRNAs were expressed in a temporal-specific manner with a very low percentage of shared lncRNAs between 24 h and 72 hpi in both tissues. Therefore, the lncRNA transcriptome profile changes as the disease progresses with high spatiotemporal specificity.

GO enrichment analyses of the neighbouring coding genes of lncRNAs modulated after NNV challenge in the head kidney revealed a large number of immune-related terms, especially after 24 h. These terms were mainly related to the activation and proliferation of immune cells, antigen presentation, immunoglobulin production and inflammation. However, the analysis of the transcriptome revealed a practically absent immune response in this tissue, and the modulated genes were mainly related to cortisol synthesis and ROS production (Lama et al., 2020). It is worth mentioning that different DNA damage-, cell cycle- and ER stress-related terms were also enriched in this tissue. It is known that oxidative stress caused by ROS production can induce DNA damage and ER stress, which could lead to cell cycle arrest (Lin et al., 2008; Yang et al., 2009; Zeng et al., 2018). Nevertheless, viruses can manipulate DNA repair pathways and cell cycle control mechanisms to facilitate their own replication (Bagga and Bouchard, 2014; Lufting, 2014). On the other hand, ER stress is also intimately related to virus activity. Viruses hijack the host translation machinery to massively produce viral proteins, affecting ER homeostasis and causing ER stress (Li et al., 2015). Moreover, ER stress also induces the production of ROS (Zeeshan et al., 2016), and ROS are an important component of the immune defence because they can kill pathogens directly by causing oxidative damage or modulating different immune mechanisms (Paiva and Bozza, 2014). It has been previously described that NNV can induce ROS in European sea bass (Lama et al., 2020) and oxidative stress-mediated cell death in fish cells (Chang et al., 2011). Because ROS are also harmful to the host, the activity of antioxidant molecules, such as glutathione, is also needed to control the damage. The term ‘positive regulation of glutathione biosynthetic process’ was also enriched among those genes flanking the lncRNAs enriched in head kidney at 72 hpi. A previous analysis of the coding genes differentially modulated in sea bass head kidney after NNV infection revealed enrichment in the oxidation-reduction process (Lama et al., 2020), which could indicate that these are mechanisms controlled by lncRNAs.

In the brain, we found that those genes located at less than 10 kb from differentially modulated lncRNAs after NNV challenge were also

enriched in immune terms both at 24 and 72 hpi. At 24 h, only one immune term was enriched in this tissue ('positive regulation of isotype switching to IgA isotypes'), which was related to antibody production. It has been described in teleosts that host antibody production is an important response to nodavirus infection even at early stages of infection (Grove et al., 2006; López-Muñoz et al., 2012; Piazzon et al., 2016; Buonocore at al., 2017), and the expression level of these immunoglobulins could be related to a higher resistance to the virus (Wu et al., 2012). Indeed, antibody production is one of the main immune mechanisms protecting the brain against neurotropic viruses (Iwasaki, 2017). However, in the transcriptome analyses, the production of antibodies seemed to be downregulated at this early sampling point (Lama et al., 2020). According to this finding, although more investigations are needed, inhibition of antibody production could be regulated by lncRNAs.

We previously observed that the main response induced by NNV in European sea bass at these early sampling points is the activation of the HPI axis, which is the stress response (Lama et al., 2020). According to this study, some stress-related terms were also enriched in the brain for the neighbouring genes of the lncRNAs modulated at 72 hpi. The activation of the stress axis observed in these same samples could lead to Ca^{2+} influx into the neurons, generating excitotoxicity, and as a consequence, neuronal damage (Arundine and Tymianski, 2003; Dong et al., 2009). Indeed, Ca^{2+} cellular homeostasis was found to be highly altered in the brain during NNV infection (Lama et al., 2020). For the neighbouring genes of the lncRNAs significantly modulated in this tissue, different calcium-related biological process terms were also enriched, and as occurred in head kidney, we also found lncRNAs flanked by genes related to the DNA damage response, which could be a consequence of excitotoxicity. Although Ca^{2+} homeostasis modulations in the brain could be a direct consequence of the stress response activated after NNV challenge, viruses can also perturb it and utilize calcium and Ca^{2+}-related proteins to benefit their own replication (Zhou et al., 2009). In fact, nodaviruses require the incorporation of Ca^{2+} ions into the viral capsid for a correct assembly process and integrity (Wu et al., 2008; Chen et al., 2015). We observed that

RGNNV, the genotype infecting European sea bass, needs Ca^{2+} to replicate correctly (Lama et al., 2020).

Although the number of annotated DEGs in the different tissues at 24 h and 72 hpi was lower compared to the number of differentially modulated lncRNAs, in general terms, the magnitude of these modulations was higher for the DEGs. This observation could suggest that small variations in lncRNA levels can have a high impact on mRNA expression. Moreover, several lncRNAs can simultaneously affect the expression of the same coding gene, and consequently, their effect can be additive. To link the coding-lncRNA response, we randomly selected four genes that were significantly modulated in the brain after viral challenge and flanked by at least one lncRNA that was also significantly affected by the infection. We observed a strong correlation between the expression of the coding genes and all the closely positioned lncRNAs. Because lncRNAs can activate or repress gene expression (Ponting et al., 2009), negative transcriptional correlations can also be observed. Because of the high modulation of Ca^{2+} homeostasis-related coding genes and lncRNAs closely located to these genes, we suggest that the expression of these genes is likely affected by lncRNAs.

Taking all these observations into account, we can conclude that there exists a high parallelism between the protein coding genes modulated by NNV challenge and the genes located near lncRNAs affected by infection. Therefore, lncRNAs seem to strongly contribute to the response against NNV. Further functional studies between significantly correlated lncRNAs and coding genes will help to elucidate the mechanism of the interactions between lncRNAs and immune genes induced after NNV infection in European sea bass.

Supplementary information accompanies this Chapter 3 at http://www.mdpi.com/2079-7737/9/7/165/s1.

Availability of data and materials. The read sequences were deposited in the NCBI Sequence Read Archive (SRA) under accesion number PRJNA589774.

3.5. REFERENCES

Agirre X, Meydan C, Jiang Y, Garate L, Doane AS, Li Z, Verma A, Paiva B, Martín-Subero JI, Elemento O, Mason CE, Prosper F, Melnick A (2019) Long non-coding RNAs discriminate the stages and gene regulatory states of human humoral immune response. *Nature Communications* 10(1):821.

Arundine M, Tymianski M (2003) Molecular mechanisms of calcium-dependent neurodegeneration in excitotoxicity. *Cell Calcium* 34:325-337.

Babicki S, Arndt D, Marcu A, Liang Y, Grant JR, Maciejewski A, Wishart DS (2016) Heatmapper: web-enabled heat mapping for all. *Nucleic Acids Research* 44(W1):W147-53.

Bagga S, Bouchard MJ (2014) Cell cycle regulation during viral infection. *Methods in Molecular Biology* 1170:165-227.

Bassing CH, Swat W, Alt FW (2002) The mechanism and regulation of chromosomal V(D)J recombination. *Cell* 109(2):S45-S55.

Boltaña S, Valenzuela-Miranda D, Aguilar A, Mackenzie S, Gallardo-Escárate C (2016) Long noncoding RNAs (lncRNAs) dynamics evidence immunomodulation during ISAV-infected Atlantic salmon (*Salmo salar*). *Scientific Reports* 6:22698.

Buonocore F, Randelli E, Tranfa P, Scapigliati G (2012) A CD83-like molecule in sea bass (*Dicentrarchus labrax*): molecular characterization and modulation by viral and bacterial infection. *Fish and Shellfish Immunology* 32(6):1179-1184.

Buonocore F, Stocchi V, Nunez-Ortiz N, Randelli E, Gerdol M, Pallavicini A, Facchiano A, Bernini C, Guerra L, Scapigliati G, Picchietti S (2017) Immunoglobulin T from sea bass (*Dicentrarchus labrax* L.): molecular characterization, tissue localization and expression after nodavirus infection. *BMC Molecular Biology* 18(1):8.

Carpenter S, Aiello D, Atianand MK, Ricci EP, Gandhi P, Hall LL, Byron M, Monks B, Henry-Bezy M, O'Neill LAJ, Lawrence JB, Moore MJ, Caffrey DR, Fitzgerald KA (2013) A long noncoding RNA

mediates both activation and repression of immune response genes. *Science* 341(6147):789-792.

Chang CW, Su YC, Her GM, Ken CF, Hong JR (2011) Betanodavirus induces oxidative stress-mediated cell death that prevented by anti-oxidants and zfcatalase in fish cells. *Plos One* 6(10):e25853.

Chaves-Pozo E, Guardiola FA, Meseguer J, Esteban MA, Cuesta A (2012) Nodavirus infection induces a great innate cell-mediated cytotoxic activity in resistant, gilthead seabream, and susceptible, European sea bass, teleost fish. *Fish and Shellfish Immunology* 33(5):1159-1166.

Chaves-Pozo E, Valero Y, Esteve-Codina A, Gómez-Garrido J, Dabad M, Alioto T, Meseguer J, Esteban MA, Cuesta A (2017) Innate cell-mediated cytotoxic activity of European sea bass leucocytes against nodavirus-infected cells: a functional and RNA-seq study. *Scientific Reports* 7(1):15396.

Chaves-Pozo E, Bandín I, Olveira JG, Esteve-Codina A, Gómez-Garrido J, Dabad M, Alioto T, Ángeles Esteban M, Cuesta A (2019) European sea bass brain DLB-1 cell line is susceptible to nodavirus: A transcriptomic study. *Fish and Shellfish Immunology* 86:14-24.

Chen NC, Yoshimura M, Guan HH, Wang TY, Misumi Y, Lin CC, Chuankhayan P, Nakagawa A, Chan SI, Tsukihara T, Chen TY, Chen CJ (2015) Crystal structures of a piscine Betanodavirus: mechanisms of capsid assembly and viral infection. *PLoS Pathogens* 11:e1005203.

Chen W, Zhang X, Li J, Huang S, Xiang S, Hu X, Liu C (2018) Comprehensive analysis of coding-lncRNA gene co-expression network uncovers conserved functional lncRNAs in zebrafish. *BMC Genomics* 19(Suppl 2):112.

Conesa A, Götz S, García-Gómez JM, Terol J, Talón M, Robles M (2005) Blast2GO: a universal tool for annotation, visualization and analysis in functional genomics research. *Bioinformatics* 21(18):3674-3676.

Dong XX, Wang Y, Qin ZH (2009). Molecular mechanisms of excitotoxicity and their relevance to pathogenesis of neurodegenerative diseases. *Acta Pharmacologica Sinica* 30:379-387.

Elling R, Chan J, Fitzgerald KA (2016) Emerging role of long noncoding RNAs as regulators of innate immune cell development and inflammatory gene expression. *European Journal of Immunology* 46(3):504-512.

Fortes P, Morris KV (2016) Long noncoding RNAs in viral infections. *Virus Research* 212:1-11.

Grove S, Johansen R, Reitan LJ, Press CM, Dannevig BH (2006) Quantitative investigation of antigen and immune response in nervous and lymphoid tissues of Atlantic halibut (*Hippoglossus hippoglossus*) challenged with nodavirus. *Fish and Shellfish Immunology* 21(5):525-539.

Guo CJ, Ma XK, Xing YH, Zheng CC, Xu YF, Shan L, Zhang J, Wang S, Wang Y, Carmichael GG, Yang L, Chen LL (2020) Distinct processing of lncRNAs contributes to non-conserved functions in stem cells. *Cell* 181:621-636.

Hu G, Tang Q, Sharma S, Yu F, Escobar TM, Muljo SA, Zhu J, Zhao K (2013) Expression and regulation of intergenic long noncoding RNAs during T cell development and differentiation. *Nature Immunology* 14:1190-1198.

Hu X, Chen W, Li J, Huang S, Xu X, Zhang X, Xiang S, Liu C (2018) ZFLNC: a comprehensive and well-annotated database for zebrafish lncRNA. *Database (Oxford)* bay114.

Hudson WH, Prokhnevska N, Gensheimer J, Akondy R, McGuire DJ, Ahmed R, Kissick HT (2019) Expression of novel long noncoding RNAs defines virus-specific effector and memory CD8+ T cells. *Nature Communications* 10(1):196.

Iwasaki A (2017) Immune regulation of antibody access to neuronal tissues. *Trends in Molecular Medicin* 23(3):227-245.

Kambara H, Niazi F, Kostadinova L, Moonka DK, Siegel CT, Post AB, Carnero E, Barriocanal M, Fortes P, Anthony DD, Valadkhan S (2014) Negative regulation of the interferon response by an interferon-induced long non-coding RNA. *Nucleic Acids Research* 42(16):10668-10680.

Kaushik K, Leonard VE, Kv S, Lalwani MK, Jalali S, Patowary A, Joshi A, Scaria V, Sivasubbu S (2013) Dynamic expression of long non-coding RNAs (lncRNAs) in adult zebrafish. *PLoS One* 8(12):e83616.

Kern C, Wang Y, Chitwood J, Korf I, Delany M, Cheng H, Medrano JF, Van Eenennaam AL, Ernst C, Ross P, Zhou H (2018) Genome-wide identification of tissue-specific long non-coding RNA in three farm animal species. *BMC Genomics* 19(1):684

Lama R, Pereiro P, Valenzuela-Muñoz V, Gallardo-Escárate C, Tort L, Figueras A, Novoa B (2020) RNA-Seq analysis of European sea bass (*Dicentrarchus labrax* L.) infected with nodavirus reveals poweful modulation of the stress response. *Veterinary Research* 51:64.

Li S, Kong L, Yu X (2015) The expanding roles of endoplasmic reticulum stress in virus replication and pathogenesis. *Critical Reviews in Microbiology* 41(2):150-164.

Lin SS, Huang HP, Yang JS, Wu JY, Hsia TC, Lin CC, Lin CW, Kuo CL, Gibson Wood W, Chung JG (2008) DNA damage and endoplasmic reticulum stress mediated curcumin-induced cell cycle arrest and apoptosis in human lung carcinoma A-549 cells through the activation caspases cascade- and mitochondrial-dependent pathway. *Cancer Letters* 272(1):77-90.

López-Muñoz A, Sepulcre MP, García-Moreno D, Fuentes I, Béjar J, Manchado M, Álvarez MC, Meseguer J, Mulero V (2012) Viral nervous necrosis virus persistently replicates in the central nervous system of asymptomatic gilthead seabream and promotes a transient inflammatory response followed by the infiltration of IgM+ B lymphocytes. *Developmental and Comparative Immunology* 37(3-4):429-437.

Luftig MA (2014) Viruses and the DNA damage response: activation and antagonism. *Annual Review of Virology* 1(1):605-625.

Novel P, M.A. Fernandez-Trujillo, J.B. Gallardo-Galvez, I. Cano, M. Manchado, F. Buonocore, E. Randelli, G. Scapigliati, M.C. Alvarez, J. Bejar (2013) Two Mx genes identified in European sea bass (*Dicentrarchus labrax*) respond differently to VNNV infection. *Veterinary Immunology and Immunopathology* 153(3-4):240-248.

Paiva CN, Bozza MT (2014) Are reactive oxygen species always detrimental to pathogens? *Antioxidants and Redox Signaling* 20(6):1000-1037.

Paneru B, Al-Tobasei R, Palti Y, Wiens GD, Salem M (2016) Differential expression of long non-coding RNAs in three genetic lines of rainbow trout in response to infection with *Flavobacterium psychrophilum*. *Scientific Reports* 6:36032.

Peng X, Gralinski L, Armour CD, Ferris MT, Thomas MJ, Proll S, Bradel-Tretheway BG, Korth MJ, Castle JC, Biery MC, Bouzek HK, Haynor DR, Frieman MB, Heise M, Raymond CK, Baric RS, Katze MG (2010) Unique signatures of long noncoding RNA expression in response to virus infection and altered innate immune signaling. *mBio* 1(5):e00206-e00210.

Pfaffl MW (2001) A new mathematical model for relative quantification in real-time RT-PCR. Nucleic Acids Research 29:2002-2007.

Piazzon MC, Galindo-Villegas J, Pereiro P, Estensoro I, Calduch-Giner JA, Gómez-Casado E, Novoa B, Mulero V, Sitjà-Bobadilla A, Pérez-Sánchez J (2016) Differential modulation of IgT and IgM upon parasitic, bacterial, viral, and dietary challenges in a perciform fish. *Frontiers in Immunology* 7:637.

Poisa-Beiro L, Dios S, Montes A, Arantguren R, Figueras A, Novoa B (2008) Nodavirus increases the expression of Mx and inflammatory cytokines in fish brain. *Molecular Immunology* 45(1):218-225.

Poisa-Beiro L, Dios S, Ahmed H, Vasta GR, Martínez-López A, Estepa A, Alonso-Gutiérrez J, Figueras A, Novoa B (2009) Nodavirus infection of sea bass (*Dicentrarchus labrax*) induces up-regulation of galectin-1 expression with potential anti-inflammatory activity. *Journal of Immunology* 183(10): 6600-6611.

Ponting CP, Oliver PL, Reik W (2009) Evolution and functions of long noncoding RNAs. *Cell* 136(4):629-641.

Rapicavoli NA, Qu K, Zhang J, Mikhail M, Laberge RM, Chang HY (2013) A mammalian pseudogene lncRNA at the interface of inflammation and anti-inflammatory therapeutics. *eLife* 2:e00762.

Reed LJ, Muench H (1938) A simple method of estimating fifty percent endpoints. *American Journal of Epidemiology* 27(3):493-497.

Rozen S, Skaletsky H (2000) Primer3 on the WWW for general users and for biologist programmers. *Bioinformatics Methods and Protocols* 132:365-386.

Sarropoulou E, Sepulcre P, Poisa-Beiro L, Mulero V, Meseguer J, Figueras A, Novoa B, Terzoglou V, Reinhardt R, Magoulas A, Kotoulas G (2009) Profiling of infection specific mRNA transcripts of the European seabass *Dicentrarchus labrax*. *BMC Genomics* 10:157.

Scapigliati G, Buonocore F, Randelli E, Casani D, Meloni S, Zarletti G, Tiberi M, Pietretti D, Boschi I, Manchado M, Martin-Antonio B, Jimenez-Cantizano R, Bovo G, Borghesan F, Lorenzen N, Einer-Jensen K, Adams S, Thompson K, Alonso C, Bejar J, Cano I, Borrego JJ, Alvarez MC (2010) Cellular and molecular immune responses of the sea bass (*Dicentrarchus labrax*) experimentally infected with betanodavirus. *Fish and Shellfish Immunology* 28(2): 303-131.

Szklarczyk D, Gable AL, Lyon D, Junge A, Wyder S, Huerta-Cepas J, Simonovic M, Doncheva NT, Morris JH, Bork P, Jensen LJ, von Mering C (2019) STRING v11: protein-protein association networks with increased coverage, supporting functional discovery in genome-wide experimental datasets. *Nucleic Acids Research* 47(D1):D607-D613.

Tarifeño-Saldivia E, Valenzuela-Miranda D, Gallardo-Escárate C (2017) In the shadow: The emerging role of long non-coding RNAs in the immune response of Atlantic salmon. *Developmental and Comparative Immunology* 73:193-205.

Tine M, Kuhl H, Gagnaire PA, Louro B, Desmarais E, Martins RST, Hecht J, Knaust F, Belkhir K, Klages S, Dieterich R, Stueber K, Piferrer F, Guinand B, Bierne N, Volckaert FAM, Bargelloni L, Power DM, Bonhomme F, Canario AVM, Reinhardt R (2014) European sea bass genome and its variation provide insights into adaptation to euryhalinity and speciation. *Nature Communications* 5:5770.

Valenzuela-Miranda D, Gallardo-Escárate C (2016) Novel insights into the response of Atlantic salmon (*Salmo salar*) to *Piscirickettsia salmonis*: Interplay of coding genes and lncRNAs during bacterial infection. *Fish and Shellfish Immunology* 59:427-438.

Valenzuela-Muñoz V, Valenzuela-Miranda D, Gallardo-Escárate C (2018) Comparative analysis of long non-coding RNAs in Atlantic and Coho salmon reveals divergent transcriptome responses associated with immunity and tissue repair during sea lice infestation. *Developmental and Comparative Immunology* 87:36-50.

Valenzuela-Muñoz V, Pereiro P, Álvarez-Rodríguez M, Gallardo-Escárate C, Figueras A, Novoa B (2019) Comparative modulation of lncRNAs in wild-type and rag1-heterozygous mutant zebrafish exposed to immune challenge with spring viraemia of carp virus (SVCV). *Scientific Reports* 9:14174.

Valero Y, Morcillo P, Meseguer J, Buonocore F, Esteban MA, Chaves-Pozo E, Cuesta A (2015) Characterization of the interferon pathway in the teleost fish gonad against the vertically transmitted nervous necrosis virus. *Journal of General Virology* 96:2176-2187.

Wang L, Park HJ, Dasari S, Wang S, Kocher JP, Li W (2013) CPAT: coding-Potential Assessment Tool using an alignment-free logistic regression model. *Nucleic Acids Research* 41(6):e74.

Wang M, Jiang S, Wu W, Yu F, Chang W, Li P, Wang K (2018) Non-coding RNAs function as immune regulators in teleost fish. *Frontiers in Immunology* 9:2801.

Wang P, Xue Y, Han Y, Lin L, Wu C, Xu S, Jiang Z, Xu J, Liu Q, Cao X (2014) The STAT3-binding long noncoding RNA lnc-DC controls human dendritic cell differentiation. *Science* 344(6181):310-313.

Ward M, McEwan C, Mills JD, Janitz M (2015) Conservation and tissue-specific transcription patterns of long noncoding RNAs. *Journal of Human Transcriptome* 1(1):2-9.

Wei N, Pang W, Wang Y, Xiong Y, Xu R, Wu W, Zhao C, Yang G (2014) Knockdown of PU.1 mRNA and AS lncRNA regulates expression of immune-related genes in zebrafish *Danio rerio*. *Developmental and Comparative Immunology* 44(2):315-319.

Wu MS, Chen CW, Liu YC, Huang HH, Lin CH, Tzeng CS, Chang CY (2012) Transcriptional analysis of orange-spotted grouper reacting to experimental grouper iridovirus infection. *Developmental and Comparative Immunology* 37(2):233-242.

Wu YM, Hsu CH, Wang CH, Liu W, Chang WH, Lin CS (2008) Role of the DxxDxD motif in the assembly and stability of betanodavirus particles. *Archives of Virology* 153:1633-1642.

Yang JS, Chen GW, Hsia TC, Ho HC, Ho CC, Lin MW, Lin SS, Yeh RD, Ip SW, Lu HF, Chung JG (2009) Diallyl disulfide induces apoptosis in human colon cancer cell line (COLO 205) through the induction of reactive oxygen species, endoplasmic reticulum stress, caspases cascade and mitochondrial-dependent pathways. *Food and Chemical Toxicology* 47(1):171-179.

Zapata A, Diez B, Cejalvo T, Gutierrez-De Frias C, Cortes A (2006) Ontogeny of the immune system of fish. *Fish and Shellfish Immunology* 20(2):126-136.

Zeeshan HM, Lee GH, Kim HR, Chae HJ (2016) Endoplasmic reticulum stress and associated ROS. *International Journal of Molecular Science* 17(3):327.

Zeng H, Nanayakkara GK, Shao Y, Fu H, Sun Y, Cueto R, Yang WY, Yang Q, Sheng H, Wu N, Wang L, Yang W, Chen H, Shao L, Sun J, Qin X, Park JY, Drosatos K, Choi ET, Zhu Q, Wang H, Yang X (2018) DNA checkpoint and repair factors are nuclear sensors for intracellular organelle stresses-inflammations and cancers can have high genomic risks. *Frontiers in Physiology* 9:516.

Zhang Q, Lai MM1, Lou YY, Guo BH, Wang HY, Zheng XQ (2016) Transcriptome altered by latent human cytomegalovirus infection on THP-1 cells using RNA-seq. *Gene* 594(1):144-150.

Zhang X, Lian Z, Padden C, Gerstein MB, Rozowsky J, Snyder M, Gingeras TR, Kapranov P, Weissman SM, Newburger PE (2009) A myelopoiesis-associated regulatory intergenic noncoding RNA transcript within the human HOXA cluster. *Blood* 113(11):2526-2534.

Zhao P, Liu S, Zhong Z, Jiang T, Weng R, Xie M, Yang S, Xia X (2018) Analysis of expression profiles of long noncoding RNAs and mRNAs in brains of mice infected by rabies virus by RNA sequencing. *Scientific Reports* 8:11858.

Zhou Y, Frey TK, Yang JJ (2009) Viral calciomics: interplays between Ca2+ and virus. *Cell Calcium* 46(1):1-17.

Chapter 4

Sea bass immunization to downsize the betanodavirus protein displayed in the surface of inactivated repair-less bacteria

Lama R[1], Pereiro P[1], Novoa B[1], Coll J[2] (2019) Sea bass immunization to downsize the betanodavirus protein displayed in the surface of inactivated repair-less bacteria. Vaccines 7:94. doi: 10.3390/vaccines7030094, ISSN 2076-393X

[1]Institute of Marine Research (IIM), Spanish National Research Council (CSIC), Eduardo Cabello 6, 36298 Vigo, Spain. [2]Biotechnology Department, National Institute for Agricultural and Food Research and Technology (INIA), La Coruña road, 28040 Madrid, Spain.

USC
UNIVERSIDADE
DE SANTIAGO
DE COMPOSTELA

4. Sea bass immunization to downsize the betanodavirus protein displayed in the surface of inactivated repair-less bacteria

4.1 INTRODUCTION

NNVs are non-enveloped particles of icosahedral symmetry enclosing two single-stranded, positive sense RNAs. One of the RNAs encodes an RdRp, while the other encodes their coat protein (C protein). According to C gene-derived protein sequences, betanodavirus isolates from Europe, Asia and Japan could be classified into 4 genotypes, but displaying only 19-23 % differences among them (Nishizawa et al., 1997; Skliris et al., 2001). Most C proteins of geographically-related betanodaviruses share up to 98-99 % of their amino acid sequence.

Different types of NNV killed vaccines have been described (Yong et al., 2017), including those made with inactivated virus (Yamashita et al., 2005; Kai et al., 2008), virus-like particles (VLP) (Lin et al., 2001; Liu et al., 2006; Thiery et al., 2006), recombinant C proteins (Husgard et al., 2001; Yuasa et al., 2002), or synthetic peptides derived from the C protein (Coeurdacier et al., 2003). Most of those have to be delivered by fish-to-fish injection such as intraperitoneal injection of formalin-inactivated betanodaviruses (Yamashita et al., 2009). Thus, an oil-adjuvanted intraperitoneal injectable vaccine that protects 12 g sea bass against the RGNNV genotype for one year has been available for emergencies since 2014 and received market authorizations in 2018 in Spain, Italy, Croatia and Greece (https://www.pharmaq.no/updates/pharmaq-has-rec/). Alternative innovative vaccination immersion protocols have been described for sea bass (Galeotti et al., 2013), and specific antibodies were induced in grouper eggs by vertical transmission from broodfish injected with inactivated NNV (Huang et al., 2017). Vaccination methods against NNV and their corresponding immune responses in European sea bass have been recently reviewed (Buonocore et al., 2019), including oral

delivery alternatives such as those using inactivated bacteria encapsulating dsRNA from NNV, and chitosan conjugated NNV DNA (Yong et al., 2017). Most recently, protection has been reported by using alive recombinant bacteria expressing the C protein sequence mixed with the feed (Gonzalez-Silvera et al., 2019). Although the use of recombinant bacteria will be most appreciated for large scale oral vaccination by avoiding stressful, labour intensive and costly delivery, the release of alive genetically modified organisms (GMOs) will have practical problems. Thus, the presence of recombinant DNA and antibiotic resistance genes in alive or even in inactivated GMOs will raise safety concerns for sustainable aquaculture.

To investigate alternatives to live or dead recombinant bacteria, we have explored here a previously reported platform consisting of formaldehyde-inactivated recombinant bacteria displaying downsized viral antigens in their surface (called spinycterins) (Coll et al., 2017). Such spinycterins were obtained by genetic fusion of selected prokaryotic anchor-motifs to the N-terminal part of small linear immunodominant viral fragments. Despite the high reduction of antigenicity caused by formaldehyde crosslinking, successful production of anti-viral antibodies was demonstrated by immersion of ultrasound-treated zebrafish and/or carps in spinycterins displaying downsized CyHV-3 herpesvirus (Coll et al., 2017). Among the safety advantages, the spinycterin inactivated condition may allow also for lyophilization and/or addition into feeds, contributing also to bypass the low temperature-dependence of fish vaccines. However, several fine-tuning details need improvement to favor further development of spinycterins for small fish vaccines. First, there is no previous evidence that shows that any spinycterin displaying downsized NNV antigens will induce protection against NNV challenge (Coll et al., 2017). Second, crosslinking by formaldehyde inactivation caused a ~80% antigenicity loss (Coll et al., 2017). Third, the yields of expression of some the anchor fusions were low or inhibited bacterial growth (Coll et al., 2017). Fourth, safety concerns may still remain when handling and releasing to the environment large amounts of recombinant bacteria and those need to be minimized even when using GMOs which may have some of their DNA intact despite inactivation. Therefore,

improvements in the above-mentioned concepts were explored in spinycterins made with downsized NNV antigens.

Because the fish host NNV antigenicity is focused on its coat protein, downsizing of the C protein was performed as a means to increase its expression levels in recombinant *Escherichia coli* while maintaining the immunogenic potential of the antigen (Costa et al., 2007; Chen et al., 2015a). To provide for bacterial surface display, several prokaryotic membrane anchor-motifs were fused to the downsized C protein. The anchor-motifs employed in this work, included those used before (Coll et al., 2017) and the P9 anchor-motif identified in the envelope of phage Φ6 (Jung et al., 2015). Because of the importance of nodaviruses in the aquaculture of commercially important fish species such as sea bass and sea bream, we chose one of them (sea bass) to validate protection of spinycterins against the NNV challenge.

To preserve the initial immunogenicity of recombinant bacteria in the resulting spinycterins, several alternative methods to formaldehyde inactivation were explored. Among the many alternatives described before, bactericidal drugs appeared to be an attractive possibility since they allow for 100 % of preservation of antigenicity, while maintaining intact the recombinant bacterial morphology and their inherent adjuvanticity. Among the described bactericidal drugs, those that target double-stranded DNA, introducing stable breaks into its strands by covalent binding and causing dead by oxidative ROS (i.e., bacterial DNA gyrase inhibitors), were preferred in contrast to those targeted to bacterial DNA-dependent RNA synthesis (i.e., rifampicins), cell-wall envelopes (wall synthesis inhibitors), and/or bacterial protein translation (synthesis inhibitors) (Molloy et al., 2000). Therefore, we explored the possibilities of some of these drugs to irreversibly inactivate surface displaying bacteria in a cost-efficient manner preferably by damaging their double stranded DNA by introducing stable breaks.

In addition, to increase safety we explored the DNA-repair deficient BLR(DE3) strain. In contrast to the BL21(DE3) *E. coli*, the derived BLR(DE3) strain cannot repair double DNA strand breaks, nor revert antibiotic-dependent ROS oxidation damage, thus making their

derived recombinants more susceptible to DNA inactivation methods (Jeong et al., 2006). Additionally, the BLR(DE3) strain is resistant to tetracycline (TetR) which is more convenient for large-scale manufacturing because it makes possible to reduce any possible contaminant bacterial growth. Furthermore, BLR(DE3) requires Isoleucine (Ileu-) in the culture media to grow (Schmidt et al., 2007), opening the possibility to develop antibiotic-independent recombinant selective methods to reduce the possibilities to spread resistant genes. All these characteristics make BLR(DE3) highly advantageous for large-scale production, but it is not yet known whether BLR(DE3) can be used to produce spinycterins.

The results obtained in this work showed that a new bacterial culture media containing soy-bean rather than casein hydrolysates made anchor-antigen expression more reproducible by delaying autoinduction and eliminating the IPTG requirement. In addition, Ciprofloxacin inactivation irreversibly damaged the DNA of the recombinant bacteria by covalent binding to the DNA strands and killed the bacteria by oxidative ROS mechanisms while preserving all antigen immunogenicity, therefore increasing safety during both manipulations and delivery of the resulting spinycterins. Finally, BLR(DE3) was a good substitute for BL21(DE3), adding another safety level. Because of all these properties, irreversibly DNA-damaged recombinant BLR(DE3) displaying downsized viral antigens may be used to further develop new adjuvant-less spinycterin vehicles for NNV antigens in an environmental safer way. These spinycterins may not only contribute to move ahead the state-of-the art of small fish viral vaccinology but also other veterinary vaccination procedures.

4.2. MATERIALS AND METHODS

4.2.1. Construction of downsized NNV coat sequence and genetic fusion to prokaryotic anchor-motifs

The frg$C_{91–220}$ sequence (amino acid residues 91–220) was derived from the C protein of NNV isolate AY284959 from *D. labrax* (Costa et al., 2007; Chen et al., 2015a). The C protein-derived sequence was fused downstream of 6 different bacterial membrane anchor-motif sequences (Table 4.1). The different constructs were genetically fused

by arbitrary flexible linkers (corresponding to the amino acid sequence GlicSerGliSer, GSGS). All the corresponding DNA sequences were chemically synthesized (GeneArt, Regensburg, Germany) and subcloned in between the NdeI and HindIII restriction sites of the pRSET prokaryotic expression plasmid which adds poly-histidine tails (polyH) at the C-terminal end of its multiple cloning site. Therefore, the general formula of the resulting recombinant constructs was: NH2-anchor + GSGS + frgC$_{91–220}$ + GSGS + polyH-COOH. The purified plasmids were then transfected by the $CaCl_2$ method into BL21(DE3) or BLR(DE3) *E. coli* strains and grown in either TB or SB media (Table 4.2) at 37 ˚C.

Table 4.1. Fused to the *N*-terminus of frgC$_{91-220}$ and resulting molecular weights.

Name	AccNum	KDa	References
frgC$_{91-220}$	AY284969	16.2	Ucko et al., 2004
Mistic + frgC$_{91-220}$	AY874162	28.9	Roosild et al., 2005; Alves et al., 2017
Nmistic + frgC$_{91-220}$	AY874162	20.0	Roosild et al., 2005; Alves et al., 2017
NTD + frgC$_{91-220}$	AJ516945	18.4	Park et al., 2013
P9 + frgC$_{91-220}$	M12921	25.6	Jung et al., 2015
YAIN + frgC$_{91-220}$	NP_414891	26.3	Leviatan et al., 2010
YBEL + frgC$_{91-220}$	NP_415176	34.8	Leviatan et al., 2010

AccNum, Gen Bank accession numbers. FrgC91–220, amino acid residues 91–220 from the C coat protein of viral nervous necrosis virus NNV (sequence accession number AY284959) (Costa et al., 2007; Chen et al., 2015a). The anchor-motif + GSGS + frgC$_{91-220}$ + GSGS + polyH DNA sequences were designed, synthesized, cloned into pRSET, used to transform *E. coli* and autoinduced in SB medium. KDa, expected molecular weight of the recombinant proteins. Mistic and N-mistic, 110 and 33 N-terminal amino acids anchor-motif from the Mistic gene from *Bacillus subtilis*. NTD, N-terminal domain of 21 amino acids anchor-motif of the exosporal BclA protein from *Bacillus anthracis*. P9, 90 amino acid anchor-motif from the coat-protein of bacteriophage Φ6. YAIN, 91 amino acid anchor-motif from the hydrophilic regulatory protein of the frmR operon of *E. coli* YBEL, 160 amino acid anchor-motif from the hydrophilic HTH-type transcriptional regulator DUF1451 family protein from *E. coli*.

4.2.2. Induction of protein expression and inactivation of antigen surface-displaying recombinant bacteria

The BL21(DE3) *E. coli* strain has been widely used for recombinant protein expression including previously reported spinycterins for fish immunization to CyHV-3 herpesvirus (Coll, 2017). The BLR (DE3) is a DNA-repair deficient transposon derivative strain

of the BL21(DE3), lacking recombinaseA (RecA-) (Goffin and Dehottay, 2017), having tetracycline resistance and requiring isoleucine for growth (Schmidt et al., 2007) (F_ ompT hsdSB(rB_ mB_) gal dcm (DE3) D(srl _ recA)306:Tn10 (TetR)) (Novagen). To produce spinycterins, BL21(DE3) or BLR(DE3) recombinant bacteria were grown overnight by strong agitation at 37 ˚C in 40 mL of TB or SB medium (see composition in Table 4.2) with 100 µg/mL of ampicillin for the BL21(DE3) strain or 100 µg/mL ampicillin, and 12.5 µg/mL tetracycline for the BLR(DE3) strain. To induce recombinant protein expression, either 0.5 mM IPTG was added every 2 h twice in TB media or autoinduction was allow to proceed during 4 days in SB media. The resulting bacteria were washed in PBS, and adjusted to a final concentration of 10^{10} cfu/mL. To irreversibly damage their DNA, Ciprofloxacin was added at 50 µg/mL, and incubated at room temperature for 2 h with agitation. The resulting spinycterins were finally washed with PBS, 20 % glycerol was added to preserve bacterial morphology, followed by storage at -20 ˚C until use.

Table 4.2. Comparison of *E. coli* culture media.

Component	Concentration, %	TB	SB
Yeast extract	2.4	X	X
Glycerol	0.8	X	X
KHPO4	0.9	X	X
KH2PO4	0.2	X	X
Tryptone	1.2	X	-
Soybean hydrolysate	4.8	-	X
Glucose	0.3	-	X

Products were from Sigma-Aldrich.

4.2.3. Characterization of the expression of pRSET-anchor + frgC$_{91–220}$ coded proteins

Confirmation of anchor + frgC$_{91–220}$ + polyH expression was performed in spinycterin pellets boiled in buffer containing SDS and mercaptoethanol. The proteins separated in gels (SDS-precast 4–20 % polyacrylamide gels from BioRad) were either stained by Coomassie-blue or transferred to nitrocellulose membranes (BioRad) for Western blotting. For blotting, the membranes were blocked with dilution buffer (0.5 % BSA, 5 % of skim milk, 0.1 % Tween-20, 0.01 % merthiolate, 0.005 % phenol red in PBS pH 6.7). Membranes were then incubated

with peroxidase labeled anti-polyH monoclonal antibody (Sigma-Aldrich). Bands were visualized using diaminobenzidine DAB stain.

4.2.4. Assay of anchor + frgC$_{91–220}$ + polyH enrichment on the bacterial surface

To assay the anchor + frgC$_{91–220}$ + polyH enrichment, the spinycterins were first "shaved" by partial digestion with 1% of trypsin during 2 h at 37 ˚C. Control undigested spinycterins were incubated in parallel with PBS. Trypsin-dependent digestion levels were then estimated by polyacrylamide gel electrophoresis (PAGE) and by ELISA.

To assay by PAGE, the amounts of recombinant bands after Coomassie blue staining of PAGE were compared between trypsin-digested and control undigested spinycterins. The resulting Coomassie-stained PAGE bands were densitometrized by Image J 1.41o (http://rsb.info.nih.gov/ij). The percentage of the recombinant protein bands relative to the total protein bands was first normalized by the formula, optical density of the recombinant anchor + frgC$_{91–220}$ + polyH band/total optical density of the corresponding spinycterin proteins. The optical densities were then expressed relative to the optical density of frgC$_{91–220}$ spinycterins by the formula, 100 x % of the anchor + frgC$_{91–220}$ + polyH/% of frgC$_{91–220}$ + polyH.

To assay by ELISA, several dilutions of the trypsin-digested and control undigested spinycterins were used to coat wells of polystyrene plates of Maxisorb 96-wells by overnight incubation to dryness at 37 ˚C. The coated solid-phases were then blocked by overnight incubation with 100 µL per well of dilution buffer (0.5 % BSA, 0.1 % Tween-20, 0.01 % merthiolate, 0.005 % phenol red in PBS pH 6.7) containing 10 µg per well of skimmed milk (Sigma-Aldrich). After washing, the wells were incubated with peroxidase-labeled anti-polyH monoclonal antibody (Sigma-Aldrich) in 50 µL per well during 60 min. After washing 3 times, the colour reaction was developed by adding 50 µL of 1 mg/mL o-phenylenediamine in citrate buffer containing 3 mM H_2O_2. Absorbances were measured by reading at dual-wave lengths at 492–620 nm to correct for individual differences between wells. PolyH binding was calculated in percentage by the formula, 100x absorbance

after trypsin digestion/absorbance of undigested samples. The percentage of absorbance was then expressed relative to frg$C_{91–220}$ spinycterins by the formula, 100 x absorbance of the anchor + frg$C_{91–220}$ + polyH/absorbance of frg$C_{91–220}$ + polyH.

4.2.5. Immunization with surface-displaying bacterins by intraperitoneal injection

Groups of 15-20 fingerling sea bass (*D. labrax*) of ~10 g of body weight were acclimatized for 30 days to sea water aquaria closed-circuits of 60 L each. Fish from two independent aquaria for each spinycterin antigen were injected with 100 µL of PBS (two independent intraperitoneal injections of 50 µL each per fish) containing 10^8 cfu of frgC_{91-220} + polyH, Nmistic + frgC_{91-220} + polyH or YBEL + frgC_{91-220} + polyH spinycterins. Non-infected, infected with the empty pRSET plasmid and non-immunized controls were also included. The fish were fed with commercial pellets and maintained at 26 ˚C during 30 days. Viral challenge was performed by intramuscular injection of 100 µL of the NNV strain 475-9/99 (2 x 10^4 $TCID_{50}$/mL) of the RGNNV genotype provided by the Instituto Zooprofilacttico delle Venize (Italy) isolated from *D. labrax (*Bovo et al., 1999). Mortalities were recorded daily. Relative percentage of survival was calculated by the formula, 100-percentage of mortality in the spinycterin-immunized NNV-challenged fish/percentage of mortality in the non-immunized NNV-challenged fish.

4.2.6. Ethic statement on fish handling

Fish care and challenge experiments were reviewed and approved by the CSIC National Committee on Bioethics under approval number ES360570202001/16/FUN01/PAT.05/tipoE/BNG, following the National Guidelines for type III experimentation (Annex X, permission RD53/2013) and the EU directive 2010/63/EU for animal experiments (http://ec.europa.eu/environment/chemicals/lab_animals/ legislation_en.htm). To record possible mortalities, the immunized fish were monitored daily 2-4 times during 1 month. MS222 was used to euthanize moribund fish by an overdose of MS222 (200 mg/mL) to minimize suffering.

4.3. RESULTS

4.3.1. Selection of the frgC$_{91-220}$ sequence from the betanodavirus C coat protein

To select an immunorelevant NNV antigen for sea bass vaccination, the C protein was chosen because it is the only target for fish neutralizing antibodies. Since a minimal antigen size favors expression on *E. coli* taking into account the additional increment of molecular size because of the fusion with a prokaryotic membrane anchor required for surface display, we studied the best way to downsize the C protein. Since targeted epitopes of both neutralizing monoclonal antibodies and serum samples from NNV-infected survivor fish were mapped at amino acid positions 1-32, 91-162 and 181-212 (Baudin-Lurencin and Richards, 1999; Costa et al., 2007), the fragment extending from the 91 to the 220 amino acid was chosen for optimal antigenic expression on *E. coli*. The frgC$_{91–220}$ contained most of the C shell domain (S-domain) located between amino acid residues 52–213 (Chen et al., 2015b) (Figure 4.1A, B), the highest hydrophilic regions of exposed amino acid residues on the viral surface (Figure 4.1A), three cysteines, all the Ca^{2+} binding sites implicated in subunit-subunit C-interactions in the viral shell structure (Chen et al., 2015b) and most of the neutralizing B-cell epitopes mentioned above (Baudin-Lurencin and Richards, 1999; Costa et al., 2007). By choosing the frgC$_{91–220}$, we avoided the highly hydrophobic 1-32 signal peptide which is deleterious to *E. coli*. We also avoided the 223-331 region that contains most of the sequence variability among NNV isolates (Skliris et al., 2001) providing a common immunogen for a wider number of NNV isolates. Finally, the three cysteins were mutated to serines during the gene synthesis to avoid the formation of *E. coli* inclusion bodies with reduced-immunogenicity.

To select for the best anchors to increase bacterial membrane expression, several prokaryotic anchor-motifs were genetically fused to frgC$_{91–220}$. Those included Mistic, Nmistic, NTD, P9, YAIN and YBEL (Roosild et al., 2005; Dvir et al., 2009a; Dvir et al., 2009b; Blain et al., 2010; Leviatan et al., 2010; Nekrasova et al., 2010; Petrovskaya et al., 2010; Park et al., 2013; Jung et al., 2015). Most of these anchor-motifs

were already described when fused to a CyHV-3 herpesvirus fragment (Coll, 2017), but the genetic fusion to P9 (Jung et al., 2015) is described here for the first time. The P9 protein of 90 amino acids constitutes the major envelope of phage Φ6. It was proposed as a bacterial anchor alternative because it facilitated the integration of 11 of 14 target proteins into the *E. coli* cell membrane (Jung et al., 2015). Therefore, the general formulas of the resulting recombinant constructs were NH2-prokaryotic membrane anchor-motif + GliSerGliSer (GSGS) linker + $frgC_{91–220}$ + GSGS linker + polyHis(H)-COOH (Figure 4.2). The expected molecular weights of the recombinant products fused to the selected prokaryotic anchors varied from 20 to 34.8 KDa while the $frgC_{91–220}$ was 16.2 KDa (Table 4.1).

4.3.2. Autoinduction media to improve anchor-fused $fgrC_{91-220}$ expression

Previous results revealed partial or total inhibition of expression of some of the anchors in the fused constructs with herpes viral proteins coded in pRSET plasmids under the control of T7/lactose promoters in BL21(DE3) *E. coli* (Coll, 2017). Most probably the presence of lactose in the casein hydrolysates of LB/TB media contributed to an early autoinduction which resulted in toxicity during the growth phase, similarly to what has been reported in other T7/lac promoter expression systems (Studier, 2005; Studier, 2014). To reduce early autoinduction, the casein hydrolysate broth (LB/TB) was substituted by soy-bean hydrolysate broth (SB). Because of the small amounts of galactose in SB, a weaker inducer than lactose, soy-bean hydrolysates may be used for delaying autoinduction to the stationary phase, thus increasing yields and reproducibility (Studier, 2005; Xu et al., 2012). Furthermore because of its plant origin, the SB medium contains no animal infectious contamination, which is important for large-scale production and release into the environment. After numerous tests, the composition of the SB media for maximal and reproducible yields of autoinducible expression of anchored $frgC_{91–220}$ resulted in the formula shown in Table 4.2.

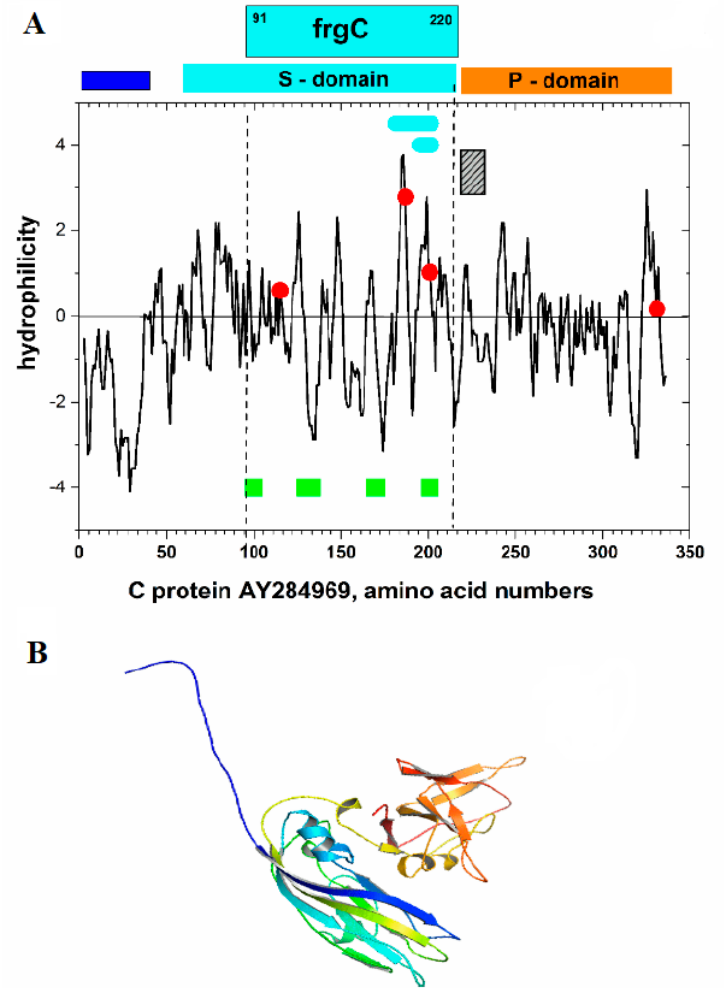

Figure 4.1. Scheme of the hydropathicity and tridimensional structure properties of frgC$_{91-220}$. A Hydropathicity plot of the coat protein C from the *D. labrax* encephalitis virus isolate DL-040899-IL (AY284969). Shell (S, blue rectangle) and protrusion (P, red rectangle) domains were located at amino acid residues 52–213 and 221–338, respectively, according to X-ray data (Chen et al., 2015b). Blue top rectangle, frgC$_{91-220}$ (amino acid residues 91–220). Blue horizontal lines inside the plot, neutralizing B-cell epitopes. Red circles, cysteine positions which were mutated to serines in the recombinant frgC$_{91-220}$. Green squares, Ca^{2+} binding sites for subunit-subunit interactions in the betanodavirus shell structure. Grey hatched rectangle, highest protein sequence variability among betanodavirus isolates corresponding to the 223-331 amino acid positions. **B** Scheme of the tridimensional structure of the C protein of the AY284969 isolate. The automatically predicted modelled structure of the C protein of the AY284969 isolate.

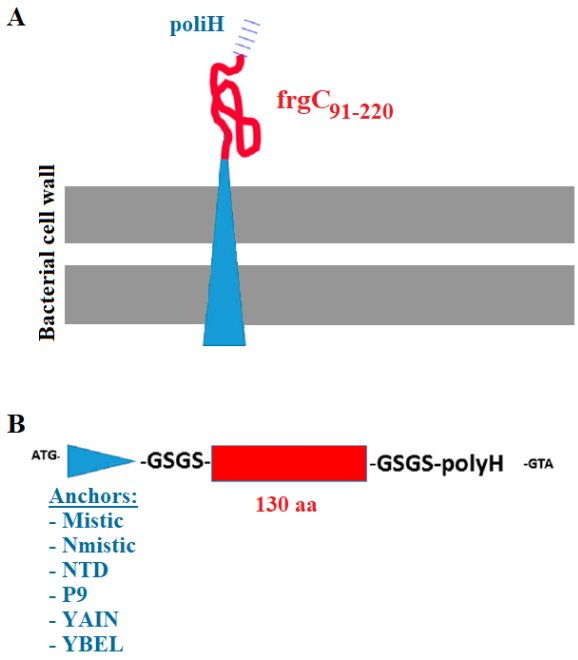

Figure 4.2. Scheme of the genetically fused constructs for bacterial surface expression of fgrC$_{91\text{-}220}$. The nucleotide sequences corresponding to the frgC$_{91\text{-}220}$ of NNV were fused downstream to each of the 6 bacterial membrane anchor-motif sequences described in Table 4.2. Red, frgC$_{91\text{-}220}$. Blue triangles, anchor-motifs. Gray, schematic bacterial membrane. Blue lines, C-terminal polyH tail.

E. coli BL21(DE3) clones transformed with each of the anchor + frgC$_{91–220}$ pRSET plasmids were selected from SB agar plates in the presence of ampicillin and grown in 2 mL SB cultures. All the recombinant proteins fused to any of the 6 anchors were efficiently expressed in *E. coli* (Figure 4.3A), in contrast to the variability previously observed when grown in TB (Coll, 2017). Densitometry estimations of each of the anchor + frgC$_{91–220}$ proteins separated by PAGE and identified by the expected molecular weights of their Coomassie-blue stained bands (Table 4.1) and western blots using anti-polyH antibodies (Figure 4.3C) varied between 4.1 to 8.4 % (n = 3) of the total stained protein in each of the *E. coli* extracts, while the estimate of the frgC$_{91–220}$ in the absence of any anchors was 4.5 ± 1.3 % (Figure

4.3B). The YBEL + frgC$_{91–220}$ spinycterins showed the highest expression level (8.4 ± 3.2 %).

We then selected one of the lower and the higher molecular weight constructs (Nmistic and YBEL, respectively) to scale up production for additional testing. The results confirmed that slightly lower but similar yields of recombinant products could be produced in 40 mL cultures. Thus, 2.4 ± 0.7 %, 2.7 ± 0.3 and 4.6 ± 2.1 % of stained protein were estimated for the frgC$_{91–220}$, Nmistic + frgC$_{91–220}$ and the YBEL + frgC$_{91–220}$ constructs, respectively (not shown).

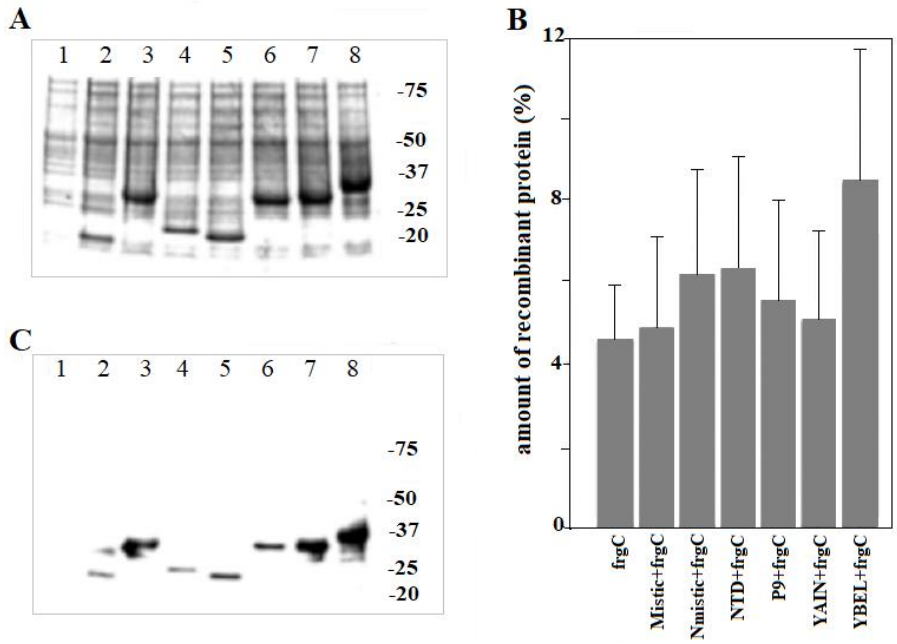

Figure 4.3. A Coomassie-blue staining and B its graphical representation and C western blotting of anchor-motif+frgC$_{91-220}$ spinycterins grown and autoinduced in SB medium. **A** BL21 (DE3) *E. coli* coding for anchor-motif + frgC$_{91-220}$ + polyH recombinant proteins analysed by Coomassie-blue staining. One representative experiment is represented. **B** Densitometry of the anchor-motif + frgC$_{91-220}$ recombinant bands stained by Coomassie. Means and standard deviations are shown (n = 3). **C** Western blotting of gels. One of 3 experiments was represented. Numbers to the right of the gels, KDa positions of molecular weight markers. The anchor-motifs of the recombinant *E. coli* in **A** and **C** corresponded to lanes: 1, empty plasmid. 2, frgC$_{91-220}$. 3, Mistic + frgC$_{91-220}$. 4, Nmistic + frgC$_{91-220}$. 5, NTD + frgC$_{91-220}$. 6, P9 + frgC$_{91-220}$. 7, YAIN + frgC$_{91-220}$. 8, YBEL + frgC$_{91-220}$.

4.3.3. Inactivation of recombinant *E. coli* by DNA-damage

To be safely handled and released to the environment, the bacteria expressing the anchor + frg$C_{91–220}$, need to be irreversibly inactivated. However, alternative inactivation methods were needed to improve the loss of antigen reactivity shown before by crosslinking with formaldehyde (Coll, 2017). Preliminary experiments performed with YBEL + frg$C_{91–220}$ BL21(DE3) *E. coli* showed no colony formation after treatment with Ciprofloxacin and Leucofloxacin at the lowest 20 µg/mL concentration tested in contrast to Oxolinic acid, Rifampicin and controls without any treatment (Figure 4.4A). Furthermore, no significant changes in the level of expressed YBEL + frg$C_{91–220}$ recombinant protein were observed when the spinycterin extracts were separated by PAGE stained with Coomassie-blue (Figure 4.4B). After exploring these results drugs damaging the bacterial DNA appeared among the most convenient since they inhibited bacterial colony formation at low concentrations preserving recombinant protein levels. To select for a suitable drug to irreversibly damage the DNA of *E. coli*, several selected antibiotics and/or base analogs (Oxolinic acid, Levofloxacin, Ciprofloxacin, BrdU, Fluoracin, Thioguanine, Rifampicin, and Mitomicin C) were screened at different concentrations for inhibition of replication of YBEL + frg$C_{91–220}$ spinycterins made in BL21(DE3) *E. coli*. According to the corresponding survival concentration-dependent curves, the most active compounds were Ciprofloxacin (CPFX) and 5-Fluoracin (Figure 4.5). CPFX was selected for further studies because it cleaves and links to DNA strands and causes oxidation-related bactericidal effects. In addition, CPFX was easily available at a low price and in contrast to some of the other drugs, up to 1,600 µg/mL did not affect the levels of recombinant protein expression, as estimated by Coomassie-blue staining of the resulting spinycterin extracts after overnight incubation (not shown).

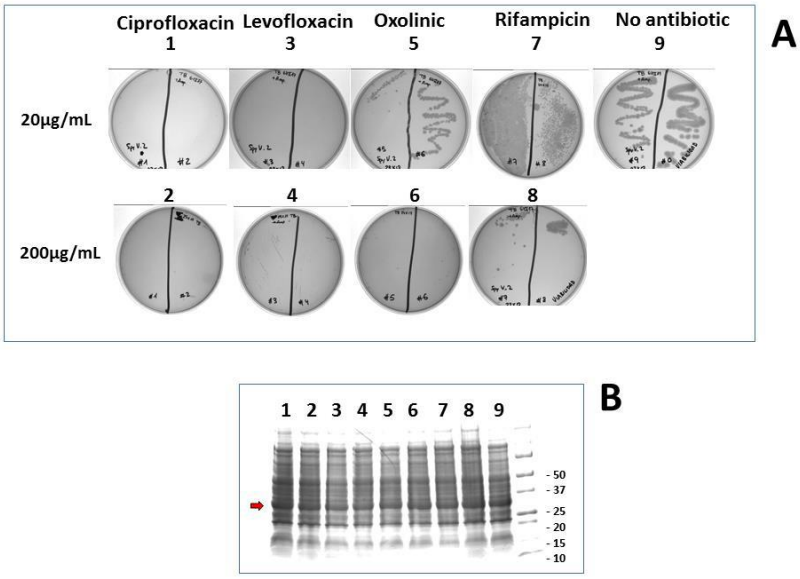

Figure 4.4. Inhibition of colony formation of YBEL + frgC91–220 spinycterins by quinolones and rifampicin for *E. coli* BL21(DE3) inactivation **(A)** and preservation of recombinant protein levels **(B)**.

4.3.4. Recombinant protein expression levels were lower when using the DNA-repair deficient BLR(DE3) *E. coli* strain

To compare the expression levels of the recombinant display constructs in the BL21(DE3) and the repair-less BLR(DE3) *E. coli*-derived spinycterins, both were grown in parallel 40 mL cultures. Results showed a higher expression level in comparison with the 2 mL cultures (Figure 4.6). However, while the $frgC_{91–220}$ was similarly expressed in the two *E. coli* strains (14.3 ± 4.5 % and 12.3 ± 3.7 %, respectively, n = 2), the expression level of the corresponding Nmistic + $frgC_{91–220}$ and YBEL + $frgC_{91–220}$ was lower when produced in the BLR(DE3) than in the BL21(DE3) strain (5.4 ± 0.4 % and 12.4 ± 0.5 %, respectively, in BLR compared to 17.7 ± 0.2 % and 36.3 ± 5.4 %, respectively, in BL21, n = 2).

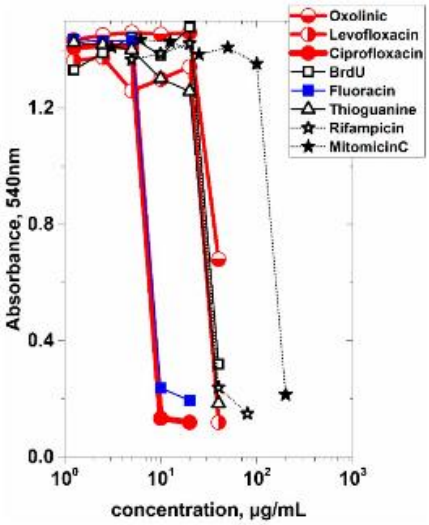

Figure 4.5. Selection of drugs for inactivation of recombinant *E. coli* BL21(DE3). Bacterial growth was estimated by absorbance at 540 nm after overnight incubation with agitation at 37 ˚C. Upper-half open red circles, Oxolinic acid. Left-half open red circles, Levofloxacin. Solid red circles, Ciprofloxacin. Open squares, 5-Bromo deoxiuridine. Solid blue squares, 5-Fluoracin. Open triangles, 6-Thioguanine. Open stars, Rifampicin. Solid starts, Mitomicin C.

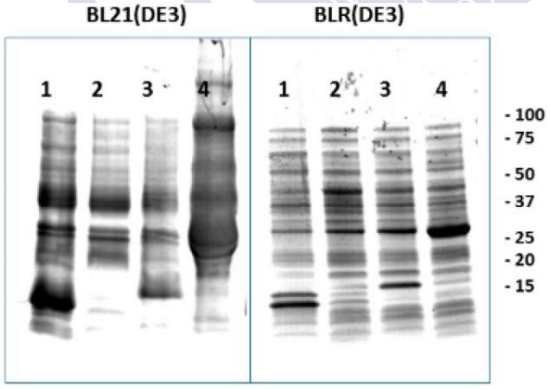

Figure 4.6. Coomassei-blue staining of polyacrylamide gel electrophoresed anchor-motif + frgC$_{91\text{-}220}$ spinycterins obtained in large amounts in BL21(DE3) and BLR(DE3) *E. coli* strains. *E. coli* coding for anchor-motif + GSGS+frgC$_{91\text{-}220}$ + GSGS + polyH recombinant proteins was obtained in either BL21(DE3) or in the repair-deficient *recA*- BLR(DE3) *E. coli* strains. Extracts were analysed as described in Figure 4.3. One of 2 experiments was represented. Numbers to the right of the gels, KDa positions of Coomassie blue stained molecular weight markers. Lanes: 1, frgC$_{91\text{-}220}$ spinycterins. 2, empty pRSET plasmid spinycterins. 3, Nmistic + frgC$_{91\text{-}220}$ spinycterins. 4, YBEL + frgC$_{91\text{-}220}$ spinycterins.

To test for the irreversibility of inactivation by the CPFX treatment, the BLR(DE3) Nmistic + frgC$_{91–220}$ or YBEL + frgC$_{91–220}$ bacteria were treated with several concentrations of CPFX and the viability of the resulting spinycterins tested by both overnight growth in TB-ampicillin-tetracycline plates and several days overgrowth in 2 mL of TB-ampicillin-tetracycline medium. No colonies nor growth could be detected after treatment with 1 µg/mL of CPFX, in contrast to untreated bacteria with an initial inocula of 10^9 cfu (not shown). This CPFX dosage was ~100-fold lower than the inactivation obtained for the BL21(DE3) strain (Figure 4.5), most probably due to the DNA-repair deficiency of the BLR(DE3) strain.

4.3.5. Surface expression of Nmistic + frgC$_{91-220}$ and YBEL + frgC$_{91-220}$ in BLR(DE3) spinycterins

To estimate the surface enrichment of frgC$_{91–220}$ in the selected spinycterins, PAGE and ELISA experiments were carried out after partially "shaving" the corresponding spinycterin surfaces by limited trypsin digestion. The higher surface exposure of frgC$_{91–220}$ should be more susceptible to trypsin digestion and therefore should show a stained-band of lower intensity by PAGE and a lower anti-polyH binding absorbance by ELISA. Surface exposure of frgC$_{91–220}$ estimated by comparing the Coomassie-blue stained bands of anchor + frgC$_{91–220}$ with those from frgC$_{91–220}$ spinycterins showed that the most exposed levels were obtained for the YBEL + frgC$_{91–220}$ spinycterins (55.5 ± 5.3 % stained band intensity remaining after trypsin digestion) followed by the Nmistic + frgC$_{91–220}$ (79.05 ± 5.8 %) spinycterins (Figure 4.7A), suggesting that the YBEL + frgC$_{91–220}$ had the highest surface exposure. The polyH binding of frgC$_{91–220}$ to peroxidase labelled anti-polyH antibodies after trypsin digestion estimated by ELISA showed again that the best levels of surface expression were obtained for the YBEL + frgC$_{91–220}$ spinycterins (60.4 ± 13.5 % anti-polyH binding after trypsin digestion) followed by the Nmistic + frgC$_{91–220}$ spinycterins (83.6 ± 40.1 %) compared to frgC$_{91–220}$ spinycterins (Figure 4.7B). Therefore, the results obtained by both methods confirmed that the surface exposure of frgC$_{91–220}$ was higher in the YBEL + frgC$_{91–220}$ than in the Nmistic + frgC$_{91–220}$ BLR(DE3) spinycterins.

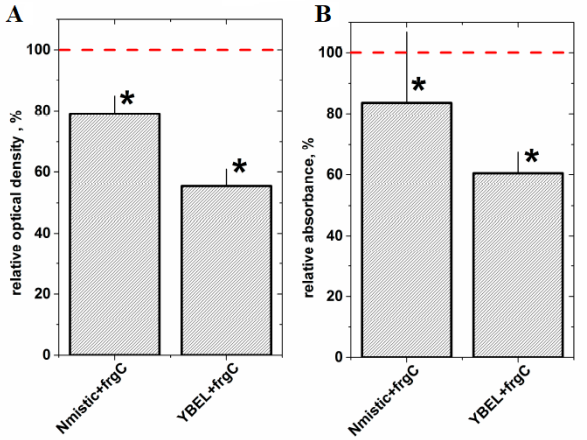

Figure 4.7. Estimation of frgC$_{91-220}$ surface enrichment by partial trypsin digestion of BLR(DE3) spinycterins followed by A PAGE and B ELISA analysis. Means and standard deviations (n = 3) are presented. Red horizontal dashed lines, mean optical density **A** and absorbance **B** of frgC$_{91-220}$ spinycterins *, significatively different from frgC$_{91-220}$ spinycterins as determined by the Student t-test ($p < 0.05$).

To explore whether additional paraformaldehyde-based crosslinking methods could be applied to inactivate spinycterins or to further inactivate CPFX-spinycterins, surface exposure of the anchor + frgC$_{91–220}$ + polyH was estimated by anti-polyH binding after paraformaldehyde treatment. Results showed that while the polyH reactivity of bacterins expressing the Nmistic + frgC$_{91–220}$ was nearly unaffected by the paraformaldehyde treatment, those expressing the larger molecular weight YBEL + frgC$_{91–220}$ lost most of their anti-polyH binding (Figure 4.8). These results showed that although alternative crosslinking methods, such as paraformaldehyde, could be used to inactivate spinycterins, these possibilities may depend on the anchor-motif employed for surface expression. The differences detected between the anti-polyH binding of the YBEL + frgC$_{91–220}$ and the Nmistic + frgC$_{91–220}$ BLR(DE3) spinycterins could be due to the larger content in primary amino-exposing lysine and arginine amino acids per mol of the highly hydrophilic YBEL anchor compared to the Nmistic anchor (7 and 14 compared to 4 and 1, respectively).

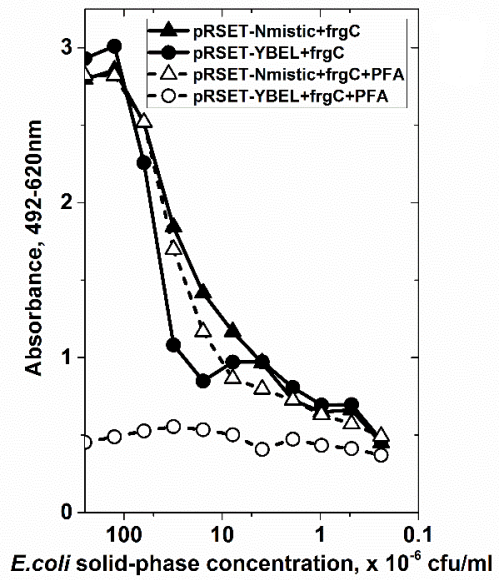

Figure 4.8. Anti-polyH binding of Nmistic + frgC$_{91-220}$ and YBEL + frgC$_{91-220}$ spinycterins without or with paraformaldehyde (PFA) treatment.

4.3.6. *In vivo* protection against NNV challenge using spinycterins obtained in BLR(DE3) *E. coli* displaying anchor + frgC$_{91-220}$

The YBEL + frgC$_{91–220}$ and the Nmistic + frgC$_{91–220}$ BLR(DE3) spinycterins were intraperitoneally injected to fingerling sea bass to validate possible protection against NNV challenge. Two independent aquaria were used to maintain the fish for each spinycterin injected. After the NNV challenge, total mortalities obtained by adding the results from each of the two aquaria resulted in 25.7 % mortality of the non-immunized but NNV-challenged controls. Similar results were obtained for the fish injected with the empty pRSET plasmid. The protection level expressed in relative percent survival was 100 % in fish injected with the YBEL + frgC$_{91–220}$ spinycterins, while it was 62.3 % in those injected with the Nmistic + frgC$_{91–220}$ spinycterins. In contrast, a survival of 2.7 % was obtained for those fish injected with the frgC$_{91–220}$ spinycterins (Figure 4.9). A correlation between protection and surface exposure levels was suggested by comparing the above-mentioned results and those from Section 4.3.5.

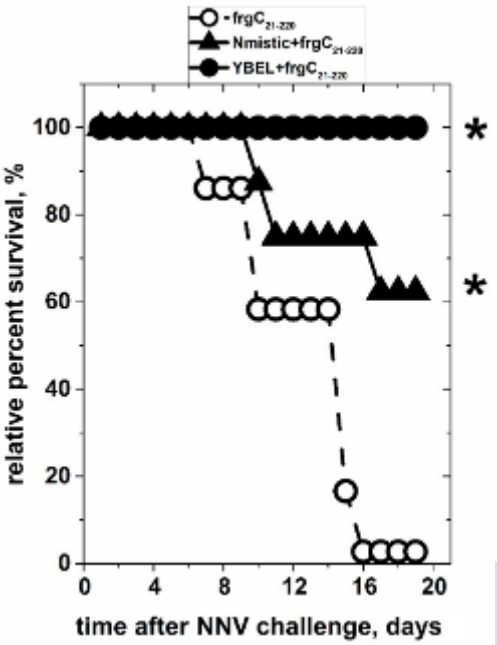

Figure 4.9. Protection to NNV challenge of sea bass juveniles after intraperitoneal injection of frgC$_{91-220}$, Nmistic + frgC$_{91-220}$ or YBEL + frgC91-220 BLR(DE3) spinycterins. *, significantly different from the frgC$_{91-220}$ survival by the Log-Rank (Mantel-Cox) test at the $p < 0.05$ level. Open circles, fish injected with frgC$_{91-220}$ spinycterins. Closed triangles, fish injected with Nmistic + frgC$_{91-220}$ spinycterins. Closed circles, fish injected with YBEL + frgC$_{91-220}$ spinycterins.

4.4. DISCUSSION

This work describes 100% protection of sea bass juveniles against NNV challenge by spinycterin vehicles and a direct correlation between bacterial surface exposure and fish protection levels. The high level of protection was obtained in the absence of adjuvants with irreversibly DNA-damaged DNA-repair-less spinycterins. Furthermore, to our knowledge, this is the first time that inactivated bacteria displaying a recombinant cystein-free downsized C NNV-terminal antigen (frgC$_{91–220}$) containing most of the epitopes targeted by fish neutralizing antibodies (B-cell epitopes) have been described for inducing protection against NNV challenge. The frgC$_{91–220}$ was fused to several prokaryotic membrane anchors to select the ones with higher membrane expression in *E. coli*. A correlation between the levels of bacterial

surface expression and fish protection was demonstrated by comparing the corresponding data obtained with YBEL + frgC$_{91–220}$ spinycterins (higher frgC$_{91–220}$ surface display and full protection) with those of Nmistic + frgC$_{91–220}$ (lower frgC$_{91–220}$ surface display and partial protection) and frgC$_{91–220}$ (lowest frgC$_{91–220}$ surface display and lowest protection) spinycterins. These relatively high protection levels were obtained despite the selected frgC$_{91–220}$ being located outside of the most important shell protrusion C-terminal domain (P domain, amino acids 214–338) in both VLP (Somrit et al., 2017) and whole virus (Chen et al., 2015b), which could had been expected to be more antigenic based only on predicted structural criteria (Figure 4.1B).

On the other hand, to improve spinycterin manufacturing, yields, reproducibility and safety, the following strategies were combined: a novel and scalable autoinduction soy-bean based media for *E. coli* expressing recombinant proteins under the control of the T7/lac promoter, inactivation through an irreversible DNA-damage alternative to traditional crosslinking inactivation, and a DNA repair-less *E. coli* strain as chassis.

A new auto-induction medium for BL21(DE3) *E. coli* culture was developed based on previous reports to reduce overexpression toxicity of some recombinant proteins (Studier, 2005; Sivashanmugam et al., 2009; Studier, 2014). Thus, we had previously found that the expression of some of the anchor-fusions to immunogenic proteins in *E. coli* under the T7/lac promoter control grown in bacterial culture media based on casein hydrolysates, such as LB or TB, were partially or totally inhibited, apparently due to toxicity during the growth phase (Coll, 2017). Since such toxicity may be caused by early autoinduction of *E. coli* due to the presence of lactose in the casein hydrolysates during their fast growth rate (Studier, 2005), we undertook a series of experiments to reduce the residual lactose content of the culture media. Those experiments lead us to develop the so-called SB medium, a bacterial culture medium based on vegetable soy-bean rather than casein hydrolysates of animal origin. To further reduce autoinduction, glucose was also added to the media as previously recommended (Studier, 2005). Using the SB media, the highest expression levels by PAGE/Western blotting were obtained for the YBEL + frgC$_{91–220}$

construct among 6 other anchor-motif alternatives. Similar higher expression results were previously reported for YBEL + frgII$_{CyHV3}$ when compared to other 6 anchor-motifs in spinycterins grown in TB media (Coll, 2017). Although their growth rate was slower in SB medium, detectable levels of recombinant protein expression could be obtained for the 6 anchor-motifs studied (*E. coli*, *B. subtilis*, phage), in contrast to the problems with some of their yields previously obtained when using the TB medium (Coll, 2017). The YBEL + frgC$_{91–220}$ construct remained with the highest level of expression among the anchor-motifs studied when cultured in SB or TB media.

After the studies on the bacterial culture media, experiments were focused in finding inhibitors of DNA replication by searching for an alternative to crosslinking for bacterial inactivation which destroyed ~80% of the bacterial surface displayed frgII$_{CyHV3}$ immunogenicity (Coll, 2017) or most of the anti-polyH binding of YBEL + frgC$_{91–220}$ spinycterins (this work). Among the possible anti-bacterial drugs s screened for inactivation, those targeting DNA replication focused in their supercoiling steps, such as those belonging to the quinolone family, appeared to be the best alternative, thus quinolones target unwinding DNA gyrase or topoisomerase II (Gram-negative bacteria) and topoisomerase IV (Gram-positive bacteria) enzymes, by interacting with double stranded DNA, covalently binding to cleavaged DNA (Collin et al., 2011) and stopping strand rejoining during DNA replication (Collin et al., 2011). Additional quinolone bactericidal irreversible effects are induced by the generation of harmful hydroxyl radicals or ROS (Kohanski et al., 2007). The above-mentioned topoisomerases are essential in bacteria but absent in higher eukaryotes, making them an attractive possibility for the present purposes. The best studied gyrase is that from *E. coli*, which has A and B subunits. The A subunit cleaves and covalently binds DNA strands, while the B subunit rejoins the strands. Inhibition of further strand cleavage/rejoining by stabilisation of the covalent gyrase-DNA complex (gyrase poisoning) shows concentration-dependent bacteriostatic or bactericidal effects (Collin et al., 2011). For instance, the CPFX quinolone exhibits a bacteriostatic reversible activity at minimal concentrations and an irreversible bactericidal activity at higher concentrations (Silva et al.,

2011; Mustaev et al., 2014). First-generation quinolones derived from nalidixic/oxolinic acids are rarely used today because of their toxicity to eukaryotic cells. Second (i.e., CPFX), third (i.e., Levofloxacin) and fourth (i.e., Gemifloxacin) generation quinolones are clinically used. After numerous experiments, CPFX was selected for this work because of its high activity at low concentrations, its covalent linking to cleavaged DNA strands, the induction of irreversible DNA-damage (bactericidal) and its low cost. Because this is an area of intensive research, new quinolones may appear in the future to cause irreversible DNA-damage of recombinant bacteria with even lower concentrations which will reduce possible concerns about the use of antibiotics to inactivate bacteria. Among the reasons mentioned above, CPFX was preferentially chosen because it cleaves the double-stranded DNA by covalently linking itself to the DNA strands (Collin et al., 2011) in a related mechanism to that of formaldehyde/paraformaldehyde crosslinking. The low concentration required and the final washing steps that remove any excess of CPFX, reduces the possibility of free CPFX being released to the environment, very much like it does with crosslinked fish vaccines. In addition, CPFX induces a ROS-dependent bacterial killing effect without affecting antigenicity, in contrast to crosslinking (Coll, 2017). To enhance safety, it may be possible to add formaldehyde/paraformaldehyde at low concentrations to some the spinycterins or to the CPFX-inactivated spinycterins, provided a crosslinking-resistant anchor-motif is used (for instance, in the case of paraformaldehyde with Nmistic + frg$C_{91–220}$ spinycterins). Therefore, in the case the use of CPFX may be rejected because of being an antibiotic, other linking/crosslinking compounds could be further explored as alternatives for spinycterin inactivation. In each particular combination of anchor-motif and immunogen care should be taken as to preserve surface display and antigenicity. In this work, we have focused on describing a minimal proof-of-concept prototype of a fish vaccine alternative platform which should be further studied by other inactivation procedures, alternative mass delivery techniques and including host innate and adaptive immune responses. In its present state-of-the-art, the described spinycterin adjuvant-less vehicles require further work to be practical.

Even though some fish vaccines based in eukaryotic expression plasmids (i.e., DNA vaccines) have been recently approved, their use is still highly controversial in Europe (Gillund et al., 2008). Therefore, using immune-relevant viral protein antigens rather than DNA may still be an alternative. Furthermore, protein antigens coded in prokaryotic rather than eukaryotic plasmid vectors (like those employed for DNA vaccines), offer safer environmental possibilities. Both of the above commented properties and the maintenance of bacterial morphology in the spinycterins described here for substituting oil-adjuvants (Zhou et al., 2002; Navot et al., 2011; Cobo et al., 2013; Labarca et al., 2015) allow easier mass delivery and lower production costs. Because of the lack of cysteins in the displayed antigen, the spinycterins described here may be also looked as a method to reduce the generation of low-immunogenicity inclusion bodies during manufacturing very often found when expressing whole heterologous proteins in recombinant bacteria. Although recent results suggested that isolated nanopellets derived from bacterial inclusion bodies may also be immunogenic (Torrealba et al., 2016), their practical use would need additional purification steps, losing their bacterial morphology and their adjuvant properties. Most probably, the use of inclusion bodies as fish vaccines will require too high concentrations. Recently, however, intact recombinant bacteria carrying their inherent adjuvanticity and coding for the whole NNV C protein have been reported to induce partial protection against NNV together with very low levels of antibodies when orally delivered to sea bass (Gonzalez-Silvera et al., 2019). Furthermore, injection of extracts corresponding to 10^{10} cfu of such recombinant bacteria per fish fully protected against NNV challenge (Gonzalez-Silvera et al., 2019). In this context, there are some practical advantages of the DNA-damaged recA- *E. coli* alternative described here when coding for surface-displayed downsized viral antigens (spinycterins) in comparison with the recombinant wild-type *E. coli* coding for the whole NNV C protein (Gonzalez-Silvera et al., 2019). For instance, as shown in this work, the injection of only 10^8 cfu per fish of morphologically intact YBEL + frgC$_{91–220}$ spinycterins fully protected against NNV challenge in the absence of any adjuvants. Furthermore, spinycterins may be better accepted in aquaculture

because they are safer due to their DNA-repair deficient *E. coli* vehicle. Other advantages may be due to the antigen downsizing concept providing a higher immunorelevant epitope density for a given mass of bacteria, and the future possibility to use spinycterins expressing mixes of different pathogen antigens in a single delivery. Additionally, because of its isoleucine deficiency, the BLR(DE3) *E. coli* strain opens up the possibility of future developing of antibiotic-free selection methods to eliminate any antibiotic resistance sequences from the vaccine vehicles and thus further increase their environmental safety.

4.5. REFERENCES

Alves NS, Astrinidis SA, Eisenhardt N, Sieverding C, Redolfi J, Lorenz M, Weberruss M, Moreno-Andres D, Antonin W (2017) MISTIC-fusion proteins as antigens for high quality membrane protein antibodies. *Scientific Reports* 7:41519.

Baudin-Laurencin F, Richards R (1999) Nodavirus Workshop. *Bulletin European Association Fish Pathologists* 19:284-285.

Blain KY, Kwiatkowski W, Choe S (2010) The functionally active Mistic-fused histidine kinase receptor, EnvZ. *Biochemistry* 49:9089-9095.

Bovo G, Nishizawa T, Maltese C, Borghesan F, Mutinelli F, Montesi F, De Mas S (1999) Viral encephalopathy and retinopathy of farmed marine fish species in Italy. *Virus Research* 63:143-146.

Buonocore F, Nunez-Ortiz N, Picchieti S, Randelli E, Stocchi V, Guerra L, Toffan A, Pascoli F, Fausto AM, Mazzini M, et al. (2019) Vaccination and immune responses of European sea bass (*Dicentrarchus labrax* L.) against betanodavirus. *Fish and Shellfish Immunology* 85:78-84.

Chen CW, Wu MS, Huang YJ, Cheng CA, Chang CY (2015a) Recognition of linear B-cell epitope of betanodavirus coat protein by

RG-M18 neutralizing mab inhibits giant grouper nervous necrosis virus (GGNNV) infection. *PLoS One* 10:e0126121.

Chen NC, Yoshimura M, Guan HH, Wang TY, Misumi Y, Lin CC, Chuankhayan P, Nakagawa A, Chan SI, Tsukihara T et al. (2015b) Crystal structures of a piscine betanodavirus: Mechanisms of capsid assembly and viral infection. *PLoS Pathogens* 11:e1005203.

Cobo C Makosch K Jung R Kohlmann K Knop K (2013) Enhanced bacterin permeability and side effects using low frequency sonophoresis at 37 kHz in rainbow trout. *Fish and Shellfish Immunology* 34(6):1648-1648.

Coeurdacier JL, Laporte F, Pepin JF (2003) Preliminary approach to find synthetic peptides from nodavirus capsid potentially protective against sea bass viral encephalopathy and retinopathy. *Fish Shellfish Immunology* 14(5):435-447.

Coll JM (2017) Fish mass immunization against virus with recombinant "spiny" bacterins. *Fish and Shellfish Immunology* 67:393-401.

Collin F, Karkare S, Maxwell A (2011) Exploiting bacterial DNA gyrase as a drug target: current state and perspectives. Applied *Microbiology Biotechnology* 92(3):479-497.

Costa JZ, Adams A, Bron JE, Thompson KD, Starkey WG, Richards RH (2007) Identification of B-cell epitopes on the betanodavirus capsid protein. *Journal of Fish Diseases* 30(7):419-426.

Dvir H, Choe S (2009a) Bacterial expression of a eukaryotic membrane protein in fusion to various Mistic orthologs. *Protein Expression and Purification* 68(1):28-33.

Dvir H, Lundberg ME, Maji SK, Riek R, Choe S (2009b) Mistic: cellular localization, solution behavior, polymerization, and fibril formation. *Protein Science* 18(7):1564-1570.

Galeotti M, Romano N, Volpatti D, Bulfon C, Brunetti A, Tiscar PG, Mosca F, Bertoni F, Marchetti MG, Abelli L (2013) Innovative vaccination protocol against vibriosis in *Dicentrarchus labrax* (L.) juveniles: Improvement of immune parameters and protection to challenge. *Vaccine* 31(8):1224-1230.

Gillund F, Kjolberg KA, von Krauss MK, Myhr AI (2008) Do uncertainty analyses reveal uncertainties? Using the introduction of DNA vaccines to aquaculture as a case. *Science of Total Environment* 407(1):185-196.

Goffin P, Dehottay P (2017) Complete Genome Sequence of *Escherichia coli* BLR(DE3), a recA-Deficient Derivative of E. coli BL21(DE3). *Genome Announcements* 5(22):e00441-17.

Gonzalez-Silvera D, Guardiola FA, Espinosa C, Chaves-Pozo E, Esteban M, Cuesta A (2019) Recombinant nodavirus vaccine produced in bacteria and administered without purification elicits humoral immunity and protects European sea bass against infection. *Fish and Shellfish Immunology* 88:458-463.

Huang SM, Cheng JH, Tu C, Chen TI, Lin CT, Chang SK (2017) A bivalent inactivated vaccine of viral nervous necrosis virus and grouper iridovirus applied to grouper broodfish (*Epinephelus coioides*) reduces hte risk of vertical transmission. *Taiwan Veterinary Journal* 43(03):1-6.

Husgard S, Grotmol S, Hjeltnes BK, Rodseth OM, Biering E (2001) Immune response to a recombinant capsid protein of striped jack nervous necrosis virus (SJNNV) in turbot *Scophthalmus maximus* and Atlantic halibut *Hippoglossus hippoglossus*, and evaluation of a vaccine against SJNNY. *Diseases of Aquatic Organisms* 45(1):33-44.

Jeong KS, Xie Y, Hiasa H, Khodursky AB (2006) Analysis of pleiotropic transcriptional profiles: a case study of DNA gyrase inhibition. *PLoS Genetics* 2:e152.

Jung Y, Jung H, Lim D (2015) Bacteriophage membrane protein P9 as a fusion partner for the efficient expression of membrane proteins in *Escherichia coli*. *Protein Expression and Purification* 116 :12-18.

Kai YH, Chi SC (2008) Efficacies of inactivated vaccines against betanodavirus in grouper larvae (*Epinephelus coioides*) by bath immunization. *Vaccine* 26(11):1450-1457.

Kohanski MA, Dwyer DJ, Hayete B, Lawrence CA, Collins JJ (2007) A common mechanism of cellular death induced by bactericidal antibiotics. *Cell* 130(5):797-810.

Labarca CC, Makhutu M, Lumsdon AE, Thompson KD, Jung R, Kloas W, Knopf K (2015) The adjuvant effect of low frequency ultrasound when applied with an inactivated *Aeromonas salmonicida* vaccine to rainbow trout (*Oncorhynchus mykiss*). *Vaccine* 33(11):1369-1374.

Leviatan S, Sawada K, Moriyama Y, Nelson N (2010) Combinatorial method for overexpression of membrane proteins in *Escherichia coli*. *Journal of Biological Chemistry* 285(31):23548-23556.

Lin CS, Lu MW, Tang L, Liu WT, Chao CB, Lin CJ, Krishna NK, Johnson JE, Schneemann A (2001) Characterization of virus-like particles assembled in a recombinant baculovirus system expressing the capsid protein of a fish nodavirus. *Virology* 290(1):50-58.

Liu W, Hsu CH, Chang CY, Chen HH, Lin CS (2006) Immune response against grouper nervous necrosis virus by vaccination of virus-like particles. *Vaccine* 24(37-39):6282-6287.

Molloy MP, Herbert BR, Slade MB, Rabilloud T, Nouwens AS, Williams KL, Gooley AA (2000) Proteomic analysis of the *Escherichia coli* outer membrane. *European Journal of Biochemistry* 267(10):2871-2881.

Mustaev A, Malik M, Zhao X, Kurepina N, Luan G, Oppegard LM, Hiasa H, Marks KR, Kerns RJ, Berger JM, Drlica K (2014)

Fluoroquinolone-gyrase-DNA complexes: two modes of drug binding. *Journal of Biological Chemistry* 289(18):12300-12312.

Navot N, Sinyakov MS, Avtalion RR (2011) Application of ultrasound in vaccination against goldfish ulcer disease: A pilot study. *Vaccine* 29(7):1382-1389.

Nekrasova OV, Wulfson AN, Tikhonov RV, Yakimov SA, Simonova TN, Tagvey AI, Dolgikh DA, Ostrovsky MA, Kirpichnikov MP (2010) A new hybrid protein for production of recombinant bacteriorhodopsin in *Escherichia coli*. *Journal of Biotechnology* 147(3-4):145-150.

Nishizawa T, Furuhashi M, Nagai T, Nakai T, Muroga K (1997) Genomic classification of fish nodaviruses by molecular phylogenetic analysis of the coat protein gene. *Applied and Environmental Microbiology* 63(4):1633-1636.

Park TJ, Heo NS, Yim SS, Park JH, Jeong KJ, Lee SY (2013) Surface display of recombinant proteins on *Escherichia coli* by BclA exosporium of *Bacillus anthracis*. *Microbial Cell Factories* 12:81.

Petrovskaya LE, Shulga AA, Bocharova OV, Ermolyuk YS, Kryukova EA, Chupin VV, Blommers MJ, Arseniev AS, Kirpichnikov MP (2010) Expression of G-protein coupled receptors in *Escherichia coli* for structural studies. *Biochemistry (Mosc)* 75(7):881-891.

Roosild TP, Greenwald J, Vega M, Castronovo S, Riek R, Choe S (2005) NMR structure of Mistic, a membrane-integrating protein for membrane protein expression. *Science* 307(5713):1317-1321.

Schmidt M, Romer L, Strehle M, Scheibel T (2007) Conquering isoleucine auxotrophy of *Escherichia coli* BLR(DE3) to recombinantly produce spider silk proteins in minimal media. *Biotechnology Letters* 29:1741-1744.

Silva F, Lourenco O, Queiroz JA, Domingues FC (2011) Bacteriostatic versus bactericidal activity of ciprofloxacin in *Escherichia coli* assessed

by flow cytometry using a novel far-red dye. *Journal of Antibiotics (Tokyo)* 64(4):321-325.

Sivashanmugam A, Murray V, Cui C, Zhang Y, Wang J, Li Q (2009) Practical protocols for production of very high yields of recombinant proteins using *Escherichia coli*. *Protein Science* 18(5):936-948.

Skliris GP, Krondiris JV, Sideris DC, Shinn AP, Starkey WG, Richards RH (2001) Phylogenetic and antigenic characterization of new fish nodavirus isolates from Europe and Asia. *Virus Research* 75(1):59-67.

Somrit M, Watthammawut A, Chotwiwatthanakun C, Ounjai P, Suntimanawong W, Weerachatyanukul W (2017) C-terminal domain on the outer surface of the *Macrobrachium rosenbergii* nodavirus capsid is required for Sf9 cell binding and internalization. *Virus Research* 227:41-48.

Studier FW (2005) Protein production by auto-induction in high density shaking cultures. *Protein Expression and Purification* 41(1):207-234.

Studier FW (2014) Stable expression clones and auto-induction for protein production in *E. coli*. *Methods in Molecular Biolgy* 1091:17-32.

Thiery R, Cozien J, Cabon J, Lamour F, Baud M, Schneemann A (2006) Induction of a protective immune response against viral nervous necrosis in the European sea bass *Dicentrarchus labrax* by using betanodavirus virus-like particles. *Journal of Virology* 80(20):10201-10207.

Torrealba D, Parra D, Seras-Franzoso J, Vallejos-Vidal E, Yero D, Gibert I, Villaverde A, Garcia-Fruitos E, Roher N (2016) Nanostructured recombinant cytokines: A highly stable alternative to short-lived prophylactics. *Biomaterials* 107:102-114.

Ucko M, Colorni A, Diamant A (2004) Nodavirus infections in Israeli mariculture. *Journal of Fish Diseases* 27(8):459-469.

Xu J, Banerjee A, Pan SH, Li ZJ (2012) Galactose can be an inducer for production of therapeutic proteins by auto-induction using *E. coli* BL21 strains. *Protein Expression and Purification* 83(1):30-36.

Yamashita H, Fujita Y, Kawakami H, Nakai T (2005) The efficacy of inactivated virus vaccine against viral nervous necrosis (NNV). *Fish Patholology* 40(1):15-21.

Yamashita H, Mori K, Kuroda A, Nakai T (2009) Neutralizing antibody levels for protection against betanodavirus infection in sevenband grouper, *Epinephelus sptemfasciatius* (Thunberg), immunized with an inactivated virus vaccine. *Journal of Fish Diseases* 32(9):767-775.

Yong CY, Yeap SK, Omar AR, Tan WS (2017) Advances in the study of nodavirus. *PeerJ* 5:e3841.

Yuasa K, Koesharyani I, Roza D, Mori K, Katata M, Nakai T (2002) Immune response of humpback grouper, *Cromileptes altivelis* (Valenciennes) injected with the recombinant coat protein of betanodavirus. *Journal of Fish Diseases* 25:53-56.

Zhou YC, Wang J, Zhang B, Su YQ (2002) Ultrasonic immunization of sea bream, *Pagrus major* (Temminck & Schlegel), with a mixed vaccine against *Vibrio alginolyticus* and *V. anguillarum*. *Journal Fish Diseases* 25(6):325-331.

USC
UNIVERSIDADE
DE SANTIAGO
DE COMPOSTELA

Chapter 5

Zebrafish as a vertebrate model to study nodavirus infections

USC
UNIVERSIDADE
DE SANTIAGO
DE COMPOSTELA

5. Zebrafish as a vertebrate model to study nodavirus infections

5.1. INTRODUCTION

The zebrafish (*Danio rerio*) is a very versatile model widely used in the study of ontogeny, developing biology, and also infectious diseases to understand the host-pathogen interactions (Kanther and Rawls, 2010; Novoa and Figueras, 2012). Zebrafish have innate and adaptive immunity resembling that of mammals and higher vertebrates. In the early stages, however, the larvae only present innate immunity, since the cells responsible of the adaptive immunity do not appear until 4 or 6 weeks post-fertilization (Lam et al., 2003), so younger larvae allow the study of innate immunity, the first line of defence against a pathogen, such as the action of primary immune cells, the macrophages (Herbomel et al., 1999) and neutrophils (Le Guyader et al., 2008), and the role of the main cytokines involved in the immune response. The zebrafish is an excellent model to study the host-pathogen interactions in early stages of larval life, due to the large number of offspring, the short generation time, the tolerance of anesthesia, the small size of the body and its transparency that allows easy imaging of the whole body by live imaging, an also the high-quality genome sequence of zebrafish enable the rapid accumulation of loss- or gain-of-function mutants and the formation of transgenic lines that allow traceability of different cell types (Cui et al., 2011; Ludwig et al., 2011; Levraud et al., 2014).

Even though no viruses are known to naturally infect zebrafish (Crim and Riley, 2012; Varela et al., 2017), various viruses (included those infecting humans) have been studied using the zebrafish as a model of infection. In the case of fish, the main diseases produced by viruses have been reproduced in zebrafish: rhabdoviruses like the spring viraemia of carp virus (SVCV) (Sanders et al., 2003; Levraud et al., 2007; Lopez-Muñoz et al., 2010; Varela et al., 2014a; Varela et al., 2014b), the snakehead rhabdovirus (SHRV) (Phelan et al., 2005), the

viral hemorrhagic septicemia virus (VHSV) (Novoa et al., 2006), the infectious hematopoietic necrosis virus (IHNV) (Ludwig et al., 2011); birnaviruses like the infectious pancreatic necrosis virus (IPNV) (LaPatra et al., 2000; Garner et al., 2003); iridoviruses as the infectious spleen and kidney necrosis virus (ISKNV) (Xu et al., 2008; Wang et al., 2008) or European sheatfish virus (ESV) (Martín et al., 2015); and nodaviruses, the nervious necrosis virus (NNV) or nodavirus (Lu et al., 2008; Morick et al., 2015).

VER disease, caused by NNV, is one of the most devastating diseases affecting commercial species around the world, such as the European sea bass (*D. labrax*). Many experiments have been carried out in European sea bass to study the interaction of the NNV with its host (Skliris and Richards, 1999) or the distribution of the virus in different tissues using immunohistochemnical assays (Mladineo, 2003), real-time TaqMan PCR (Panzarin et al., 2010), one-step qRT-PCR (Mazelet et al., 2011), and *in situ* hybridation (Lopez-Jimena et al., 2011). In the last years, NGS technologies have been used to understand the transcriptome response of European sea bass during a nodavirus infection both *in vitro*, infecting sea bass leukocytes (Chaves-Pozo et al., 2017) and brain cells (DLB-1 cell line) (Chaves-Pozo et al., 2019), and *in vivo*, studying the brain and head kidney of infected animals (Lama et al., 2020).

Despite of the importance of this disease, there are not many studies that take advantage of the benefits of zebrafish to investigate the NNV infection. In 2007, Furusawa et al. tried to establish experimental infections for adult zebrafish but without success (Furusawa et al., 2007). Later, Lu et al. were able to reproduce the NNV infection in zebrafish (Lu et al., 2008) which could be used as an *in vivo* model for studying viral pathogenesis and the immune responses after treatments with different compounds (Morick and Saragovi, 2017).

In this chapter, we sought to improve the knowledge of the VER disease through the use of zebrafish as NNV infection model, taking advantage of different imaging methods and transgenic fish lines with the aim of comparing different routes of infection, observing the behaviour of infected larvae and analysing the immune response against the virus.

5.2. MATERIALS AND METHODS

5.2.1. Fish

Embryos and larvae used in this study were obtained from our experimental facility, where the zebrafish were cultured using established protocols (Westerfield, 2000; Nüsslein-Volhard and Dahm, 2002). Different fish lines were used: wild type (WT) zebrafish, AB wild type line (AB), Tübingen wild type line (TU), transgenic line Tg(*mpx*:GFP), in which neutrophils are labelled, transgenic line Tg(*mpeg*:mCherry), in which macrophages are labelled, transgenic line Tg(*lyz*:DsRed2), in which myeloid lineage and lysozyme-expressing cells are labelled, and transgenic line Tg(*fli*:GFP), in which endothelial cells are labelled. The eggs were obtained according to protocols described in The Zebrafish Book (Westerfield, 2000) and maintained at 28 °C in egg water (5 mM NaCl, 0.17 mM KCl, 0.33 mM $CaCl_2$, 0.33 mM $MgSO_4$, and 0.00005% methylene blue).

5.2.2. Virus

The viral strain 475-9/99, belonging to the RGNNV genotype of the family *Nodaviridae*, was kindly provided by the Institute Zooprofilattico delle Venezie (Italy) after isolation from diseased sea bass (Bovo et al., 1999). The virus was propagated in the snakehead-fish cell line SSN-1 (ECACC 96082808) cultured in L-15 medium (Gibco), supplemented with 2mM L-glutamine (Gibco), 2 % FBS (Gibco), and 1 % penicillin/streptomycin solution (Invitrogen), with incubation at 25 °C until the cytopathic effect. The supernatants were harvested and centrifuged at 4,000 xg to eliminate cell debris. The supernatant was stored at -80 °C until use, and this viral stock was titrated into 96-well plates using the Reed-Müench method (1938).

5.2.3. Infection of larvae with NNV

The fish larvae were infected by 4 different routes at 3 and 14 days post-fertilization (dpf). Zebrafish larvae were anesthetized in E3 egg water containing 160 µg/mL MS-222 (Sigma-Aldrich), placed on an agarose plate and individually microinjected as described by Benard (2012). NNV was diluted at appropriate concentration (10^6 $TCDI_{50}$/mL) in L15 medium with 0.1 % phenol red (as visible marker to the injection

of the solution into the larvae) just before microinjection of 2 nL of viral suspension to infected larvae, or 2 nL of L15 to uninfected larvae. Larvae were infected through microinjection into the head (via brain), the duct of Cuvier (via DC) and intramuscularly (via IM), and also by immersion in water containing 10^6 $TCDI_{50}$/mL NNV. Then, larvae were maintained in Petri dishes at 28 °C on a 12 h light-dark cycle. Mortality was recorded daily using 3 replicates of 10 larvae each. Experiments were repeated 3 times.

5.2.4. Imaging: fluorescence microscopy, video record and confocal microscopy

Transgenic larvae were infected by 4 different routes at 3 dpf and, after 1, 2 and 3 dpi, images of whole larvae were taken using a Nikon AZ100 fluorescence microscope. Larvae were anaesthetized with a 0.01% of MS-222 solution. The different immune cells labelled in the transgenic lines were counted using a macro of ImageJ program (Schneider et al., 2012) to calculate the percentage of cells that migrated to the brain during infection.

To analyse the swimming behaviour of the fish larvae, two Petri dishes of 10 larvae each, inoculated by the same route, one containing infected larvae and the other uninfected control larvae, were placed in the same plane of a video recording for 2 consecutive minutes. Recordings of 3 and 14 dpf larvae were made at 3, 6 and 10 dpi with a Leika camera of 48 Mpx and the images were processed with Photoshop and Chemotaxis and Migration Tool program, according to the manufacturer's instructions. The data obtained allowed us to follow larvae movements calculating the velocity, the accumulated and Euclidean distances and the directionality to compare the swimming behaviour between infected and uninfected control larvae.

A whole-mount inmunohistochemistry was done as follows. Transgenic larvae Tg(*mpx*:GFP) and Tg(*fli*:GFP) and WT larvae were infected at 3 dpf for 24 and 72 h. Then, larvae were fixed O/N at 4 °C in 4 % paraformaldehyde (PFA) diluted in phosphate-buffered saline containing 0.1 % Tween-20 (PBST). Larvae were washed twice in PBST. Larvae were dehydrated in a graded series of methanol /PBST solution (25 % for 5 min, 50 % for 10 min and 75 % for 5 min), and

stored in 100 % methanol O/N at -20 °C. For immunofluorescence processing, larvae were rehydrated in a graded series of methanol /PBST solution (75 % for 5 min, 50 % for 10 min and 25 % for 5 min) and washed 4 times for 5 min with PBST. Larvae were bleached by the incubation for 5 min in bleaching solution (0.8 mL of KOH 10 %, 0.3 mL of H_2O_2 30 %, 0.1 mL of Tween-80 and 8.8 mL of distilled water), then washed twice 5 min in PBST. Permeabilization was achieved by the incubation with proteinase K at 10 µg/mL. After 2 h at 37 °C, larvae were washed twice in PBST and incubated in Tween-20 2 % in PBS 1 day at RT. Larvae were washed and blocked in 1 % Tween-20/PBS and 10 % lamb serum O/N at RT. The primary antibodies 6G7 (antigen tubulin beta III, DSHB) at 5 µg/mL for WT larvae, and anti-sea bass encephalitis virus (anti-DIEV) (Aranguren et al., 2002) at 1:4,000 for all larvae, were diluted in antibody solution (0.2 % Tween-20/PBS and 10 % lamb serum) for 3 days at 4 °C. Larvae were washed O/N, and then, incubated for 2 days in antibody solution with Alexa Fluor 488 anti-mouse (for labelling 6G7) or Alexa Fluor 546 anti-rabbit (for labelling anti-DIEV) (Invitrogen), at 1:1,000 and 1:500, respectively. Secondary antibodies were washed O/N in PBST, and stained with DAPI 1 h RT. After 3 washes with PBS, larvae were stored at 4 °C until examination. Confocal images of fixed larvae were taken using a TSC SPE confocal microscope (Leica). The images were processed using the LAS-AF (Leica Application Suite Advanced Fluorescence) program.

5.2.5. Evaluation of NNV load and immune gene analysis by qPCR

To evaluate the progress of the NNV infection in zebrafish, larvae were infected via brain and collected at 1, 3, 5 and 7 dpi. Whole larvae were harvested under RNAse-free conditions in pools of 4 larvae each. Total RNA was isolated using the Maxwell® RSC simplyRNA Tissue kit (Promega) in accordance with the manufacturer's instructions. cDNA synthesis was performed with the NZY First-Strand cDNA Synthesis Kit (NZYtech) using 0.2 µg of total RNA. The qPCR reactions were performed using specific primers designed with the Primer 3 software (Rozen and Skaletsky, 2000), and their efficiencies were previously tested according to the protocol described by Pfaffl

(Pfaffl, 2001). Individual qPCR reactions were conducted in 25-µl reaction volumes using 12.5 µL of SYBR GREEN PCR Master Mix (Applied Biosystems), 10.5 µL of ultrapure water (Sigma-Aldrich), 0.5 µL of each specific primer (10 µM) and 1 µL of cDNA template. All reactions were performed using technical triplicates in the 7300 Real-Time PCR System thermocycler (Applied Biosystems) with an initial denaturation step (95 °C, 10 min), followed by 40 cycles of a denaturation step (95 °C, 15s) and one hybridization-elongation step (60 °C, 1 min). The relative gene expression was calculated using the Pfaffl method (Pfaffl, 2001) and using *18S ribosomal RNA* (*18s*) as a reference gene.

Viral replication was detected by the relative gene expression of the NNV coat protein gene (RNA2) (Kuo et al., 2011). Several zebrafish genes were evaluated; their sequences are listed in Table 5.1.

5.2.6. Statistical analysis

Kaplan-Meier survival curves were analyzed with a log-rank (Mantel-Cox) test. For the remaining experiments, the results were represented graphically as the mean ± standard error of mean (SEM) and significant differences were obtained using a Student's t-test and displayed as *** ($0.0001 < p < 0.001$), ** ($0.001 < p < 0.01$) or * ($0.01 < p < 0.05$).

5.2.7. Ethic statement on fish handling

All the experimental procedures were reviewed and approved by the CSIC National Committee of Bioethics under appoval number ES360570202001/17/FUN.01/INM06/BNG.

5.3. RESULTS

5.3.1. Comparison of infection routes, age and zebrafish WT line in the model of NNV infection

To determine the most efficient route of infection with NNV, wild-type zebrafish larvae were infected 3 dpf through 4 different routes: a) via brain, by microinjection directly into the area of the head between the eyes reaching the brain that is the target tissue of NNV, b) via duct

of Cuvier (DC), to produce a systemic and local infection, c) intramuscularly (IM), microinjecting into the muscle in the middle of the back, and d) by bath, by immersing the larvae in a viral suspension (Figure 5.1).

Table 5.1. Sequence of the primer pairs used in this study.

Primer name	Direction	Primer sequence
NNV Coat protein	Forward	GACGCGCTTCAAGCAACTC
	Reverse	CGAACACTCCAGCGACACAGCA
18S	Forward	ACCACCCACAGAATCGAGAAA
	Reverse	GCCTGCGGCTTAATTTGACT
il1b	Forward	TTCCCCAAGTGCTGCTTATT
	Reverse	AAGTTAAAACCGCTGTGGTCA
tnfa	Forward	ACCAGGCCTTTTCTTCAGGT
	Reverse	GCATGGCTCATAAGCACTTGTT
il6	Forward	TCAACTTCTCCAGCGTGATG
	Reverse	TCTTTCCCTCTTTTCCTCCTG
ifnphi1	Forward	GAGCACATGAACTCGGTGAA
	Reverse	TGCGTATCTTGCCACACATT
mxe	Forward	AGTCACCCAATGTCAGTGCA
	Reverse	GCTGAGAGATGTACTGGTTC
nlrc3	Forward	CGAAAGCTCACCACACTCAA
	Reverse	AGCCACTGTTCCCAAATCAC
mpx	Forward	TCCAAAGCTATGTGGGATGTGA
	Reverse	GTCGTCCGGCAAAACTGAA
marco	Forward	AAGGACCCACAGGACAACAG
	Reverse	ATGTGGTGATGCTCCTCCTC

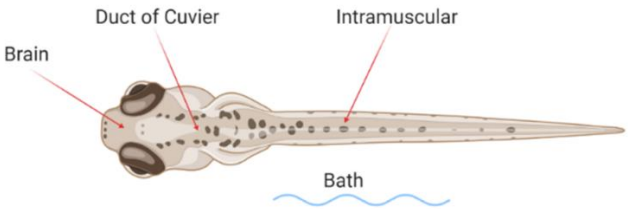

Figure 5.1. Routes of infection: a) via brain, b) via duct of Cuvier, c) intramuscularly, and d) by bath.

Our results showed that the most effective route that caused significantly higher mortalities after infection with NNV was via brain, being the survival of the larvae only 56 % compared to their uninfected controls, followed by the intramuscular microinjection in which survival of the infected larvae was 62 %. Infections via duct of Cuvier or via bath did not show significantly different mortality compared to the uninfected controls (Figure 5.2A).

To analyse the effect of larvae age on the susceptibility to a NNV infection, we also infected 14 dpf larvae using the same infection routes and conditions as the previous experiment and recorded the mortalities again in parallel. We could observe that the mortalities of infected larvae were not significantly different compared to the uninfected controls (Figure 5.2B).

Once we verified that the route through microinjection via brain in 3 dpf larvae was the one that caused a lower survival of the infected larvae, we wanted to determine if different zebrafish wild-type lines could show modified sensitivity against NNV infection. Therefore, 3 dpf larvae of WT, AB and TU wild-type lines were infected by microinjection via brain and mortalities were recorded daily. The 3 wild-type lines showed significant differences in the mortality of the infected larvae respect to their uninfected controls, being the WT those with the lowest survival (Figure 5.3). For that reason, WT zebrafish larvae of 3 dpf were used in successive experiments.

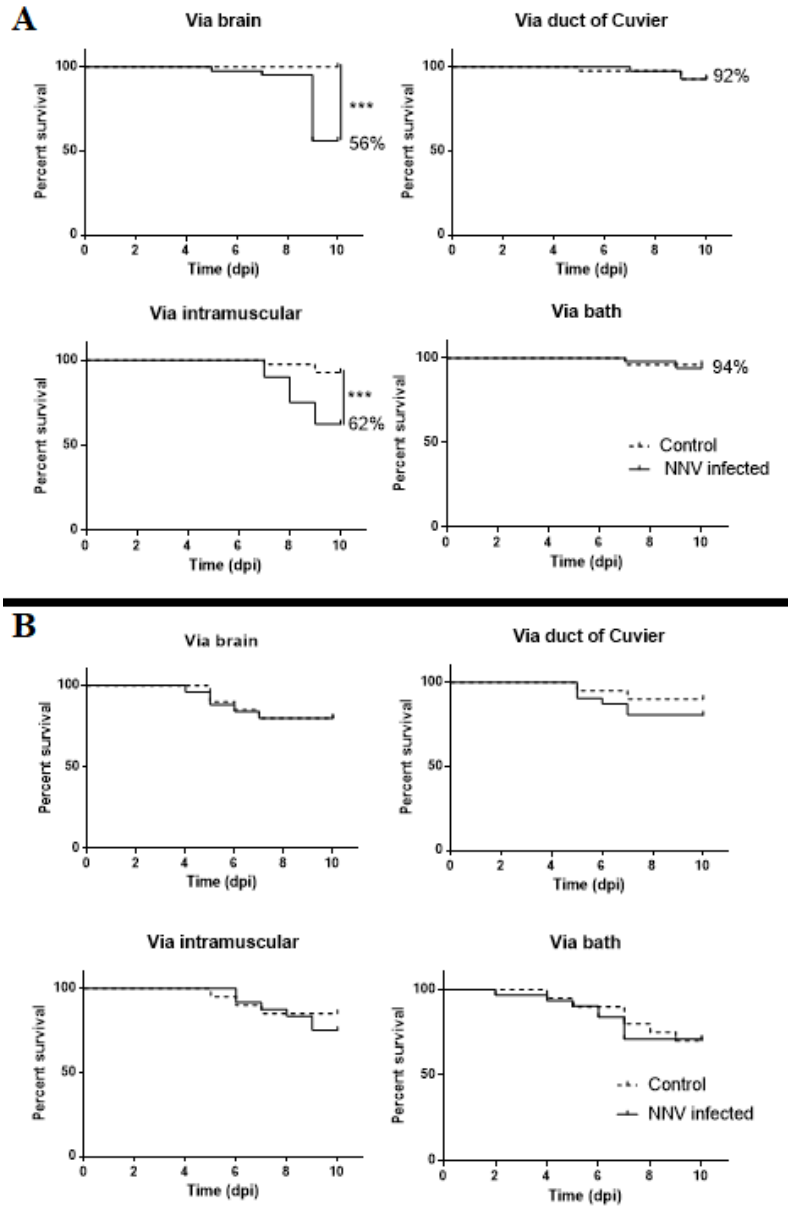

Figure 5.2. Kaplan-Meier survival curves of NNV infected and uninfected larvae challenged through different infection vias. A Larvae infected at 3 days post-fertilization. **B** Larvae infected at 14 days post-fertilization. Significant differences were displayed as follows: ***, 0.0001 > p-value > 0.001; **, 0.001 > p-value > 0.01; *, 0.01 > p-value > 0.05.

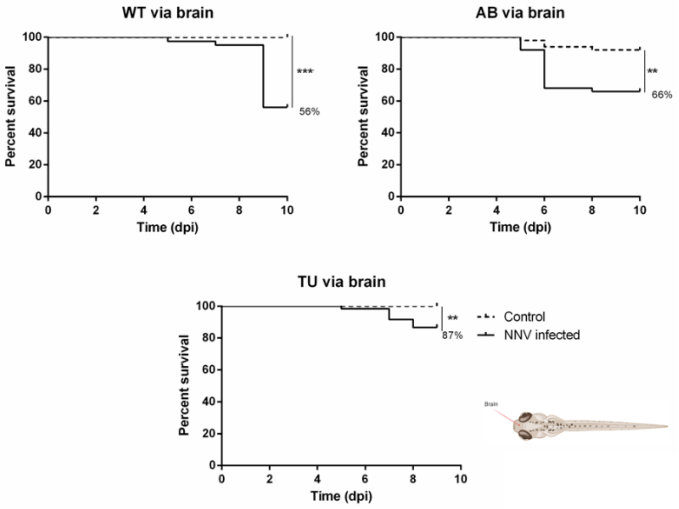

Figure 5.3. Kaplan-Meier survival curves of NNV infected and uninfected different wild-type strains of zebrafish larvae challenged via brain. Larvae infected 3 days post-fertilization.

5.3.2. Use of transgenic lines to study the migration of immune cells to infection site (CNS)

The existence of transgenic lines in zebrafish provides an easy-to-use working tool that gives us very useful information. To study the immune response of zebrafish to NNV infection, different transgenic lines were used. The transgenic line Tg(*lyz*:DsRed2) was used to detect cells expressing lysozyme c gene (*lyz*), myeloid precursors with lysozyme activity. The transgenic line Tg(*mpx*:GFP) was used to detect cells expressing myeloperoxidase gene (*mpx*), a specific marker of differentiated neutrophils. The transgenic line Tg(*mpeg*:mCherry) was used to detect cells with macrophage-expressed gen (*mpeg*) (macrophages). The larvae were infected by 4 infection routes and these cells were counted at 1, 2 and 3 dpi. The number of cells that migrated to the brain after infection was determined. The data represented the difference in the amount of cells in infected larvae compared with uninfected control larvae (control FC = 1 in the dot line).

There was a greater migration of Lyz+ cells at 48 and 72 hpi and greater migration of neutrophils at 24 and 48 hpi to the brain when the infection was carried out via brain. Infection by the other routes was not

able to cause a migration of these main immune cells to the target organ of the virus. No macrophage migration to the brain was observed by any route of infection.

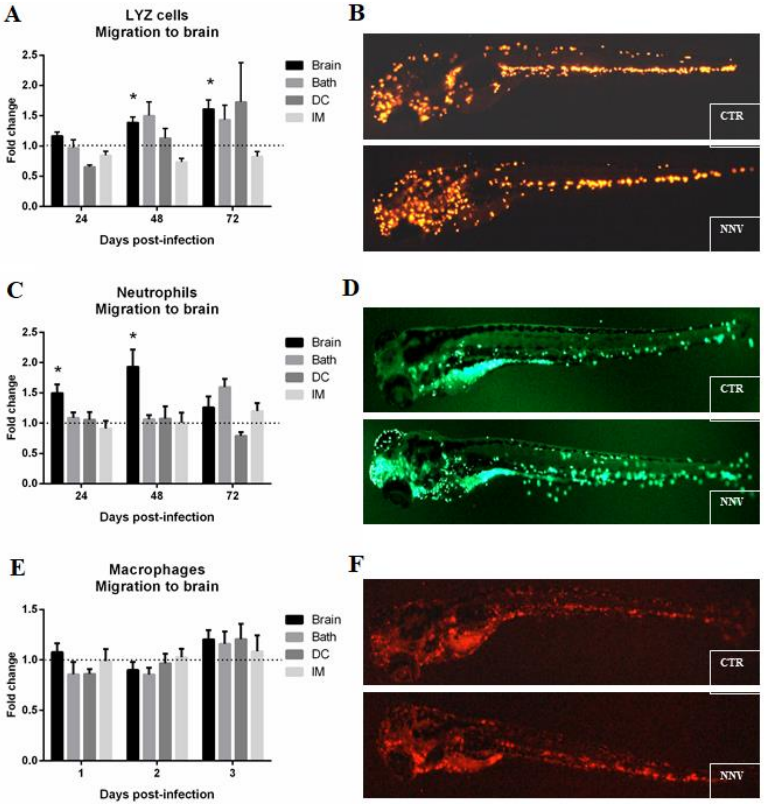

Figure 5.4. Counting labeled immune cells in transgenic larvae. Different immune cells labelled in the transgenic lines were counted using a macro of ImageJ program to calculate the percentage of cells that migrated to the brain during infection **A B** Transgenic line Tg(*lyz*:DsRed2). **C D** Transgenic line Tg(*mpx*:GFP). **E F** Transgenic line Tg(*mpeg*:mCherry). Larvae were infected by the 4 infection routes analyzed in this study and these cells were counted at 1, 2 and 3 dpi. The number of cells that migrated to the brain after NNV infection (**A C E**) were calculated. The data represent the difference in the amount of cells in infected larvae compared with uninfected control larvae (control FC = 1 in the dot line). Means ± standard errors of means were calculated. Significant differences were displayed as follows: ***, 0.0001 > p-value > 0.001; **, 0.001 > p-value > 0.01; *, 0.01 > p-value > 0.05. **B D F** Photo examples of larvae microinjected in brain at 2 dpi.

5.3.3. Behavioral observation by video tracking

We further investigate the swimming behaviour of 3 and 14 dpf zebrafish larvae by video tracking to determine if the infection produced changes on other measurable parameters of the fish, like velocity (mm/sec), accumulated distance (mm) of larvae path, Euclidean distance (mm) (length of straight line between larvae start-point and end-point), and directionality (calculated by comparing the Euclidean distance to the accumulated distance, it represents a measurement of the directness of larvae trajectories). Data shown represented the fold change of infected larvae against their uninfected controls (FC = 1, dot lines).

In figure 5.5A, in 3 dpf larvae, the velocity, directionality and Euclidean distance were found to be significantly different in almost all comparisons between infected and uninfected larvae, regardless of the infection route used, and the most of them disappear after 10 dpi. However, in 14 dpf larvae (Figure 5.5B), there were fewer differences between infected and uninfected larvae, and differences in directionality remaining mainly in the later days of infection (6 and 10 dpi). Figure 5.5C was an example of the maximum projections used for the analysis of the videos.

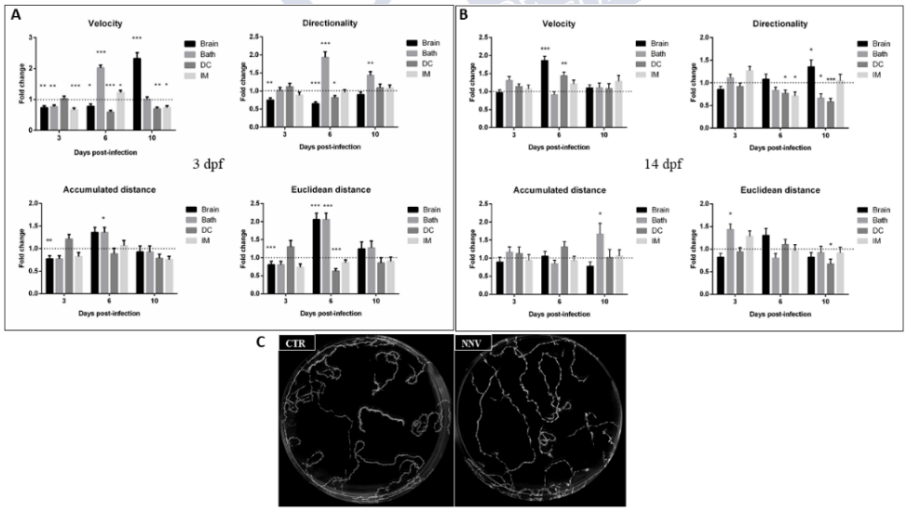

Figure 5.5. Video tracking of 3 (A) and 14 dpf (B) zebrafish larvae. Tracking of videos taken at different times of infection (3, 6 and 10 dpi); NNV infected and

uninfected control WT larvae challenged through different infection vias. Data shown represent the fold change of infected larvae against their uninfected controls (Control FC = 1, dot lines): velocity, directionality, accumulated distance and Euclidean distance. **C** Example of maximal projection of the video of the infected larvae via brain at 6 dpi. Means ± standard errors of means were calculated. Significant differences were displayed as follows: ***, 0.0001 > p-value > 0.001; **, 0.001 > p-value > 0.01; *, 0.01 > p-value > 0.05.

5.3.4. Confocal imaging detecting the position of NNV

Whole-mount immunohistochemistry is a very powerful tool that offers the use of zebrafish as a working model, it allows to locate antigen-antibody interactions without the need to prepare sections of the larvae. Thus, using the anti:DIEV antibody, we were able to locate the NNV inside the larva to found possible colocalization sites with different cells or tissues that could be responsible for the distribution of the virus throughout the organism. We started with the study of neutrophils in transgenic larvae (Tg *mpx*:GPF), having found a greater migration of these cells towards the site of infection (Figure 5.4C), but after the whole-mount inmunohistochemistry, we did not observe any colocalization point with the virus labeling, which would eliminate the theory that this immune cells may participate in the transport of the virus to the brain (Figure 5.6).

We continued with the study of the endothelium using the transgenic line Tg(*fli*:GFP), in case the infection could have a systemic origin and travel through this tissue, but we were only able to observe how the virus took a form similar to the endothelium shape (Figure 5.7A). When we analyzed this colocalization in depth, representing in a graph the red signal of the virus against the green signal of the endothelium, it could be found that although there was a similar distribution of the labels, the virus was not found within the endothelial cells, NNV surrounds the endothelium (Figure 5.7B).

Furthermore, due to the neurotropic nature of the virus we labeled the central nervous system in WT larvae, with the 6G7 antibody that binds the tubulin III of the radial glia cells. At first glance, the distribution of the virus was not similar to that of CNS labeling, and when making an analysis of the orthogonal projection of the photographs, we did not find colocalization sites (Figure 5.8).

This was a first approach to study the possible strategies of neuroinvasion of the NNV.

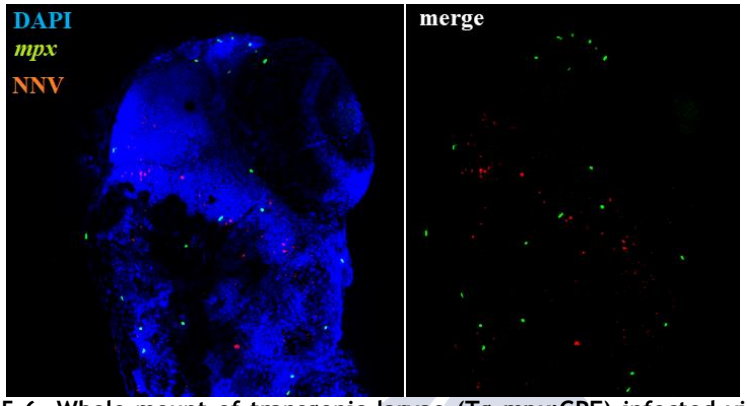

Figure 5.6. Whole-mount of transgenic larvae (Tg *mpx*:GPF) infected via brain with NNV 1 dpi. Photo of larva head displaying neutrophils in green, NNV in red and DAPI in blue. Second photo displays only the neutrophils and NNV.

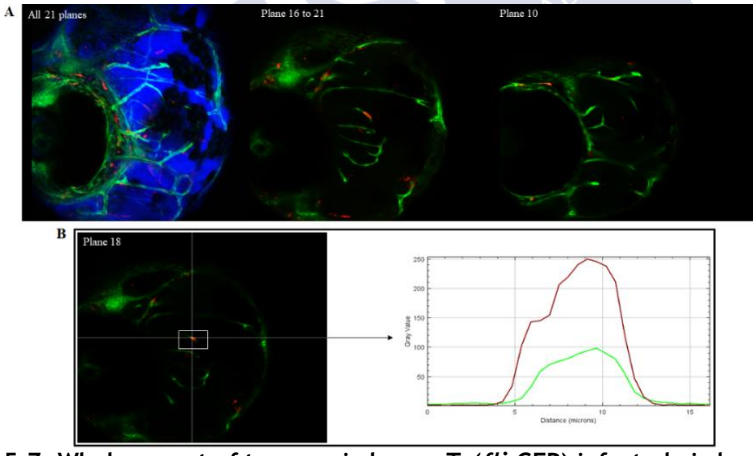

Figure 5.7. Whole-mount of transgenic larvae Tg(*fli*:GFP) infected via brain with NNV 1 dpi. A Series of photos of larva head with the maximum projection of 21 planes, only from planes 16 to 21 or only one plane, plane 10, to observe the different locations of the virus in the head of the larva. **B** Photograph of the orthogonal of a possible colocalization point marked, which was analyzed with a graph of the distance between the two labels, the red of the NNV and the green of the endothelium.

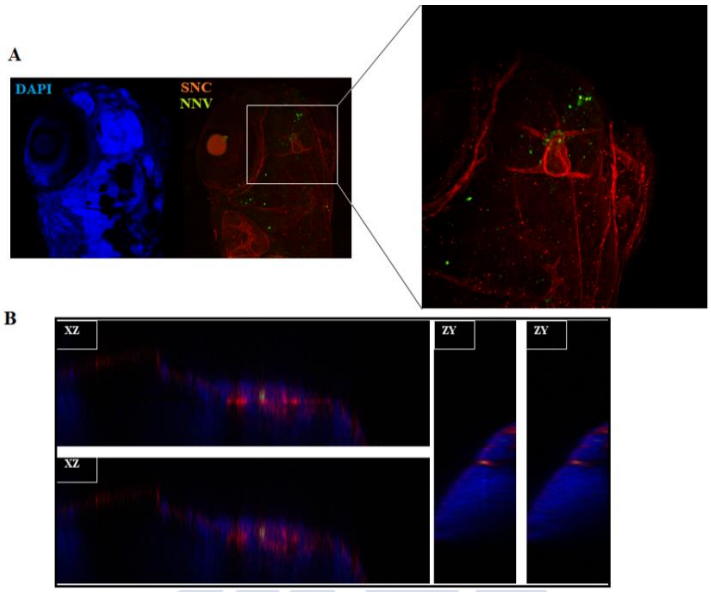

Figure 5.8. Whole-mount of transgenic WT larvae infected via brain with NNV 1 dpi. A Photo of larva head displaying NNV in green, tubulin III in red and DAPI in blue. **B** Photos of orthogonal analysis in single planes.

5.3.5. Time course of NNV infection and zebrafish genes expression

New experiments were conducted to follow the expression of both viral and zebrafish genes by qPCR. After infection of zebrafish larvae via brain with NNV, the expression of the gene coding for the capsid protein increased over the infection time (Figure 5.9A).

Concerning the expression of the host immune genes (Figure 5.9B), the expression of the proinflammatory cytokines *il1b* and *tnfa*, interferon *ifnphi1*, interferon induced gene *mxe* or the NOD-like receptor gene *nlrc3*, significantly increased during infection. The proinflammatory cytokine gene *il6* also showed an increased expression after infection although this was not significantly different from that found in control fish. The *mpx* gen, a specific marker of differentiated neutrophilic granulocytes (Elomaa et al., 1995), and specially, the macrophage receptor, *marco*, also showed an increment of their expression after infection. Therefore, we could confirm an immune

reaction of the zebrafish larvae to an infection with NNV and an increase in the viral load in the infected larvae over time.

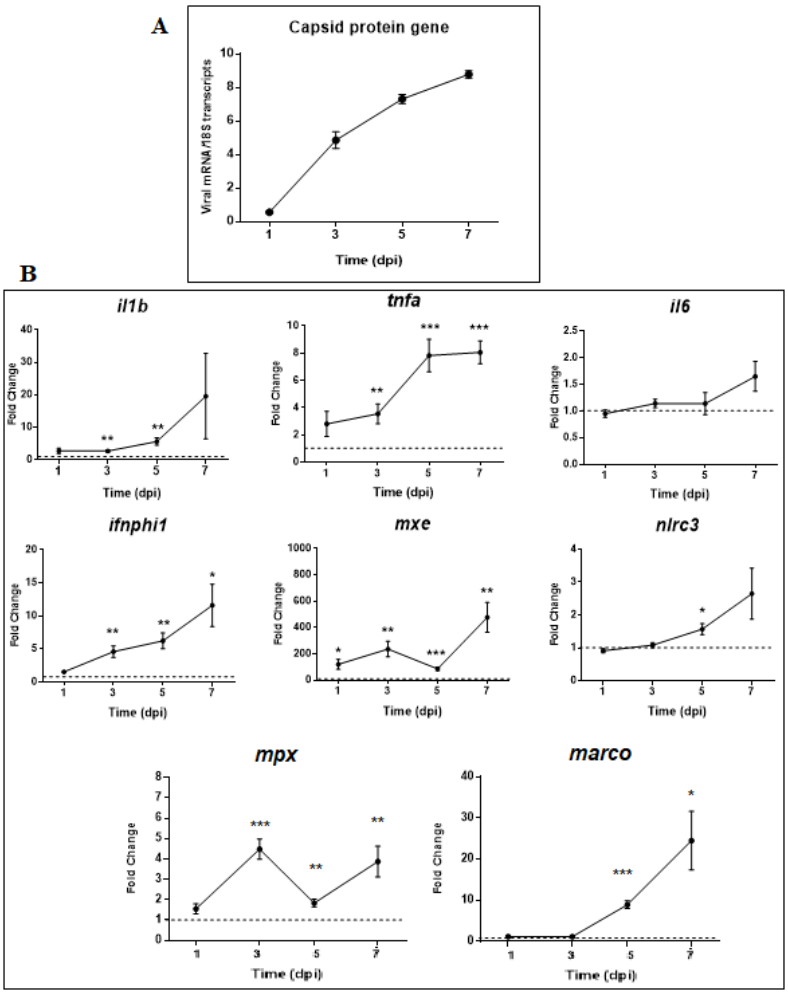

Figure 5.9. Study of gene expression by qPCR. **A** Quantification of NNV capsid protein gene transcripts as a measure of the viral amount in the larvae over different times of infection. **B** Expression of immune genes in NNV infected and uninfected larvae at different times of infection. Each sample (three technical replicates) was normalized to the 18S zebrafish gene and standardized with respect to its uninfected control (5 biological replicates, pools of 4 larvae each). Dot bar marks the uninfected control fold change (1). Means ± standard errors of means were calculated. Significant differences were displayed as follows: ***, 0.0001 > p-value > 0.001; **, 0.001 > p-value > 0.01; *, 0.01 > p-value > 0.05.

5.4. DISCUSSION

It is well known that zebrafish provides significant advantages for understanding host-pathogen interactions in the context of a complete vertebrate. For this reason, it is widely used for biomedical research (Lin et al., 2016). Although in 2007, Furusawa et al., reported that zebrafish was not susceptible to NNV (2007), later Lu was able to reproduce the nodavirus infection in this fish species (Lu et al., 2008). Although VER disease produces important economic losses in cultured fishes around the world, few studies have conducted to establish the disease in the zebrafish model. In 2008, zebrafish has been a study model of the response of interferon to an acute or persistent NNV infection using adults infected by peritoneal injection and larvae microinjected with NNV (it is not specified where the microinjection is performed or the age of the larvae) and techniques such as RT-PCR, immunoblot and histopathology (Lu et al., 2008), and afterwards, Morick described the infection by bath of zebrafish larvae (Morick et al., 2015), and also the protection conferred by ribavirin treatment against infection of larvae by bath, studying the immune genes using real time RT-PCR (Morick and Saragovi, 2017).

However, these works did not fully used all the advantages that this model species offers us. In this study we wanted to propose the use of zebrafish as a model species for this disease and to use techniques that allow us a deeper understanding of what happens during this viral disease.

First, we wanted to determine the most effective route of infection, in order to carry out our studies. After the infection of 3 dpf larvae via brain, duct of Cuvier, intramuscularly, and via bath we could assess that the route that offered a lower percentage of survival against NNV was the microinjection via brain, followed by the microinjection via intramuscular. Exposure of the larvae to the virus by bath did not reach any statistically different mortality than the control group, so we may not find that "infection window" at 4 dpf described by Morick (Morick et al., 2015). Furthermore, we wanted to check if the age of the larvae influenced the infection with NNV using any route of infection. In this way, 14 dpf larvae were infected under the same conditions than the 3 dpf larvae (both viral load, infection volume or incubation temperature

and time), and no significant mortalities could be detected. Therefore, the older the larvae become, the more resistance they offer to this virus. This could be due to a more developed immune system or because of the differences produced by the beginning of the feeding of the larvae that do not allow us to verify the effect of the virus as well as it occurs in younger larvae that do not have to be fed daily removing this variable. Thus, infection via brain in 3 dpf zebrafish larvae would be more effective for subsequent studies of the VER disease in this fish species. Moreover, the advantages of using younger larvae were a shorter waiting time to obtain the fish for experimentation, greater experimentation power as they were still optically transparent, which made possible the use of imaging techniques to study transgenic larvae, whole-mount immunohistochemistry and other visualization techniques.

One of the main characteristic symptoms produced by NNV is erratic swimming in infected fish. The small size of the zebrafish allows us to better control the experimental conditions *in vivo*, since its storage does not require very large spaces so certain variables, as the temperature, are more controlled. In addition, for this work, this characteristic allowed us to study the swimming behavior of several infected individuals compared with the respective non-infected controls under the same camera approach, thus eliminating possible interference effects. In this way, we were able to analyze different characteristics of fish behavior, such as velocity, accumulated distance, Euclidean distance and directionality of swimming. In 3 dpf larvae, we were able to observe that whatever the infection route was, the larvae used to present a significant alteration of any of the swimming characteristics analyzed, being the velocity the one that presents greater statistical differences between infected and non-infected controls. In 14 dpf larvae, these differences in the behavior of the infected larvae gradually disappear, although it can still be observed that the virus has some effect on the swimming behavior of the larvae. The NNV may not be capable of producing significant mortalities at this age, but it does affect the swimming behavior of the larvae, it may be affecting certain areas of the brain of the fish.

After observing the mortalities produced by NNV through brain infection in 3 dpf larvae, we verified how mortality was associated with a greater replication of the virus. The expression of different immune genes of the zebrafish larvae throughout this infection was also modulated. An increase in the gene expression of proinflammatory cytokines such as *tnfa* and *il1b* was observed by qPCR analysis. This increase in pro-inflammatory cytokines was also observed in different organisms infected with NNV, such as Atlantic halibut (Overgard et al., 2012), sea bass and seabream (Poisa-Beiro et al., 2008), turbot (Montes et al., 2010), zebrafish (Morick et al., 2015) or orange-spotted groupers (Huang et al., 2016). The expression of TNFα is much higher in species susceptible to NNV, such as sea bass, compared to its expression in species resistant to NNV, seabream, which indicated that this pro-inflammatory cytokine may be responsible for a large inflammatory reaction in the areas of infection of this virus, such as the brain, retina and spinal cord, producing a neurodegenerative process that the fish is not able to overcome (Poisa-Beiro et al., 2008).

Mx apparently plays an important role in viral immunity in larvae, in which the adaptive immune response is not fully functional (Novoa and Figueras, 2012) showing a non-specific protection against a range of RNA viruses during early stages of organisms (Lin et al., 2006) so, we studied the gene expression in zebrafish larvae infected with NNV, detecting a high expression of *mxe* gene. This high and prolonged expression over time can also be seen in other fish during a NNV infection, such as barramundi (Wu and Chi, 2007), grouper (Chen et al., 2006), seabream (Poisa-Beiro et al., 2008), sea bass (Scapigliati et al., 2010) or turbot (Park et al., 2009; Montes et al., 2010). The cytokine involved in the regulation of defense response to virus by host, the *ifnphi1* gene, also increment its expression after 3 dpi. Like IL-1β, IL-6 is also a cytokine involved in different immune processes like acute phase reaction, and although in other fish infected with NNV it increases its gene expression (Overgard et al., 2012), it does so at a very early time of infection, so we may not be seeing regulation of *il6* in our infection model. The possible effect of *nlrc3* expression during a viral infection in fish should be further studied, its expression *in vivo* has been studied in fish in face of a stimulus with poly I:C, an analogue of

dsRNA virus (Li et al., 2015; Paria et al., 2016), or after an infection with channel catfish hemorrhage reovirus (CCRV) in channel catfish (Li et al., 2012), showing all these cases a positive regulation of *nlrc3*, but we can also detect a downregulation of *nlrc3* in the brain and the head kidney of infected sea bass at 24 hpi (Lama et al., 2020), maybe due to the lack of other proinflammatory cytokines like TNFa and IL1b (Álvarez et al., 2017). In our experimental infections of zebrafish larvae we found an upregulation of this gene at 5 dpi, matching the regulation of the other proinflammatory cytokines.

The expression of two genes expressed by the two main immune fish cell types was also analyzed, the *mpx* gene, a myeloid-specific peroxidase which is a specific marker of differentiated neutrophilic granulocytes, and the *marco* gene, a macrophage receptor with collagenous structure, specific marker of macrophages, both already present in 2 dpf larvae (Elomaa et al., 1995; Lieschke et al., 2001). These two genes were upregulated during a NNV infection, so we used transgenic lines of zebrafish to analyze the migration on these inmune cells to brain and found that infection via brain causes the migration of neutrophils to the site of infection. We also used the transgenic line where myeloid lineage and lysozyme-expressing cells are labelled, and we were able to observe a migratory trend similar to that of neutrophils, Lyz+ cells migrate to the brain when infection is carried out via brain. This similar migratory trend such as neutrophils may be due because of the expression of the *mpx* gene largely overlaps with the expression of the *lyz* gene in zebrafish larvae (Su et al., 2007).

Neuroinvasion is a rare phenomenon, but certain neuronal viruses, such as NNV, have the ability to colonize the CNS. The strategies to reach the brain, a highly protected organ, can be by camouflage in immune cells, such as neutrophils or macrophages, that have permission to enter and protect the brain, this is the so-called ‘Trojan horse’ strategy. Another strategy is to infect endothelial cells from microvessels that reach the brain to irrigate it, and also through numerous axons that connect the CNS with the periphery (Passoni et al., 2017). By whole-mount immunohistochemistry and imaging of fixed samples, we could study the distribution of the NNV in the head of zebrafish larvae. We were not able to find colocalization of the virus

with the neutrophils, eliminating the possibility that these cells were the carriers of the virus throughout the animal's body. We also did not find colocalization between the labelled endothelial cells in the Tg(*fli*:GFP) larvae and the virus, suggesting that the NNV may not be traveling through the endothelium of the larvae. It was possible to visualize the virus associated to some glial neurons, however most of the virus staining does not coincide with the 6G7 antibody staining suggesting that the virus should be replicating in othe cell type. More work should be done to determine which are possible targets of the NNV infection.

In conclusion, this work reaffirms the foundations for the zebrafish to be considered the model of infection, not only of the NNV, but of many other fish viruses that are hard to study *in vivo* due to the difficult obtaining of the affected species or its maintenance in the laboratory.

5.5. REFERENCES

Álvarez CA, Ramírez-Cepeda R, Santana P, Torres E, Cortés J, Guzmán F, Schmitt P, Mercado L (2017) Insights into the diversity of NOD-like receptors: Identification and expression analysis of NLRC3, NLRC5 and NLRX1 in rainbow trout. *Molecular Immunology* 87:102-113.

Aranguren R, Tafalla C, Novoa B, Figueras A (2002) Experimental transmission of encephalopathy and retinopathy induced by nodavirus to sea bream, *Sparus aurata* L., using different infection models. *Journal of Fish Diseases* 25:317-324.

Benard EL, Van der Sar AM, Ellett F, Lieschke GJ, Spaink HP, Meijer AH (2012) Infection of zebrafish embryos with intracellular bacterial pathogens. *Journal of Visualized Experiments* (61):e3781.

Binesh CP (2013) Mortality due to viral nervous necrosis in zebrafish *Danio rerio* and goldfish *Carassius auratus*. *Diseases of Aquatic Organisms* 104:257-260.

Bovo G, Nishizawa T, Maltese C, Borghesan F, Mutinelli F, Montesi, F, De Mas S (1999) Viral encephalopathy and retinopathy of farmed marine fish species in Italy. *Virus Research* 63:143-146.

Chaves-Pozo E, Valero Y, Esteve-Codina A, Gómez-Garrido J, Dabad M, Alioto T, Meseguer J, Esteban MA, Cuesta A (2017) Innate cell-mediated cytotoxic activity of European sea bass leucocytes against nodavirus-infected cells: a functional and RNA-seq study. *Scientific Reports* 7:15396.

Chaves-Pozo E, Bandín I, Olveira JG, Esteve-Codina A, Gómez-Garrido J, Dabad M, Alioto T, Esteban MA, Cuesta A (2019) European sea bass brain DLB-1 cell line is susceptible to nodavirus: a transcriptomic study. *Fish and Shellfish Inmunology* 1:14-24.

Chen YM, Su YL, Lin JHY, Yang HL, Chen TY (2006) Cloning of an orange-spotted grouper (*Epinephelus coioides*) Mx cDNA and characterisation of its expression in response to nodavirus. *Fish and Shellfish Immunology* 20:58-71.

Crim MJ, Riley LK (2012) Viral diseases in zebrafish: What is known and unknown. *ILAR Journal* 53(2):135-143.

Cui C, Bernard EL, Kanwal Z, Stockhammer OW, vand der Vaart M, Zakrzewska A, Spaink HP, Meijer AH (2011) Infectious disease modeling and innate immune function in zebrafish embryos. *Methods in cell biology* 105:273307.

Elomaa O, Kangas M, Sahlberg C, Tuukkanen J, Sormunen R, Liakka A, Thesleff I, Kraal G, Tryggvason K (1995) Cloning of a novel bacteria-binding receptor structurally related to scavenger receptors and expressed in a subset of macrophages. *Cell* 80(4):603-609.

Furusawa R, Okinaka Y, Uematsu K, Nakai T (2007) Screening of freshwater fish species for their susceptibility to a betanodavirus. *Diseases of Aquatic Organisms* 77:119-125.

Garner JN, Joshi B, Jagus R (2003) Characterization of rainbow trout and zebrafish eukaryotic initiation factor 2α and its response to endoplasmic reticulum stress and IPNV infection. *Developmental and Comparative Immunology* 27:217-231.

Herbomel P, Thisse B, Thisse C (1999) Ontogeny and behaviour of early macrophages in the zebrafish embryo. *Development* 126:3735-3745.

Huang Y, Yu Y, Yang Y, Yang M, Zhou L, Huang X, Qin Q (2016) Antiviral function of grouper MDA5 against iridovirus and nodavirus. *Fish and Shellfish Immunology* 54:188-196.

Kanther M, Rawls JF (2010) Host-microbe interactions in the developing zebrafish. *Current Opinion in Immunology* 22(1):10-19.

Kuo HC, Wang TY, Chen PP, Chen YM, Chuang HC, Chen TY (2011) Real-time quantitative PCR assay for monitoring of nervous necrosis virus infection in grouper aquaculture. *Journal of Clinical Microbiology* 49:1090-1096.

Lam S, Chua H, Gong Z, Lam T, Sin Y (2003) Development and maturation of the immune system in zebrafish, *Danio rerio*: a gene expression profiling, in situ hybridization and immunological study. *Developmental and Comparative Immunology* 28:9-28.

Lama R, Pereiro P, Valenzuela-Muñoz V, Gallardo-Escárate C, Tort L, Figueras A, Novoa B (2020) RNA-Seq analysis of European sea bass (*Dicentrarchus labrax* L.) infected with nodavirus reveals powerful modulation of the stress response. *Veterinay Research* 51:64.

LaPatra SE, Barone L, Jones GR, Zon Li (2000) Effects of infectious hematopoietic necrosis viru and infectious pancreatic necrois virus infection on hematopoietic precursors of zebrafish. *Blood Cells, Molecules, and Diseases* 26(5):256-259.

Le Guyader D, Redd MJ, Colucci-Guyon E, Murayama E, Kissa K, Biolat V, Mordelet E, Zapata A, Shinomiya H, Herbomel P (2008) Origins and unconventional behavior of neutrophils in developing zebrafish. *Blood* 111(1):132-41.

Levraud JP, oudinot P, Colin I, Benmansour A, Peyrieras N, Herbomel P, Lutfalla G (2007) Identification of the zebrafish IFN receptor:

implications for the origin of the vertebrate IFN system. *Journal of Immunology* 178(7):4385-4394.

Levraud JP, Palha N, Langevin C, Boudinot P (2014) Through the looking glass: witnessing host-virus interplay in zebrafish. *Trends in Microbiology* 22(9):490-497.

Li J, Kong L, Gao Y, Wu C, Xu T (2015) Characterization of NLR-A subfamily members in miiuy croaker and comparative genomics revealed NLRX1 underwent duplication and lose in actinopterygii. *Fish and Shellfish Immunology* 47(1):397-406.

Li M, Wang QL, Lu Y, Chen SL, Li Q, Sha ZX (2012) Expression profiles of NODs in channel catfish (*Ictalurus punctatus*) after infection with *Edwardsiella tarda*, *Aeromonas hydrophila*, *Streptococcus iniae* and channel catfish hemorrhage reovirus. *Fish and Shellfish Immunology* 33(4):1033-1041.

Lieschke GJ, Oates AC, Crowhurst MO, Ward AC, Layton JE (2001) Morphologic and functional characterization of granulocytes and macrophages in embryonic and adult zebrafish. *Blood* 98(10):3087-3096.

Lin CH, John JAC, Lin CH, Chang CY (2006) Inhibition of nervous necrosis virus propagation by fish Mx proteins. *Biochemical and Biophysical Research Communications* 351:534-539.

Lin CY, Chiang CY, Tsai HJ (2016) Zebrafish and Medaka: new model organisms for modern biomedical research. Journal of *Biomedical Science* 23:19.

López-Jimena B, Alonso MC, Thompson KD, Adams A, Infante C, Castro D, Borrego JJ, Garcia-Rosado E (2011) Tissue distribution of Red Spotted Grouper Nervous Necrosis Virus (RGNNV) genome in experimentally infected juvenile European seabass (*Dicentrarchus labrax*). *Veterinaty Microbiology* 154:86-95.

López-Muñoz A, Roca FJ, Sepulcre MP, Meseguer J, Mulero V (2010) Zebrafish larvae are unable to mount a protective antiviral response against waterborne infection by spring viremia of carp virus. *Developmental and Comparative Immunology* 34:546-552.

Lu MW, Chao YM, Guo TC, Santi N, Evensen O, Kasani SK, Hong JR, Wu JL (2008) The interferon response is involved in nervous necrosis virus acute and persistent infection in zebrafish infection model. *Molecular Immunology* 45:1146-1152.

Ludwig M, Palha N, Torhy C, Briolat V, Colucci-Guyon E, Brémont M, Herbomel P, Boudinot P, Levraud JP (2011) Whole-body analysis of a viral infection: vascular endothelium is a primary target of infectious hematopoietic necrosis virus in zebrafish larvae. *PLoS Pathogens* 7(2):e1001269.

Martín V, Mavian C, López Bueno A, Molina A, Díaz E, Andrés G, Alcami A, Alejo A (2015) Establishment of a zebrafish infection model for the study of wild-type and recombinant European sheatfish virus. *Journal of Virology* 89(20):10702-10706.

Mazelet L, Dietrich J, Rolland JL (2011) New RT-qPCR assay for Viral Nervous Necrosis Virus detection in sea bass, *Dicentrarchus labrax* (L.): application and limits for hatcheries sanitary control. *Fish and Shellfish Immunology* 30:27-32.

Mladineo I (2003) The immunohistochemical study of nodavirus changes in larval, juvenile and adult sea bass tissue. *Journal of Applied Ichtyology* 19:366-370.

Montes A, Figueras A, Novoa B (2010) Nodavirus encehalopathy in turbot (*Scophthalmus maximus*): Inflammation, nitric oxide production and effect of anti-inflammatory compounds. *Fish and Shellfish Immunology* 28:281-288.

Morick D, Figenbaum O, Smirnov M, Fellig Y, Inbal A, Kotler M (2015) Mortality caused by bath exposure of zebrafish (*Danio rerio*)

larvae to nervous necrosis virus is limited to the fourth day postfertilization. *Applied and Environmental Microbiology* 81(10):3280-3281.

Morick D, Saragovi A (2017) Inhibition of nervous necrosis virus by ribavirin in a zebrafish larvae model. *Fish and Shellfish Immunology* 60:537-544.

Novoa B, Romero A, Mulero V, Rodriguez I, Fernandez I, et al. (2006) Zebrafish (*Danio rerio*) as a model for the study of vaccination against viral haemorrhagic septicemia virus (VHSV). Vaccine 24:3924-3931.

Novoa B, Figueras A (2012) Zebrafish: model for the study of inflammation and the innate immune response to infectious diseases. *Advances in Experimental Medicine and Biology* 946:253-275.

Nüsslein-Volhard C, Dahm R (2002) Zebrafish: a practical approach. *Oxford University Press, New York, NY*.

Overgard AC, Nerland AH, Fiksdal IU, Patel S (2012) Atlantic halibut experimentally infected with nodavirus shows increased levels of T-cell marker and IFNγ transcripts. *Developmental and Comparative Immunology* 37:139-150.

Panzarin V, Patarnello P, Mori A, Rampazzo E, Cappellozza E, Bovo G, Cattoli G (2010) Development and validation of a real-time TaqMan PCR assay for the detection of betanodavirus in clinical specimens. *Archives of Virology* 155:1193-1203.

Paria A, Deepika A, Sreedharan K, Makesh M, Chaudhari A, Purushothaman CS, Rajendran KV (2016) Identification of Nod like receptor C3 (NLRC3) in Asian seabass, *Lates calcarifer*: Characterisation, ontogeny and expression analysis after experimental infection and ligand stimulation. *Fish and Shellfish Immunology* 55:602-612.

Park KC, Osborne JA, Montes A, Dios S, Nerland AH, Novoa B, Figueras A, Brown LL, Johnson SC (2009) Immunological responses

of turbot (*Psetta maxima*) to nodavirus infection or polyriboinosinic acid (pIC) stimulation, using expressed sequences tags (ESTs) analysis and cDNA microarrays. *Fish and Shellfish Immunology* 26:91-108.

Passoni G, Langevin C, Palha N, Mounce BC, Briolat V, Affaticati P, De Job E, Joly JS, Vignuzzi M, Saleh MC, Herbomel P, Boudinot P, Levraud JP (2017) Imaging of viral neuroinvasion in the zebrafish reveals that Sindbis and chikungunya viruses favour different entry routes. *Disease Models and Mechanisms* 10(7):847-857.

Pfaffl MW (2001) A new mathematical model for relative quantification in real-time RT-PCR. *Nucleic Acids Research* 29:2002-2007.

Phelan P, Pressley M, Witten P, Mellon M, Blake S, et al. (2005) Characterization of snakehead rhabdovirus infection in zebrafish (*Danio rerio*). *Journal of Virology* 79:1842-1852.

Poisa-Beiro L, Dios S, Montes A, Aranguren R, Figueras A, Novoa B (2008) Nodavirus increases the expression of Mx and inflammatory cytokines in fish brain. *Molecular Immunology* 45:218-225.

Reed LJ, Müench H (1938) A simple method of estimating fifty percent endpoints. *The American Journal of Epidemiology* 27(3):493-497.

Rozen S, Skaletsky H (2000) Primer3 on the WWW for general users and for biologist programmers. *Methods in Molecular Biology* 132:365-386.

Sanders G, Batts W, Winton J (2003) Susceptibility of zebrafish (*Danio rerio*) to a model pathogen, spring viremia of carp virus. *Comparative Medicine 53*(5):514-521.

Scapigliati G, Buonocore F, Randelli E, Casani D, Meloni S, Zarletti G, Tiberi M, Pietretti D, Boschi I, Manchado M, Martin-Antonio B, Jimenez-Cantizano R, Bovo G, Broghesan F, Lorenzen N, Einer-Jensen K, Adams S, Thompson K, Alonso C, Bejar J, Cano I, Borrego JJ, Alvarez MC (2010) Cellular and molecular immune responses of the

sea bass (*Dicentrarchus labrax*) experimentally infected with betanodavirus. *Fish and Shellfish Immunology* 28:303-311.

Schneider CA, Rasband WS, Eliceiri KW (2012) NIH Image to ImageJ: 25 years of image analysis". *Nature methods* 9(7):671-675.

Skliris GP, Richards RH (1999) Induction of nodavirus disease in seabass, *Dicentrarchus labrax*, using different infection models. *Virus Research* 63:85-93.

Su F, Juarez M, Cooke CL, LaPointe L, Shavit JA, Yamaoka JS, Lyons SE (2007) Differential regulation of primitive myelopoiesis in the zebrafish by Spi-1/Pu.1 and C/ebp1. *Zebrafish* 4:187-199.

Varela M, Díaz-Rosales P, Pereiro P, Forn-Cuní G, Costa MM, Dios S, Romero A, Figueras A, Novoa B (2004a) Interferon-induced genees of the expanded IFIT famil show conserved antiviral activities in non-mammalian species. *PLoS one* 9:e100015.

Varela M, Romero A, Dios S, van der Vaart M, Figueras A, Meijer AH, Novoa B (2014b) Cellular visualization of macrophage pyroptosis and interleukin-1β release in a viral hemorrhagic infection in zebrafish larvae. *Journal of virology* 88(20):12026-12040.

Wang ZL, Xu XP, He BL, Weng SP, Xiao J, Wang L, Lin T, Liu X, Wang Q, Yu XQ, He JG (2008) Infectious spleen and kidney necrosis virus OFR48R functions as a new viral vascular endothelial growth factor. *Journal of Virology* 82(9):4371-4383.

Westerfield M (2000) The zebrafish book. A guide for the laboratory use of zebrafish (*Danio rerio*). *University of Oregon Press, Eugene, OR.*

Wu YC, Chi SC (2007) Cloning and analysis of antiviral activity of a barramundi (*Lates calcarifer*) Mx gene. *Fish and Shellfish Immunology* 23:97-108.

Xu X, Zhang L, Weng S, Huang Z, Lu J, Lan D, Zhong X, Yu X, Xu A, He J (2008) A zebrafish (*Danio rerio*) model of infectious spleen and kidney necrosis virus (ISKNV) infection. *Virology* 376:1-12.

USC
UNIVERSIDADE
DE SANTIAGO
DE COMPOSTELA

Chapter 6

General discussion and Conclusions

USC
UNIVERSIDADE
DE SANTIAGO
DE COMPOSTELA

6 General discussion and conclusions

6.1. GENERAL DISCUSSION

This Doctoral Thesis aims a deeper knowledge of the effect of a nodavirus infection in a susceptible species such as sea bass (*Dicentrarchus labrax*). As described in **Chapter 1**, sea bass is a species of great commercial value and nodavirus negatively impacts on aquaculture economy.

In **Chapter 2** of this Doctoral Thesis, a transcriptomic analysis of nodavirus infection on brain, the main target organ of the virus, and the head kidney, the main immune organ of fish, was carry out. Instead of a clear immune or antiviral response, almost a complete picture of the response of the HPI axis was drawn, with the interconnection of these two organs. So far, it is the first time that such a clear response of this axis has been found in teleost fish when faced with a viral infection. The biosynthesis of the main stress hormone, cortisol, orchestrates a series of changes that lead to the regulation of pituitary hormones that modify neuronal processes in the brain, causing neuronal damage explaining the symptoms so characteristic of the VER disease. As the time of infection progresses, the cells try to protect themselves by passing from the state of excitotoxicity, caused by the influx of calcium into the cell due to the excitability of glutamate receptors, to the state of neuroprotection, lowering the calcium levels inside cells. This chapter may change our immunological vision in detrimental to analyze the functions of the HPI axis, protecting neurons from the entire hormonal storm produced in the fish and that affects so many biological processes. The neuroprotection seen at 72 hpi may occurs too late, it would be necessary to study the possibility of stopping all the previous neuronal damage, being able to stop the spread of the virus and the effects that causes in the brain of the fish. The transcriptomic study of this axis in a nodavirus resistant species such as the seabream (*Sparus*

aurata), could elucidate which pathways would be more effective to intervene.

The study of lncRNAs in **Chapter 3** is an attempt to better understand the response observed in the transcriptome. The use of the same samples allows us to eliminate those sequences that are being translated into proteins and focus on those sequences that miss them and that may be acting as regulators of the fish's response to the virus. We were able to verify that there is an important parallel response between the expression of the proteins and the regulation of the lncRNAs that surround them. Although in our transcriptome the immune response was not clearly represented, several terms related to immune processes were found when the enrichment analysis of GO terms of genes that surround the lncRNA differentially expressed in the head kidney were analyzed. We could also find stress-related processes of the endoplasmic reticulum, which is related to our observations of ROS production at early stages of infection described in **Chapter 2**. Among the regulated lncRNAs in the brain, we also observed regulated immune processes related to immunoglobulin production, important when fighting neurotropic viruses and also a modulation of the calcium homeostasis within the cell, already detected in the transcriptome. Thus, the relationship with terms of stress in the head kidney and calcium in the brain refers us to the regulation of the HPI axis. The discovery that lncRNAs modulate some of the most regulated processes at protein level suggests that modulation of the expression of lncRNAs could be an effective tool against viral infection.

While this technology is still in development, **in Chapter 4** we described the steps to achieve a vaccine with lower cost and greater environmental safety. We focused in the use of bacterias that expressed on their surface the so-called *spinycterins*, a fragment of the protein of the virus capsid attached by a prokaryotic anchor. By using a shorter protein C fragment that contains most of the antigenicity, we were able to maximize bacterial expression. In addition, the autoinduction medium in which bacteria were grown was improved to avoid loss of immunogenicity and the overexpression of toxicity that occurs with certain recombinant proteins. The safety of the vaccine was also increased by the use of an *E. coli* strain incapable of repairing damage

in its DNA, thus being able to inactivate them effectively and irreversibly. All the improvements analyzed in this chapter will allow furthers advances in the development of new vaccines with prototypes that avoid the use of adjuvants.

In **Chapter 5** we wanted to assess if the zebrafish (*Danio rerio*) was a good study model for the VER disease. Obtaining and maintaining commercial fish species is not always easy, and extensive facilities are required for their maintenance. The zebrafish is a vertebrate model that does not require large facilities or important efforts for its maintenance, it allows to obtain a large number of individuals and we can control factors such as the traceability of the families that are being used. In this chapter, we reproduce the VER disease in zebrafish that will allow a better understanding of the relationship between the nodavirus and its host. We determined the best route of infection and the age at which this fish species was infected more effectively. Tools used in this study, such as the use of transgenic fishes or tecniques as whole mount immunohistochemistry, may be further developed in the future for the study of different treatments that can alleviate the fatal consequences produced by the VER disease

USC
UNIVERSIDADE
DE SANTIAGO
DE COMPOSTELA

6.2. CONCLUSIONS

1. RNA-Seq analysis of the brain and head kidney of sea bass juveniles showed that there was a modest modulation of immune-related genes in the brain, the target organ of this virus.

2. The nodavirus induces a complete alteration of the hypothalamic-pituitary-interrenal axis after infection, connecting processes regulated by hormones, neurotransmitters and their receptors in the brain and the synthesis of cortisol, the main stress hormone, in the head kidney.

3. After infection, lncRNAs were also modulated in sea bass and enrichment analysis of the neighbouring coding genes of the modulated lncRNAs revealed many terms related to the immune response and viral infectivity but also related to the stress response. A strong correlation between the expression of the lncRNAs and their flanking coding genes was observed.

4. The so-called spynicterins exert immunization of European sea bass juveniles against nervous necrosis virus. The use of *E. coli* displaying at their surface a downsized nodavirus coat antigen provides potential to develope cost effectivenness and safer vaccines.

5. Although after 14 days post fertilization zebrafish are resistant to the nodavirus infection, 3 dpf larvae infected by brain microinjection could be a valid infection model for nodavirus since they are susceptible to the disease and a clear modulation of the expression of immune genes is observed.

USC
UNIVERSIDADE
DE SANTIAGO
DE COMPOSTELA

Resumo en galego

PROCURA DE NOVAS ESTRATEXIAS PARA O CONTROL DE ENFERMIDADES VIRAIS NA ACUICULTURA

Capítulo 1: Introdución

Unha das especies animais que conseguiu maior éxito na historia da acuicultura europea é a robaliza mediterránea (*Dicentrarchus labrax* L.). En menos de 15 anos, a produción de robaliza que procede da acuicultura pasou duns poucos miles de toneladas a preto de 164.000 toneladas en 2015 (FAO, Food and Agriculture Organization), fronte a só as case 6.500 toneladas obtidas mediante pesca segundo datos do MAPAMA (Ministerio de Agricultura e Pesca, Alimentación e Medio Ambiente) do mesmo ano. España ocupa o cuarto lugar na clasificación mundial de pesca de robaliza, e o terceiro en produción de robaliza en acuicultura, seguindo a tendencia mundial.

O estrés ó que se someten as robalizas e outros animais en condicións de cultivo considérase un factor importante corresponsable de brotes de enfermidades, polo que xeralmente os esforzos para mellorar a cría céntranse en reducir este estrés. Estes brotes teñen efectos importantes na produción comercial e poderían interromper a expansión da industria nalgúns países, particularmente na acuicultura mediterránea. Outro problema é a falta de terapéuticos eficaces autorizados na maioría dos países europeos, polo que o coñecemento sobre os mecanismos moleculares e xenéticos de resistencia a patóxenos e as características específicas da resposta inmune fronte a diversos axentes infecciosos debería beneficiar enormemente o desenvolvemento de vacinas e terapias eficaces. Desta maneira evitaríase o uso de antimicrobianos que poderían chegar ao medio ambiente e causar un efecto prexudicial sobre a saúde humana.

A robaliza mediterránea vese afectada por enfermidades infecciosas de todo tipo, aínda que a enfermidade que causa maiores

perdas económicas é a retinopatía e encefalopatía viral (VER), cuxo axente causal é o virus da necrose nerviosa (NNV) ou nodavirus. O NNV pertence ao xénero *Betanodavirus*, que se clasifica en 4 xenotipos debido a unha pequena variación na secuencia do ARN2 (rexión T4): RGNNV (red-spotted grouper nervous necrosis virus), BFNNV (barfin flounder nervous necrosis virus), TPNNV (tiger puffer nervous necrosis virus) e SJNNV (striped jack nervous necrosis virus). Estes xenotipos infectan a especies que habitan en rangos distintos de temperatura, sendo o xenotipo RGNNV o causante da enfermidade na robaliza.

Aínda que esta enfermidade afecta principalmente a larvas e xuvenís, alcanzando mortalidades do 100 %, tamén se observaron importantes mortalidades en peixes de tamaño comercial e adultos. Debido á súa natureza neurotrópica, o nodavirus afecta principalmente ó sistema nervioso central, causando vacuolización no cerebro, retina e espiña dorsal dos peixes infectados.

O nodavirus é un virus pequeno non envolto, cun diámetro duns 25 nm e simetría icosaédrica. Seu xenoma viral bisegmentado consta de duas cadeas de ARN sinxelas de sentido positivo. O ARN1 codifica a ARN polimerasa dependente de ARN (RdRp), e o ARN2 codifica a proteína estructural da cápside, que está asociada co arresto do ciclo celular e a súa acumulación induce unha fervenza dependente de caspasa que remata na apoptosis celular. Ademáis, fórmase un fragmento subxenómico do ARN1, o chamado ARN3, que codifica dúas proteínas non estructurais, a proteína B1 que xoga un rol antinecrótico en estadíos temperáns da infección, e a proteína B2 que suprime o ARN de interferencia de las células infectadas e actúa como factor necrótico en estadíos tardíos da infección.

De momento, esta enfermidade viral prevense evitando a exposición dos animais ao nodavirus e refórzanse as boas prácticas de manexo, como prácticas xerais de hixiene, tratamento da auga con luz UV e a desinfección dos tanques. Actualmente a vacinación está restrinxida ao xenotipo RGNNV con dúas vacinas inactivadas mortas con formalina no mercado da acuicultura.

Os peixes teleosteos son o grupo animal máis primitivo que posúe un sistema inmune completo, que consta dunha inmunidade innata ou inespecífica e unha inmunidade adaptativa ou específica. Aínda que

adoitan describirse por separado, estas dúas partes da inmunidade van da man para manter os niveis de inmunocompetencia do hóspede o máis altos posible.

A resposta inmunitaria innata considérase esencial á hora de facer fronte a unha infección vírica, está mediada por mecanismos celulares e humorais. A nivel humoral, unha infección por betanodavirus *in vivo* mostra unha gran amplificación da expresión de distintas citoquinas proinflamatorias involucradas no roteiro antiviral dos interferóns. Esta resposta de citoquinas conleva un patrón de inflamación que podería estar implicado na formación de vacuolizacións no sistema nervioso central, características desta enfermidade infecciosa. A nivel celular, a actuación de células citotóxicas non específicas, células natural-killer e linfocitos T citotóxicos mestúrase coa actuación de distintas proteínas antivirais.

A inmunidade adaptativa mellora cada vez que o hóspede ten contacto cun patóxeno específico. A produción de inmunoglobulinas por parte das células B é un factor crítico á hora de recoñecer, neutralizar e eliminar o patóxeno. As células T promoven a destrución das células infectadas para que o virus non se disemine polo resto do organismo. A maior expresión de marcadores de células B e T foi demostrada ante unha infección con nodavirus, suxerindo o seu papel activo contra a infección e abrindo unha xanela ao desenvolvemento de vacinas máis eficaces que incrementen esta resposta adaptativa.

O obxectivo da presente Tese Doutoral foi profundar no coñecemento da resposta ante unha infección con nodavirus. O uso de ferramentas bioinformáticas permítenos un estudo en maior profundidade das interaccións entre hóspede e patóxeno, polo que se utilizou a secuenciación de ARN de alto rendemento (RNA-Seq) para analizar a resposta transcriptómica completa da robaliza europea ante o nodavirus, así como a súa posible modulación por ARNs longos non codificantes do xenoma (lncRNAs). Como materia de estudo usouse o cerebro, o principal órgano diana do virus, e o ril anterior, implicado na resposta inmunitaria. Esta foi a primeira vez que a análise dun RNA-Seq mostrou unha interacción de roteiros neuroendocrinos e sistema inmune a través do eixo hipotálamo-pituiratio-interrenal (HPI) durante unha infección con nodavirus, e tamén o involucramento de varios

lncRNAs na resposta a nodavirus. Mentres estas técnicas avanzan a pasos axigantados, quixemos mellorar a inmunización da robaliza contra o nodavirus. Desenvolveuse unha vacina con bacterias recombinantes de *Escherichia coli* con fragmentos virais na súa superficie (*spynicterins*), mellorando a seguridade ambiental e a súa rendibilidade ao non requirir adxuvantes. Tamén comprendemos durante o desenvolvemento desta Tese Doutoral, a relativa dificultade de traballar con especies de alto valor comercial, así quíxose establecer ao peixe cebra como modelo de infección do nodavirus para aproveitar moitas das ferramentas que nos pode proporcionar.

Capítulo 2: A análise do RNA-Seq da robaliza europea (*Dicentrarchus labrax* L.) infectada con nodavirus revela unha potente resposta de estrés

Como se comentou na introdución, realizouse o estudo transcriptómico da robaliza europea ante unha infección con nodavirus, polo gran valor comercial desta especie animal e a gran taxa de mortalidade que este virus causa nela. Aínda que hai varios estudos que utilizan o RNA-Seq para entender os efectos do nodavirus a través do perfil transcriptómico de células infectadas *in vitro* e en órganos e texidos de animais infectados *in vivo*, esta foi a primeira vez que se analizou a resposta transcriptómica completa da robaliza europea ante unha infección con nodavirus. Os órganos seleccionados para este estudo foron o cerebro, pola natureza neurotrópica do virus, e o ril anterior, por orquestrar a resposta inmune do animal. Tomáronse mostras dos tecidos a dous tempos de infección (24 e 72 horas post-infección, hpi) facendo grupos de 3 individuos e tendo finalmente 3 réplicas biolóxicas de estudo en cada condición. A secuenciación realizouse utilizando a tecnoloxía Illumina HiSeq 4000 e a análise destas secuencias resultantes levouse a cabo utilizando o programa CLC Genomics Workbench v. 11.0.2. Esta análise de alto rendemento do transcriptoma proporcionou 28.044.852 lecturas (*reads*) por mostra, cunha lonxitude media de 101 pares de bases (pb). Estas *reads* foron ensambladas *de novo* en 347.317 contigs, dos cales se anotou con éxito o 10,2 % fronte á base de datos da plataforma UniprotKB/Swiss-Prot. Grazas á análise do RNA-Seq puidemos obter os xenes diferencialmente expresados (DEG) entre os

individuos infectados e os individuos control non infectados. Como consecuencia da natureza neurotrópica do nodavirus, a resposta transcriptómica no cerebro foi moito maior que en ril. No cerebro obtivéronse 4.062 transcritos regulados de maneira significativa a 24 hpi, e 1.478 a 72 hpi. Con todo, o número de transcritos regulados no ril foi menor, só houbo 32 e 76 DEGs a 24 e 72 hpi, respectivamente. Ao realizar a análise de enriquecemento de termos GO, os procesos biolóxicos máis representativos en cerebro estaban relacionados co transporte de ións e procesos regulados por calcio ou mediados por diferentes neurotransmisores e os seus receptores. No ril, os termos GO enriquecidos estaban relacionados con procesos biolóxicos de oxidación-redución, biosíntesis de glucocorticoides e metabolismo de esteroles.

A pesar de que no ril os xenes inmunes esperados non se atopaban significativamente modulados pola infección viral, atopáronse algúns destes xenes diferencialmente expresados no cerebro, aínda que en baixa proporción. Observouse unha regulación case completa do eixo HPI, que ademais presentaba un cambio completo da modulación dos xenes relativos a este eixo, estando regulados de maneira positiva ás 24 hpi e de maneira negativa ás 72 hpi. Este cambio de regulación correlacionouse cunha síntese activa de cortisol no ril, a principal hormona do estrés, ás 24 hpi. Ao realizar experimentos nos cales se inxectaron robalizas con cortisol e se infectaron con nodavirus, puidemos comprobar que este estrés causado polo cortisol beneficiaba ao virus na súa replicación e alcanzaba mortalidades maiores durante a súa infección. Isto puido ser debido a que o cortisol modula a resposta inmune provocando inmunosupresión. Ademais, encontráronse regulados varios tipos de neurotransmisores implicados na excitación neuronal a través de correntes iónicas, e isto, xunto ao análise do roteiro de sinalización do calcio que tamén se atopaba alterado nos dous tempos, púidose identificar que os principais reguladores da homeostase do calcio estaban afectados pola infección con nodavirus e que seguían o mesmo patrón de modulación que os xenes do eixo HPI ao estar intimamente ligados estes dous roteiros.

A hiperactivación dos receptores de glutamato a 24 hpi pode xerar excitotoxicidade e un influxo excesivo de calcio ao interior celular, o

que incrementa a produción de especies reactivas de osíxeno (ROS), mecanismos prexudiciais para a célula. Así, levaronse a cabo experimentos tanto *in vitro* como *in vivo* que nos demostraron que a infección por nodavirus mostra a tempos curtos unha produción significativa de ROS, e a medida que pasa o tempo esta produción de ROS redúcese, do mesmo xeito que a cantidade de calcio no interior celular. Ademais, o uso de quelantes intracelulares de calcio reduciu a produción de ROS significativamente, tanto en células infectadas como non infectadas. Tamén se comprobou que a menor dispoñibilidade de calcio no interior celular reduce a replicación do nodavirus. Desta maneira, tanto a sobrecarga como a falta de calcio son prexudiciais para o virus.

Este traballo supón a primeira vez que se describe a modulación completa do eixo HPI ante unha infección cun virus neurotrópico en teleosteos.

Capítulo 3: Posible participación de lncRNAs na modulación da resposta transcriptómica da robaliza europea ante unha infección con nodavirus

Neste capítulo da presente Tese Doutoral, quíxose comprobar se a resposta transcriptómica que atoparamos na robaliza ante unha infección con nodavirus estaba orquestrada en parte por lncRNAs. Os lncRNAs representan unha parte de ARNs non codificantes cunha lonxitude sobre 200 nucleótidos e que se transcriben da mesma maneira que os ARN mensaxeiros. En peixes, aínda que os estudos funcionais son limitados, existen varias publicacións que describen a modulación de lncRNAs ante distintos estímulos con atención especial no sistema inmune. A identificación da funcionalidade dos lncRNAs en peixes baséase na función proteica dos xenes codificantes. Para esto, anotáronse os *contigs* contra unha base de proteínas de peixes teleósteos incluidas nas bases de datos NCBI GenBank y UniProt/Swiss-Prot para descartalos, xunto aqueles *contigs* con máis de 200 nucleótidos e posibles marcos de lectura (ORFs). A continuación, utilizouse a ferramenta Coding Potential Assessment Tool (CPAT) para descartar as secuencias con potencial codificador. Os *contigs* que pasaron tódolos filtros consideráronse lncRNAs putativos e foron analizados para

detectar os transcritos diferencialmente modulados e a súa posible posición no xenoma de *Dicentrarchus labrax*.

O 69 % dos *contigs* (240.274) foron anotados contra secuencias de proteínas de peixes teleósteos, e dos *contigs* non anotados, un total de 12.158 pasaron tódoslos filtros para ser considerados posibles lncRNAs. O 95,96 % destos *contigs* mapeáronse con éxito ante o xenoma de *D. labrax*. De novo, como ocurría ca regulación transcriptómica no capítulo anterior, a modulación de lncRNAs foi maior no cerebro que no ril, posiblemente pola natureza neurotrópica do virus. En ambos tecidos, o número de lncRNAs regulados de maneira positiva foi maior que aqueles regulados de maneira negativa a 24 hpi, e estas diferenzas reducíronse considerablemente ás 72 hpi.

Extraéronse os xenes codificantes que flanqueaban aos lncRNAs diferencialmente expresados e realizouse un enriquecemento de termos GO dos mesmos. No ril atopáronse numerosos termos relacionados coa inmunidade a 24 hpi. Con todo, esta representación inmune diluíase a 72 hpi. No cerebro, a 24 hpi a presenza de termos inmunes foi practicamente nula, aínda que compartía co ril a existencia de termos involucrados no dano do ADN, así como numerosos procesos relacionados coa ubiquitinización. Tamén se atoparon procesos biolóxicos relacionados coa homeostase do calcio, o que podería explicar en parte a gran regulación transcriptómica de canles e proteínas de unión a calcio descritos no capítulo anterior desta Tese Doutoral. Ás 72 hpi, a representación de termos inmunes incrementouse en cerebro e tamén apareceron termos relacionados co estrés, do mesmo xeito que en ril ao mesmo tempo de infección.

Neste traballo púidose correlacionar a expresión de certos lncRNA coa expresión dos seus xenes codificantes veciños, así detectáronse lncRNA que correlacionan de maneira significativa para xenes diferencialmente expresados relacionados coa inmunidade, e tamén para os xenes que regulan as diferenzas na homeostase do calcio detectadas a nivel transcriptómico durante a infección con nodavirus. Os lncRNAs parecen contribuír en gran medida á resposta transcriptómica contra o nodavirus.

Capítulo 4. Inmunización da robaliza cun fragmento da proteína do betanodavirus exposta na superficie de bacterias inactivadas sen mecanismo de reparación

Como se comentou na introdución, existen 4 xenotipos dentro do xénero *Betanodavirus* que se clasifican acorde á secuencia xénica que codifica a proteína da cápside (proteína C), mostrando só un 19 ou 23 % de diferenzas entre eles. A maioría das proteínas C dos betanodavirus xeograficamente relacionados comparten ata un 98 ou 99 % da súa secuencia aminoacídica e esta proteína estrutural é a única diana dos anticorpos neutralizantes do peixe. Así, a maioría de vacinas que se describiron contra nodavirus, ademais de utilizar o virus completo morto ou inactivado, centráronse en vacinas baseadas en cápsides baleiras (virus-like particles, VLP), na proteína C recombinante ou en péptidos sintéticos derivados da proteína C.

Neste traballo, fíxose uso das chamadas *spinycterins*, fragmentos de antíxenos virais expresados na superficie de bacterias recombinantes, con distintas ancoraxes de membrana procariotas unidos a un fragmento da proteína viral C. Para preservar a inmunoxenicidade que se perde ao inactivar as bacterias recombinantes co uso do formaldehido, probouse un fármaco bactericida que introduce cortes estables nas cadeas do ADN das bacterias recombinantes mediante unha unión covalente, causando a súa morte por estrés oxidativo. Para que este dano fose irreversible, elixiuse a cepa de *E. coli* BLR(DE3), incapaz de reparar cortes na dobre cadea de ADN. Ademais, esta cepa é resistente á tetraciclina, podendo producirse a gran escala e evitar contaminación da vacina con outros microorganismos, e tamén require Isoleucina no seu medio de cultivo para poder seleccionar os recombinantes sen depender de antibióticos e reducir así a posibilidade de diseminación de xenes resistentes e poder ser manipulada con seguridade.

Para elixir o mellor fragmento da proteína C para a inmunización, fíxose unha análise dos epítopos tanto de anticorpos monoclonais neutralizantes como de mostras de soro de peixes sobreviventes a unha infección con NNV e mapeáronse as súas posicións aminoacídicas. Elixiuse o fragmento que contén os aminoácidos dende a posición 91 á 220 ($frgC_{91\text{-}220}$) xa que presenta as rexións máis hidrofílicas para ser

expostas na superficie das bacterias recombinantes e tamén representa unha das secuencias con menor variabilidade entre as cepas de NNV, proporcionando un inmunóxeno común para un maior número de cepas do virus. Ademais, as tres cisteínas foron mutadas a serinas durante a síntese xénica para evitar a formación de corpos de inclusión na bacteria *E. coli*, os cales reducirían a inmunoxenicidade.

Fusionáronse distintas anclaxes procariotas con este frg$C_{91\text{-}220}$ para comprobar cal sería o que incrementase en maior medida a súa expresión na membrana bacteriana. Tras unha dixestión con tripsina, puidose comprobar que a anclaxe procariota que expoñía en maior medida o frg$C_{91\text{-}220}$ era a anclaxe YBEL, seguida da anclaxe Nmistic.

Por último, levouse a cabo a inmunización de robalizas cas *spinycterins* YBEL+ frg$C_{91\text{-}220}$ y Nmistic + frg$C_{91\text{-}220}$ expresadas na cepa BLR(DE3), inxectáronse intraperitonealmente e tras 30 días dende a inmunización realizouse unha infección con NNV inxectándoo intramuscularmente. No grupo control non inmunizado e infectado con NNV alcanzouse unha mortalidade do 25,7 %, ó igual que no grupo infectado co plásmido vacío pRSET. O nivel de protección expresado en porcentaxe relativa de supervivencia foi do 100 % naqueles peixes inxectados cas *spinycterins* YBEL+ frg$C_{91\text{-}220}$, e dun 62,3 % naqueles peixes inxectados cas *spinycterins* Nmistic + frg$C_{91\text{-}220}$. Aqueles peixes inxectados con *spinycterins* que non iban unidas a unha anclaxe procariota, solo levando o frg$C_{91\text{-}220}$, presentaron unha supervivencia relativa de tan só o 2,7 %. Puidose observar unha gran correlación entre o nivel de exposición do antíxeno e o nivel de inmunización ante a infección.

Desta maneira, neste capítulo da presente Tese Doctoral centrámonos en describir un prototipo mínimo como alternativa de vacina para peixes que debería estudarse máis a fondo mediante outros procedimentos de inactivación, técnicas alternativas de administración masiva e incluíndo respostas inmunitarias innatas e adaptativas do hóspede.

Capítulo 5. O peixe cebra como modelo vertebrado para o estudo de infeccións con nodavirus.

O peixe cebra (*Danio rerio*) é un modelo de traballo moi versátil utilizado amplamente para estudos de ontoxenia, bioloxía do desenvolvemento e enfermidades infecciosas para comprender as interaccións entre hóspede e patóxeno. Aínda que non se coñecen virus que infecten de maneira natural ao peixe cebra, o seu uso como modelo de infección permitiu o estudo de varias enfermidades causadas por virus, tanto de humanos como de peixes. E a pesar da importancia da enfermidade VER, non existen moitos estudos que aproveiten os beneficios do peixe cebra para investigar a infección con nodavirus.

Despois de probar distintas vías de infección e idades larvarias, puidemos determinar que canta máis idade tiña a larva, máis complicado era que presentase síntomas de infección. As maiores mortalidades obtéñense cando o virus foi microinyectado directamente no cerebro de larvas de 3 días post-fertilización (dpf). Baixo estas mesmas condicións, existía unha maior migración cara ao sitio de infección de neutrófilos e células que expresan lisozima, implicadas na resposta inmune. Este seguimento celular puido realizarse *in vivo* cun microscopio de fluorescencia grazas ao pequeno tamaño das larvas, a transparencia do seu corpo e a existencia de liñas transxénicas con distintas liñas celulares marcadas. Estas características tamén permitiron a marcaxe inmunohistoquímica do virus e certas proteínas de interese, dándonos unha ferramenta ca cal intentar descubrir as células ou texidos que o virus utiliza para distribuírse o longo do corpo dos peixes infectados.

Os principais síntomas do nodavirus son a natación errática dos peixes afectados pola infección, xa que o virus actúa a nivel neuronal e tamén provoca a curvatura da espiña dorsal. Así, quixemos detectar as variacións no movemento das larvas, atopando diferenzas significativas na velocidade ou dirección da natación das larvas infectadas comparadas con aquelas non infectadas.

A maior mortalidade das larvas infectadas no cerebro correlacionouse cunha maior expresión da proteína da cápside do nodavirus a lo longo do tempo. A análise da expresión de distintos xenes mediante qPCR amosounos unha maior expresión xenes que

codifican citoquinas proinflamatorias como o *tnfα* e *il1β* ou a proteína *mxe* que son indicativas de que o peixe está reaccionando ante o virus.

Este último capítulo pecha a Tese Doctoral reafirmando as bases para que o peixe cebra sexa considerado o modelo de infección, non só do nodavirus, senon de moitos outros virus de peixes que son difíciles de estudar *in vivo* debido á difícil obtención das especies afectadas ou polo seu mantemento no laboratorio